

**DESIGN, SYNTHESIS AND STUDY OF A FEW DONOR-  
ACCEPTOR-DONOR (D-A-D) MOLECULES AS  
MOLECULAR PROBES AND LOGIC GATES**

THESIS SUBMITTED TO  
**THE UNIVERSITY OF KERALA**  
FOR THE DEGREE OF  
**DOCTOR OF PHILOSOPHY**  
IN CHEMISTRY  
UNDER THE FACULTY OF SCIENCE

*By*  
**S. SREEJITH**



PHOTOSCIENCES AND PHOTONICS GROUP  
CHEMICAL SCIENCES AND TECHNOLOGY DIVISION  
NATIONAL INSTITUTE FOR INTERDISCIPLINARY SCIENCE AND TECHNOLOGY  
CSIR, TRIVANDRUM - 695019  
KERALA, INDIA

SEPTEMBER 2009

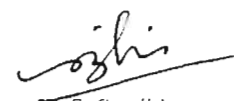
Dedicated to...

**My Parents**

## DECLARATION

I hereby declare that the matter embodied in the thesis entitled: “**Design, Synthesis and Study of a few Donor-Acceptor-Donor (D-A-D) Molecules as Molecular Probes and Logic Gates**” is the result of the investigations carried out by me at the Photosciences and Photonics Group, Chemical Sciences and Technology Division, National Institute for Interdisciplinary Science and Technology (NIIST), CSIR, Trivandrum, under the supervision of Dr. A. Ajayaghosh and the same has not been submitted elsewhere for any other degree.

In keeping with the general practice of reporting scientific observations, due acknowledgement has been made wherever the work described is based on the findings of other investigators.

  
S. Sreejith

National Institute for Interdisciplinary Science and Technology  
(NIIST)

*(Formerly Regional Research Laboratory)*



Council of Scientific & Industrial Research  
(CSIR)

Industrial Estate P.O., Trivandrum - 695 019  
Kerala, INDIA



A. Ajayaghosh, F. A. Sc.  
Scientist  
Photosciences and Photonics Section  
Chemical Sciences and Technology  
Division

Tel: 91-471-2515 306  
Fax: +91-471-2491 712  
E-mail: [ajayaghosh62@gmail.com](mailto:ajayaghosh62@gmail.com)

September 8, 2009

CERTIFICATE

This is to certify that the work embodied in the thesis entitled: “**Design, Synthesis and Study of a few Donor-Acceptor-Donor (D-A-D) Molecules as Molecular Probes and Logic Gates**” has been carried out by Mr. S. Sreejith under my supervision at the Photosciences and Photonics Group of the National Institute for Interdisciplinary Science and Technology (NIIST), CSIR, Trivandrum and the same has not been submitted elsewhere for a degree.

A. Ajayaghosh  
(Thesis Supervisor)

## ACKNOWLEDGEMENTS

*It is with great pleasure that I extend my deep sense of gratitude to Dr. A. Ajayaghosh, my thesis supervisor, for suggesting the research problem, for his constant guidance, valuable suggestions, support and encouragement, leading to the successful completion of this work. His assurance at the time of crisis, especially for standing by me in days of hardship is gratefully acknowledged.*

*I would like to express my gratitude to Prof. M. V. George for his constant encouragement and inspiration during my stay at the National Institute for Interdisciplinary Science and Technology (NIIST), Trivandrum.*

*I wish to thank Dr. B. C. Pai, Acting Director, NIIST and Professor T. K. Chandrashekar and Dr. G. Vijay Nair (Former Directors), NIIST, Trivandrum for providing necessary facilities and infrastructure of the laboratory for carrying out the work.*

*I would also like to acknowledge:*

- *Dr. Suresh Das, Head, Chemical Sciences and Technology Division, Dr. K. R. Gopidas, Dr. D. Ramaiah, and Dr. K. George Thomas, scientists of the Photosciences and Photonics Group, for their help and valuable suggestions.*
- *Dr. E. Arunkumar, Ms. Priya Carol, Dr. Reji Varghese and Dr. C. Vijayakumar former members of the Photosciences and Photonics Group for their help and advice.*
- *Special word of thanks to my colleague Ms. K. P. Divya who helped me with experiments and for fruitful discussions, criticism and suggestions with regard to work and manuscripts.*
- *Mr. Shyam Krishna and Mr. Sai Shyam, Biotechnology Division, NIIST for plasma analysis experiments and Ms. V. N. Anupama, Environmental Technology Division, NIIST for fluorescence microscopy experiments.*
- *Dr. P. Jayamurthy, Agroprocessing and Natural Products Division, NIIST for providing cell lines and whole hearted support during cell imaging and labelling experiments.*
- *Mr. Robert Philip and Mrs. Sarada Nair for general help and support.*
- *Dr. V. K. Praveen, Dr. P. Chithra, Mr. S. Mahesh, Mr. S. Santhosh Babu, Mr. S. Srinivasan, Mr. S. Prasanth Kumar, Mr. Anesh Gopal, Mr. P. Anees, Dr. Saji Alex, Mr. Jomon Mathew, Mr. S. Ramakrishnan, Mr. K. V.*

- Ratheesh, Mr. Jathish Kumar, Ms. K. S. Anju and other members of Photochemistries and Photonics Group for their help and cooperation.*
- *Mrs. Saumini Mathew for NMR spectra, Mrs. S. Viji for HRMS and Elemental Analysis.*
  - *Members of the Organic Chemistry Section for general help.*
  - *All my teachers at St. Thomas College, Kozhencherry and Marthoma College, Thiruvalla especially Dr. Thomas Mathew, Dr. Raju Thomas and Dr. Koshy John for their constant encouragement at different stages of my academic career.*
  - *Council of Scientific and Industrial Research (CSIR) and Department of Science and Technology (DST), Government of India for financial assistance.*

*I am deeply and forever indebted to my parents for their constant source of love, inspiration and blessings. Finally I would like to thank my brother, friends and relatives for their excellent support and encouragement.*

*S. Sreejith*

*Trivandrum  
September 2009*

## CONTENTS

		Page
	<b>Declaration</b>	i
	<b>Certificate</b>	ii
	<b>Acknowledgements</b>	iii
	<b>Preface</b>	vii
<b>Chapter 1</b>	<b>Organic Chromophores as Molecular Probes and Logic Gates: An Overview</b>	<b>1-39</b>
1.1	Abstract	1
1.2	Introduction	2
1.3	Molecular Probes for Zinc Ions	4
1.4	Squaraine Based Molecular Probes	12
1.5	Concept of Molecular Logic Operations: From Molecular Probes to Logic Gates	22
1.5.1	Chemically Driven Molecular Logic Gates	27
1.6	Objectives of the Present Investigation	33
1.7	References	34
<b>Chapter 2</b>	<b>A Near Infrared (NIR) Squaraine Dye for the Detection of Amino-thiol Content in Blood Plasma</b>	<b>40-76</b>
2.1	Abstract	40
2.2	Introduction	41
2.3	Results and Discussion	47
2.3.1	The Design Strategy	47
2.3.2	Synthesis of the Squaraine based Probes <b>Sq1a</b> and <b>Sq1b</b>	48
2.3.3	Absorption and Emission Spectra of the Bispyrroles <b>15a</b> and <b>15b</b>	50
2.3.4	Absorption and Emission Studies of <b>Sq1a</b> and <b>Sq1b</b>	51
2.3.5	Thiol Detection	53
2.3.6	Human Blood Plasma Analysis	59
2.4	Conclusions	66
2.5	Experimental Section	67
2.6	References	74

<b>Chapter 3</b>	<b>Bipyridine based Fluorophores for the Detection of Zinc Ions under Cellular and Aqueous Environments</b>	<b>77-114</b>
3.1	Abstract	77
3.2	Introduction	78
3.3	Results and Discussion	86
3.3.1	Synthesis of Zn <sup>2+</sup> Probes	86
3.3.2	Optical Properties	87
3.3.3	Solid State Quantum Yield Measurements of <b>CBP</b>	91
3.3.4	Circular Dichroism Studies of <b>CBP</b>	92
3.3.5	Cation Binding Properties of <b>CBP</b>	93
3.3.6	Design of Reusable Dipstick Probe for Zinc Ions using <b>CBP</b>	98
3.3.7	Cation Binding Properties of <b>GBP</b>	102
3.3.8	Cell Imaging Study with <b>GBP</b>	103
3.4	Conclusions	105
3.5	Experimental Section	106
3.6	References	112
<b>Chapter 4</b>	<b>Excited State Charge Transfer Modulation and Molecular Logic Operations in a Bipyridine Integrated Fluorophore</b>	<b>115-147</b>
4.1	Abstract	115
4.2	Introduction	116
4.3	Results and Discussion	122
4.3.1	The Design Strategy	122
4.3.2	Synthesis of <b>10</b>	123
4.3.3	Optical Properties of <b>10</b>	125
4.3.4	Absorption and Emission Studies of <b>10</b> in Presence of Different Chemical Inputs	128
4.3.5	Logic Operations of <b>10</b>	133
4.3.6	Paper Microfluidic Demonstration of Fluorescence Modulation with Various Inputs	138
4.4	Conclusions	140
4.5	Experimental Section	141
4.6	References	145
	<i>List of publications and patents</i>	148
	<i>Posters presented at conferences</i>	149

## PREFACE

Design of organic chromophores which selectively respond to various analytes has attracted wide scientific and technological interests. Among this, molecules which show distinct optical responses with specific analytes are essential for developing molecular probes or the so called "chemosensors and chemodosimeters". Similarly, molecules which can be switched between two stable states, with respect to chemical inputs are capable of encoding binary digital inputs in a memory device. Thus, molecular probes and molecular logic gates are the two sides of the same coin. Therefore, molecules that act as switches and logic gates to process information in molecular electronics or computing are important. The present thesis entitled "***Design, Synthesis and Study of a few Donor-Acceptor-Donor (D-A-D) Molecules as Molecular Probes and Logic Gates***" embodies the result of our efforts to develop new molecular probes for the detection of biorelevant analytes as well as new fluorophores for molecular logic operations.

The thesis is comprised of four chapters. The first chapter is an overview of molecular probes and logic gates where the optical and electronic properties of donor-acceptor-donor based systems are made use of. In this chapter, a general discussion on the basic concept of molecular probes and molecular logic gates are provided. The recent progress made in this area are highlighted with some of the important examples on molecular systems used as probes for biorelevant analytes and logic gates emphasizing the various design strategies adopted.

The second chapter describes a new strategy for the detection of thiols and thiol containing amino acids in human blood plasma using a NIR squaraine dye. The detection is based on the activation of fluorescence by thiol induced breaking of conjugation in the squaraine backbone. The squaraine probe selectively responds to thiols and aminothiols which allow their ratiometric detection due to the generation of new, noninterfering absorption and emission bands. Since the detection is based on absorption and emission changes due to the analyte specific generation of new

chromophores, other impurities do not interfere with sensitivity. Application of the probe is illustrated with the quantitative detection of the total aminothiols content in human blood plasma which has tremendous biological and clinical relevance. Using this probe, we have shown that the aminothiol content is high in the blood of heavy smokers which is responsible for many heart diseases.

In the third chapter we discuss the synthesis, biological as well as analytical application of two fluorescent bispyrrole derivatives. Pyrrole end capped 5, 5' divinyl 2, 2' bipyridyl systems are excellent ratiometric probes for the specific detection of  $Zn^{2+}$ . A bispyrrole derivative with glycol side chain has been synthesized and used for imaging  $Zn^{2+}$  ions in MCF-7 cell lines using epifluorescence microscopy. A chiral side chain attached bispyrrole, exhibited high solid state luminescence and hence could be used for the detection of  $Zn^{2+}$  ions in aqueous analytical solutions. The solid state fluorescence ( $\Phi_f = 0.462$ ) of the chiral derivative was high when compared to the one with an achiral side chain ( $\Phi_f = 0.018$ ). This property of chiral derivative is exploited for the preparation of a fluorescence "dipstick" for the detection of  $Zn^{2+}$  ions in aqueous medium. Details of the synthesis, optical properties and use in the fabrication of reusable dipstick fluorescence probe for the detection of  $Zn^{2+}$  ions are also described.

A strongly fluorescent bipyridine based donor-acceptor-donor (D-A-D) type receptor molecule which can perform multiple basic logic operations such as AND, INHIBIT, IMPLICATION and 3-input INHIBIT etc, with different chemical inputs is discussed in the fourth chapter. The modulation of ICT (Intramolecular charge transfer) induced intrinsic fluorescence property of the fluorophore, using three different chemical inputs, generating three different fluorescence states from the same molecular backbone is exploited for logic operations. Four different basic logic gates with different information outputs could be achieved using this simple strategy. A combined logic operation has been defined by using the full fluorescence response of this new molecule. Apart from the illustration of the logic operations in solution, we have used a

paper microfluidic technique to demonstrate the fluorescence changes and logic operations on a solid substrate.

In summary, in this thesis, a systematic investigation on the synthesis and studies of a few donor-acceptor-donor (D-A-D) based molecules are described. The new molecules were used for the detection of various biorelevant analytes such as low molecular weight aminothiols and  $Zn^{2+}$  ions and for the imaging of biological cells. By making use of the fluorescence modulation with external inputs, a molecular logic gate was also developed which can perform various logic operations. Thus, the present thesis attempts to bridge between two important areas namely, molecular probes and molecular logic gates with a few fluorescent molecules.

---

#### References

1. A. Ajayaghosh, P. Carol, S. Sreejith, *J. Am. Chem. Soc.* **2005**, *127*, 14962.
2. P. Carol, S. Sreejith, A. Ajayaghosh, *Chem. Asian J.* **2007**, *2*, 338.
3. S. Sreejith, K. P. Divya, A. Ajayaghosh, *Chem. Commun.* **2008**, 2903.
4. S. Sreejith, P. Carol, P. Chithra, A. Ajayaghosh, *J. Mater. Chem.* **2008**, *18*, 264.
5. S. Sreejith, K. P. Divya, A. Ajayaghosh, *Angew. Chem. Int. Ed.* **2008**, *47*, 7883.

---

### Organic Chromophores as Molecular Probes and Logic Gates: An Overview

---

#### 1.1. Abstract

*Design of organic chromophores which selectively respond to various analytes has attracted wide scientific and technological interests. Among these molecules, fluorophores which give distinct fluorescence response with specific analytes are preferred for developing molecular probes due to the high sensitivity of fluorescence emission with respect to a specific analyte. They are widely used as chemosensors (reversible detection) or chemodosimeters (one time detection) and also for the imaging of biological tissues. On the other hand, molecules which can be switched between two stable states, with respect to chemical inputs are capable of encoding binary digital inputs in a memory device. Thus, molecules that act as switches and logic gates to process information in molecular electronics or computing are important. In this chapter, an overview of the literature on molecular systems that are used as probes for biorelevant analytes and for logic operations, emphasizing the various design strategies adopted are discussed. Finally the aim and outline of the thesis are presented.*

## 1.2. Introduction

Molecular probes or the so called “chemosensors and chemodosimeters” are the molecules of synthetic origin that are able to bind selectively and reversibly, an analyte of interest with a concomitant change in one or more properties such as absorption and/or emission characteristics.<sup>1</sup> It may also result in changes of redox potentials, translocation of molecular fragment within the supramolecular assembly (which may also be associated with changes in optical or electrochemical properties as well), chemical reactivity, or magnetic properties. Among the different molecular probes, fluorescence based probes have many advantages: fluorescence measurements are usually very sensitive (single molecule detection is possible), low cost, easily performed, and versatile, offering sub nanometer spatial resolution with submicron visualization and sub millisecond temporal resolution.<sup>2</sup> Furthermore, many opportunities exist for modulating the photophysical properties of a fluorophore, such as the proton, energy and electron transfer processes, heavy atom effects, changes of electronic density, and the destabilization of a nonemissive  $n-\pi^*$  excited state.<sup>3,4,5</sup> This offers, a wide range of possibilities for tailoring efficient luminescent chemosensors.

Fluorescent sensors can be either based on ‘fluorogenic chelating agents’ or ‘fluoroionophores’ with separate fluorophore and ionophore linked with or without a spacer. They may undergo an analyte specific fluorescence change due to the modulation of excited state physical properties via photoinduced energy or

electron transfer. 'Fluoroionophores' with an appropriate combination of the fluorophore and ionophores are the most widely used strategy in probe design.<sup>6</sup> For one time detection of an analyte, chemodosimeters are used which show irreversible fluorescence quenching or color bleaching. Design of fluorescent molecular probes by incorporating the following two features enhances the efficiency of probes: (i) easily distinguishable fluorescent states before and after binding event, (ii) generation of ratiometric fluorescent signals.

Many of the fluorescent chemosensors can be considered as molecular switches.<sup>4</sup> Any chemical system that can exist in at least two different forms with distinguishable physical properties in a reversible fashion is regarded as molecular switches. They are molecules or molecular systems that can modulate their optical or electrical properties upon interaction with external stimuli such as anions, cations, or neutral molecules. They are the simplest tools that can transmit information on events occurring at a molecular scale to the macroscopic world. In the case of fluorescence monitoring, the quantum yield should change from very small ( $\Phi \ll 1$ ) to high ( $\Phi \approx 1$ ), or vice versa, and the shift of the emission band should be larger than the corresponding band halfwidth. If the change in the absorption or emission can be switched "on" and "off" in response to a chemical input, binary digital logic operations can be addressed with molecular systems, resulting in molecular logic gates. Therefore, design of intelligent functional organic fluorophores which respond to specific analytes are useful either as

molecular probes for the detection of a specific analyte or as information processing channels for implementing future miniaturized computing devices. In the present chapter, the recent developments in the field of molecular probes are discussed with special emphasis on zinc ion specific chromophores. Subsequently, an overview of squaraine dye based molecular probes is presented. Finally, the concept of molecular logic gates and some recent development in this area is discussed.

### **1.3. Molecular Probes for Zinc Ions**

Zinc is the second most abundant transition metal ion in the human body, where it has multiple roles in both intra- and extracellular functions.<sup>7-12</sup> A large number of proteins and enzymes have been identified to contain  $Zn^{2+}$ . Zinc is reported to be responsible for neurological disorders such as Alzheimer's disease, amyotrophic lateral sclerosis (ALS), Parkinson's disease, and epilepsy.<sup>13</sup> Furthermore, zinc plays a crucial role in insulin secretion and apoptosis. The World Health Organization estimates that more than 40% of the children in Africa and Asia have stunted growth associated with limited dietary zinc.<sup>14</sup> The extent to which conditions of zinc deficiency persist today is difficult to determine because of the lack of suitable biochemical markers for zinc ions. Besides growth, numerous body functions are affected by zinc ions, including the immune, endocrine, and gastroenterological systems. The huge scope for the exploration of the diverse physiological roles of biological zinc demands sensitive and

noninvasive techniques for real-time detection and imaging. The relative concentration of free  $Zn^{2+}$  within biological cells varies from 1 nM in the cytoplasm of many cells to 1 mM in the vesicles of presynaptic neurons in the human brain.<sup>15</sup> Although, the total concentration of zinc ions in a cell is relatively high, the concentration of free zinc, which is not strongly bound to proteins, is extremely low. The estimation of free zinc has proved to be difficult with classical methods. These concerns make it a top priority of chemists to develop selective and efficient probes for zinc ions.

The growing contributions of zinc homeostasis to neurophysiology and neuropathology have prompted interest in devising new ways to detect  $Zn^{2+}$  in biological and analytical samples.  $Zn^{2+}$  is a difficult analyte to monitor owing to its closed shell  $3d^{10}4s^0$  electronic configuration and the absence of oxidation-reduction activity within biological environments. As such, conventional techniques (e.g., NMR, EPR, and electronic absorption spectroscopy) are largely ineffective for this spectroscopically silent metal ion. Atomic absorption spectroscopy (AA) provides a sensitive and selective method for zinc detection and has been used to track release of zinc into extracellular fluid after neuronal stimulation.<sup>16</sup> However, this technique has limited spatial resolution and is destructive to the sample.

As  $Zn^{2+}$  is invisible to most analytical techniques, fluorescence technique stands out as the method of choice.<sup>17</sup> This method utilizes a probe molecule that

recognizes  $Zn^{2+}$  and emits a specific wavelength upon binding, which in turn allows tracking of zinc ions in live cells with fluorescence microscopy. A fluorescent molecular probe consists of a fluorophore attached to a chelating agent or an ionophore with or without a spacer group.<sup>4,12</sup> Analyte binding results in either enhancement or change in the emission intensity of the probe.

Effective fluorescent probes for imaging metal ions in living cellular systems must meet several strict requirements.<sup>18</sup> Most importantly, the probe should be selective for a specific metal ion over other biologically abundant cations, including those that exist at much higher cellular concentrations (for example,  $Na^+$ ,  $K^+$ ,  $Mg^{2+}$  and  $Ca^{2+}$ ). Principles of coordination chemistry, including preferred donor numbers and ligand field geometries, as well as hard-soft acid-base considerations, are critical for designing and obtaining metal selective responses. A turn-on emission increase or shift in the excitation/emission profiles is preferred over a turn-off emission quenching response to maximize spatial resolution using light microscopy. Because, a metal responsive probe is inherently involved in complex equilibria with endogenous ligands within the cell, probes must be matched with dissociation constants ( $K_d$ ) appropriate to the system under study. Furthermore, high optical brightness values can lower the amount of dye needed for cellular applications, which minimizes the potential for altering endogenous cellular distribution. Dyes that have visible light excitation and emission are desirable in order to minimize sample damage and reduce auto fluorescence.

Finally, probes must also be compatible with biological systems: they must be water soluble, they must allow for examination of extracellular, intracellular or subcellular regions, and they must be nontoxic (though potential toxicity is a difficult trait to predict). Addressing the challenge of meeting both chemical and biological constraints is critical to developing useful tools for cellular applications.

Many fluorescent sensors utilize the principle of photoinduced electron transfer (PET) for the signaling of the binding process.<sup>19,20</sup> Metal coordination to the receptor unit makes it a less efficient electron donor to an attached fluorophore. Thus, the native fluorescence of the fluorophore is restored. This signaling is highly selective for the analyte. Sensors operating according to this principle are known as CHEF (chelation-enhanced fluorescence) type sensors (Figure 1.1).<sup>19,20</sup>

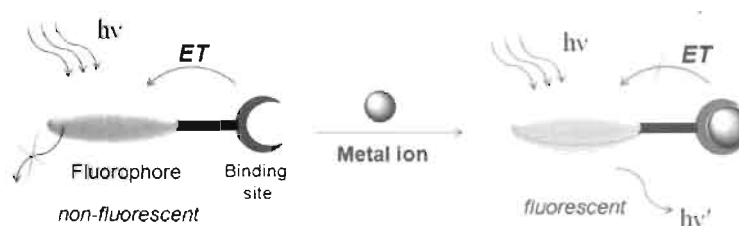


**Figure 1.1.** Schematic representation of CHEF-type fluorescent sensor for metal ions.

The amino nitrogen of di-2-phenylpicolylamine (DPA) ligand is a good electron donor in PET process. DPA based sensor **1** is a typical PET sensor for protons and post transition metal ions like zinc (Chart 1.1).<sup>21</sup> Upon binding of the

metal ion, the quenching process is interrupted and the fluorescence quantum yield is increased. In order to shift the excitation wavelength to the visible region, fluorescein and its derivatives were used as fluorophores. Only the anionic form of the fluorescein emits strongly, which means that the pKa values are an important factor for the pH dependent performance. Attachment of electron withdrawing groups renders better performance in a much broader pH range. When the fluorophores are connected to DPA, the electron transfer from the DPA facilitates quenching of the fluorescence.<sup>22</sup> This process is interrupted when the amino nitrogen coordinates with Zn<sup>2+</sup>. A few examples of fluorescent enhancement based probes are shown below (Chart 1.1).

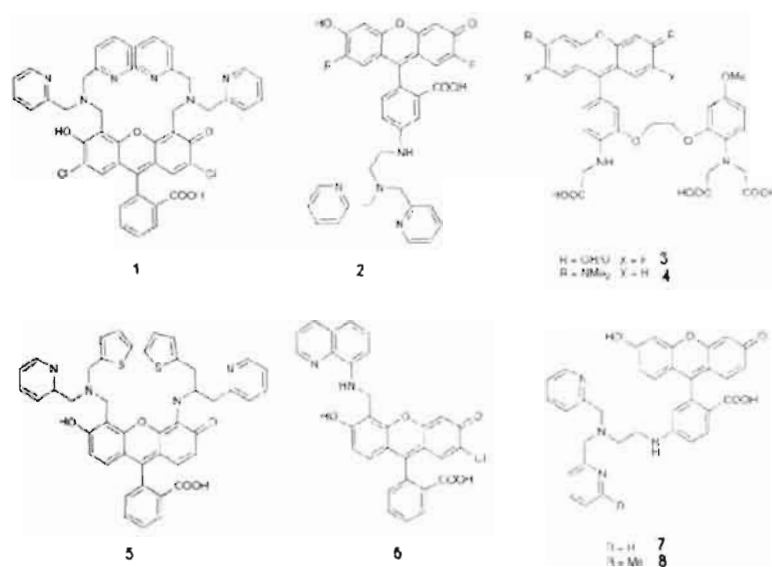


**Chart 1.1.** A few examples of turn-on fluorescent probes for Zn<sup>2+</sup>.

Fluorescence intensity based probes are useful for visualizing uptake, release and redistribution of  $Zn^{2+}$  in many cellular applications. However, potential variations in excitation intensity, sample thickness, probe concentration and artefacts associated with the local cellular environments can preclude reliable quantitative measurements. A strategy to avoid these issues is through ratiometric imaging with chemosensors.<sup>23</sup> A ratiometric probe responds upon binding to an analyte with a shift in its emission maximum, which may or may not be concomitant with an increase in emission. This shift in the emission maximum should be enough to distinguish coexisting  $Zn^{2+}$ -free and  $Zn^{2+}$ -bound species, allowing the ratio of their emission intensities. Together with the known binding constant of the sensor, the unknown zinc concentration can be derived. Assuming identical solvent influences of fluorescence of the  $Zn^{2+}$ -free and  $Zn^{2+}$ -bound species, a ratiometric signal is internally calibrated. The principle of a ratiometric probe is shown in Figure 1.7.<sup>12</sup>

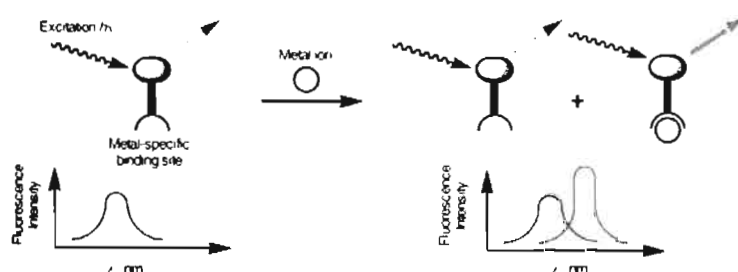


**Figure 1.2.** Schematic representation of ratiometric detection of metal ions.

FuraZin (**9**) and IndoZin (**10**) are ratiometric  $Zn^{2+}$  sensors derived from the classic Fura and Indo  $Ca^{2+}$  probes and operate via an internal charge transfer (ICT) mechanism, in which metal ion binding modulates the electron donating properties of the electron rich receptor in its photoexcited state (Chart 1.2).<sup>24</sup>  $Zn^{2+}$  complexation causes shift in the absorption band of **9** from 378 nm to 330 nm with a constant emission centered at 510 nm. In contrast, **10** maintains a constant absorption maximum at 350 nm however exhibits a blue shift of its emission wavelength from 480 nm to 395 nm upon binding  $Zn^{2+}$ . **9** and **10** have moderate  $Zn^{2+}$  affinities ( $K_d \sim 3.0 \mu M$ ) with good selectivity over  $Ca^{2+}$  and  $Mg^{2+}$ , and the former has been used to show that rapid zinc uptake into cellular vacuoles. **12** and **13** are a Fura-inspired pair of ratiometric  $Zn^{2+}$  sensors bearing DPA-type receptors for specific  $Zn^{2+}$  detection. The ethyl ester of **11** is cell permeable and can image labile  $Zn^{2+}$  in RAW 264.7 macrophages.<sup>25</sup>

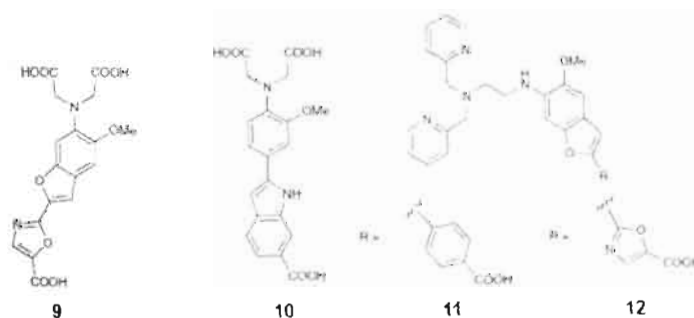
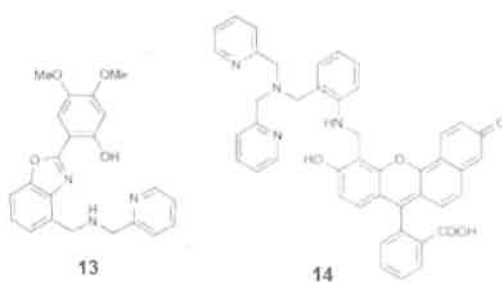


**Chart 1.2.** A few examples of ratiometric fluorescent probes for  $Zn^{2+}$ .

Henary *et al.*<sup>26</sup> and Taki *et al.*<sup>27</sup> have exploited the excited state intramolecular proton transfer (ESIPT) processes in benzimidazole and benzoxazole frameworks for the development of  $Zn^{2+}$ -specific ratiometric fluorophores. When unbound, the receptor moiety is involved in hydrogen bonding between heteroatoms of the receptor. Upon coordination to  $Zn^{2+}$ , the disruption of hydrogen bonding induces a shift in the emission and absorption.<sup>26</sup> The Zinbo series of ratiometric  $Zn^{2+}$  probes rely on this property and use a benzoxazole scaffold with a phenolic component to generate up to an 82-fold change in emission ratio upon interaction with  $Zn^{2+}$ .<sup>28</sup> Zinbo-5 (**13**) has been used with two-photon excitation to record ratiometric images of real-time changes in intracellular  $Zn^{2+}$  concentration in fibroblast cells.

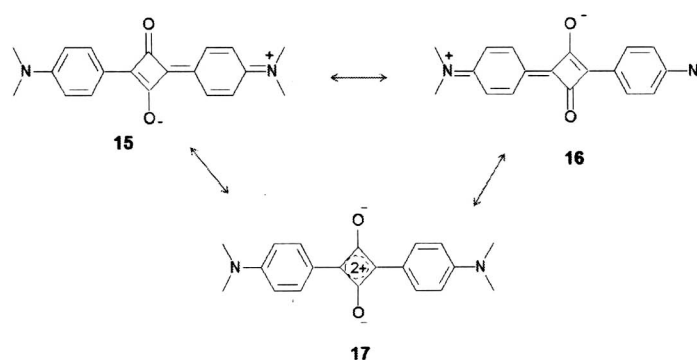


Zin-naphthopyr-1 (**14**) implements a seminaphthofluorescein architecture that, in its *apo* form, exhibits two absorption ( $\lambda = 503$  nm and 539 nm) and emission ( $\lambda = 528$  nm and 604 nm) bands in the visible region. **14** forms a strong 1:1 complex with  $Zn^{2+}$  ( $K_d = 0.55$  nM) and displays a major emission band centered at 624 nm with a minor peak at 545 nm. The  $I_{624}/I_{528}$  ratio increases from

0.4 to 7.1 upon addition of  $\text{Zn}^{2+}$  and maintains good selectivity over abundant cellular cations. Confocal microscopy experiments verify that the diacetate derivative of **14** is membrane permeable and can image, in real-time, the NO-induced release of  $\text{Zn}^{2+}$  in live COS-7 cells.<sup>29</sup>

#### 1.4. Squaraine Based Molecular Probes

Squaraine dyes (Squaraines) are ideally suited for designing molecular probes due to their favorable optical properties, which get perturbed with polarity of solvents, temperature and ionic inputs.<sup>30</sup> Squaraines belong to a class of polymethine dyes with a resonance stabilized zwitterionic structure.<sup>31</sup> A representative example is shown in Scheme 1.1.



Scheme 1.1.

Squaraines typically contain an electron deficient central four member ring and two electron donating groups in a donor-acceptor-donor (D-A-D) form. The intense absorption and emission properties of squaraines, which are associated

with the donor-acceptor-donor charge transfer, are suitable for the design of molecular probes for specific analytes. These dyes possess typically narrow and very intense absorption bands ( $\epsilon > 10^5$ ) at the red end of the visible spectral window and fluorescence bands of a mirror image shape with high fluorescence quantum yield ( $\Phi > 0.1$ ). Binding of substrates can occur either to the oxygen atom of the electron deficient cyclobutene ring or to an ionophore which is attached to the dye which perturbs the electronic property of the dye. The binding of the analyte is signaled in the form of a measurable change in the absorption, emission or redox properties.

A large number of squaraines have been used as chemosensors<sup>32-35</sup> and chemodosimeters<sup>36,37</sup> for the detection of a variety of analytes including alkali, alkaline, transition metal ions and low molecular weight aminothiols using various “probe responding” mechanisms. For example, the azacrown appended squaraines **18** and **19** are sensitive towards alkali and alkaline earth metal cations.<sup>38,39</sup> The 1, 2-bis (2'-aminophenoxy)ethanetetraacetic acid based squaraine **20** is sensitive to  $\text{Ca}^{2+}$  ions.<sup>40</sup> The 2, 3, 3-trimethyl-3H-indole derived squaraine dye **21** showed three levels of signals based on the concentration of  $\text{Zn}^{2+}$  ions (Chart 1.3).<sup>41</sup>

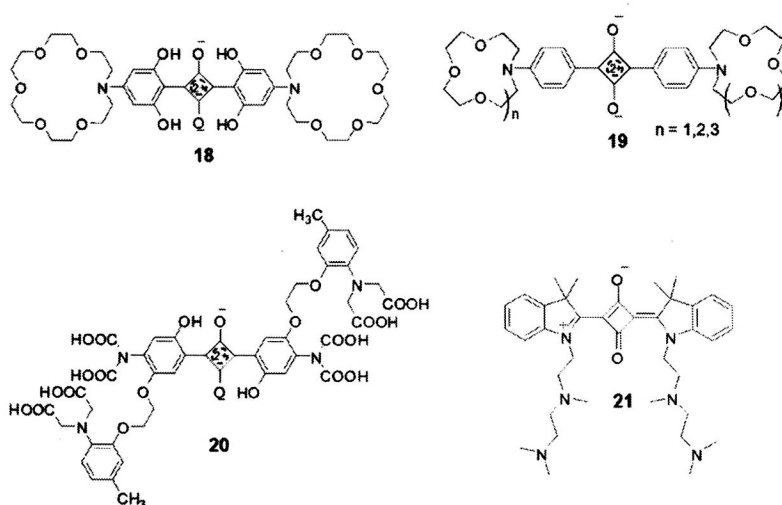


Chart 1.3

Even though squaraines are found suitable for the detection of a variety of cations, the selectivity and sensitivity in most of the cases are not very promising. This limitation has led to further studies on the design of squaraine based molecular probes for better selectivity and sensitivity.

The pyrrole derived polysquaraines having different podand chains are reported to exhibit selectivity towards alkali metal cations when compared to the analogous squaraine dye **23**. For example, the polysquaraine **22** is selective to  $\text{Li}^+$  over  $\text{Na}^+$  and  $\text{K}^+$  (Chart 1.4). Although there is no change in the absorption spectrum of the polymer, considerable enhancement in the fluorescence emission is observed upon  $\text{Li}^+$  binding. However, the model squaraine **23** shows very weak

response to  $\text{Li}^+$  revealing the crucial role of the polysquaraine back bone in the signal amplification process.<sup>42,43</sup>

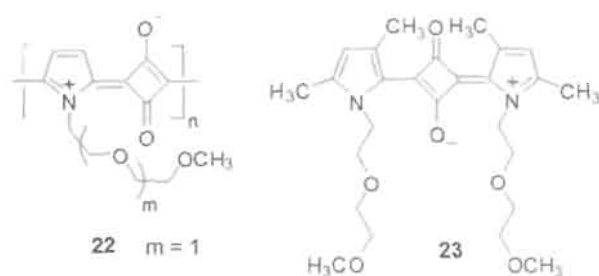
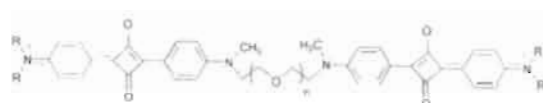


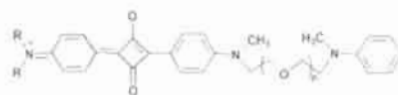
Chart 1.4

Squaraines are known to form “H” (blue shift) and “J” (red shift) type aggregates in appropriate solvents. In majority of the cases, they favor the blue shifted “H” aggregates with strong quenching of the emission. This phenomenon has been reported to the detection of specific cation such as  $\text{Ca}^{2+}$  and  $\text{Mg}^{2+}$ . The idea involves the induced folding of the squaraine dye **24** with  $\text{Ca}^{2+}$  or  $\text{Mg}^{2+}$ .<sup>44,45</sup> Formation of a folded structure or the sandwich dimer results in the dramatic change of the spectral properties of the dye which can be followed visually through colorimetry or monitoring the changes in the emission spectrum of the dye (Figure 1.3).



24 a-f

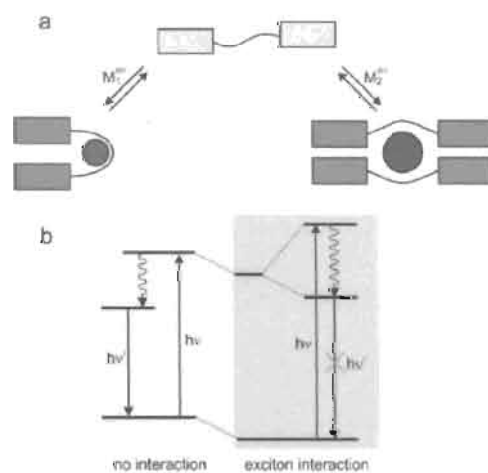
24 a  $n = 1$ ,  $R = C_4H_9$       24 d  $n = 4$ ,  $R = CH_3$   
 24 b  $n = 2$ ,  $R = C_4H_9$       24 e  $n = 5$ ,  $R = CH_3$   
 24 c  $n = 3$ ,  $R = CH_3$       24 f  $n = 6$ ,  $R = CH_3$



25 a-c

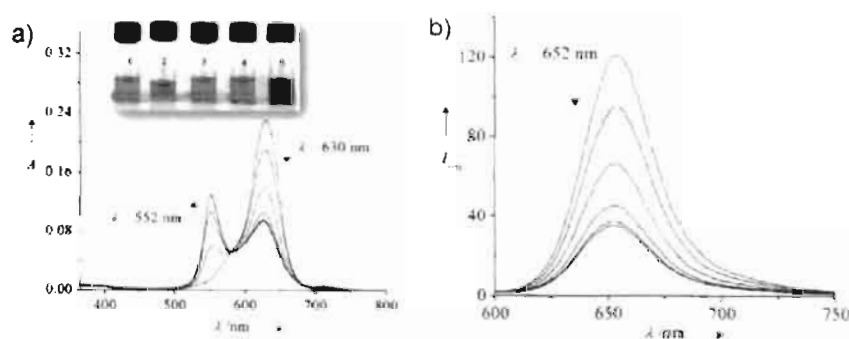
25 a  $n = 1$ ,  $R = C_2H_5$       25 c  $n = 3$ ,  $R = CH_3$   
 25 b  $n = 2$ ,  $R = CH_3$

Chart 1.5



**Figure 1.3.** Different cation binding modes of a bis-squaraine dye connected with a flexible polyether linker which operates based on cation driven exciton interaction (a). The corresponding energy diagrams showing allowed and forbidden transitions (b).

The bichromophores **24a-f** (Chart 1.5) show strong perturbation in the absorption and emission spectra with high selectivity toward alkaline earth metal cations, particularly to  $\text{Mg}^{2+}$  and  $\text{Ca}^{2+}$  ions. However, no optical response was noticed against alkali metal ions. The bichromophore **24 e** with five oxygen atoms in the podand chain shows high selectivity to  $\text{Ca}^{2+}$ . The binding is visible to the naked eye due to the color change from light blue to deep purple blue (Figure 1.4).

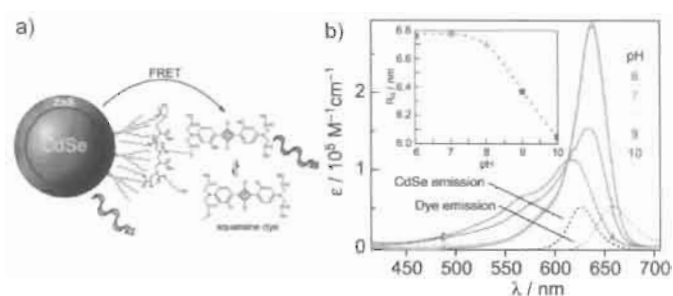


**Figure 1.4.** Change in the a) absorption and b) emission ( $\lambda_{\text{exc}} = 580 \text{ nm}$ ) spectra of **24** in acetonitrile upon addition of  $\text{Ca}^{2+}$  ions. Inset shows visible color change of the bichromophore ( $n = 5$ ) in acetonitrile upon addition of  $\text{Ca}^{2+}$ ; (1) in the absence of metal salts, (2)  $\text{Mg}^{2+}$ , (3)  $\text{Na}^+$ , (4)  $\text{K}^+$  and (5)  $\text{Ca}^{2+}$ .

The change in the optical properties is associated with the exciton interaction between the chromophores due to the cation steered folding of the molecule and not due to a simple reorganization of the electronic structure as a result of the cation binding. This is clear from the fact that, although the monochromophores **25 a-c** (Chart 1.5) binds to cations, no change in the optical properties could be noticed. Even though these dyes show remarkable response towards  $\text{Ca}^{2+}$  and

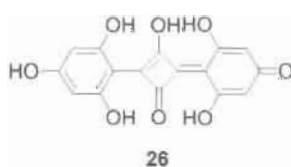
$Mg^{2+}$  in acetonitrile, their practical applications is limited due to the tendency of the dye to aggregate under aqueous conditions even in the absence of cations. Therefore, challenges remain towards the development of squaraine based probes for any analytes which could be useful in aqueous conditions without self-aggregation of the dye units.

A new ratiometric nanocrystal based pH sensor was developed by conjugating a squaraine dye with an equilibrium response to an analyte to the surface of CdSe/ZnS nanocrystal (NC).<sup>46</sup> The sensor was constructed from a colloidal CdSe nanocrystal that is coated with an outer layer of ZnS. Phosphine oxide ligands are encapsulated with an amphiphilic polymer upon which a pH sensitive squaraine dye is conjugated. Upon excitation, the CdSe/ZnS nanocrystal may either fluoresce or transfer energy to the squaraine dye. The sensing action of the NC-squaraine conjugate is imparted by the modulation of the FRET efficiency arising from the overlap of the pH sensitive dye absorption spectrum with pH sensitive quantum dot emission (Figure 1.5). A ratiometric response to pH was observed owing to the modulation of FRET efficiency between the emissive NC and dye conjugated to the nanocrystal surface.



**Figure 1.5.** a) Schematic diagram showing a sensor constructed from colloidal CdSe nanocrystal (NC) which is affixed with a pH sensitive squaraine dye. b) The pH dependent absorption profile of squaraine dye. Shown in gray and black dashed lines are emissions of the dye and NC at pH 6.0. Inset shows changes in the critical distance for FRET with pH.

Squaraines have been reported useful in detecting biorelevant analytes such as bovine serum albumin (BSA) and Heparin, based on fluorescence as well as colorimetric changes. The squaraine dye **26** binds to BSA selectively with high association constant ( $1.4 \pm 0.1 \times 10^6 \text{ M}^{-1}$ ).<sup>47</sup> The site selective binding can be visualized through dual mode recognition of visual color change from pinkish (squaraine dye alone) to bluish in presence of bovine serum albumin (BSA). An 80-fold enhancement in the fluorescence was observed upon binding to BSA (Figure 1.6).



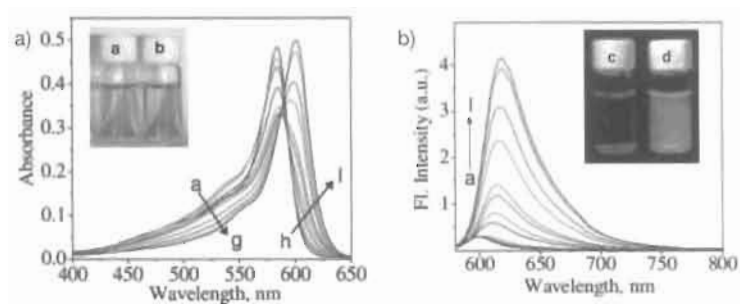


**Figure 1.6.** Changes in the absorbance and fluorescence intensity of **26** ( $3 \mu\text{M}$ ) with the addition of BSA in phosphate buffer. Insets show visual color change and fluorescence change before and after the addition of BSA.

In another report, the squaraine dye **27** has been shown to be a protein indicator, which noncovalently interacts with BSA and provides dramatic color change from orange to deep purple (Figure 1.7).<sup>18</sup>

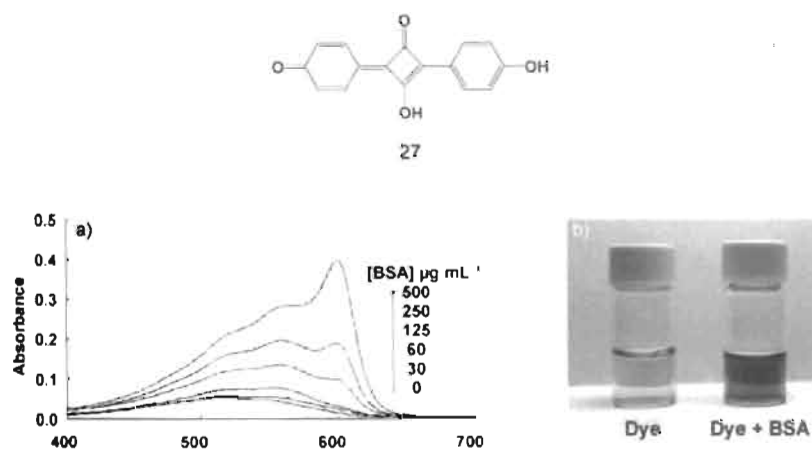
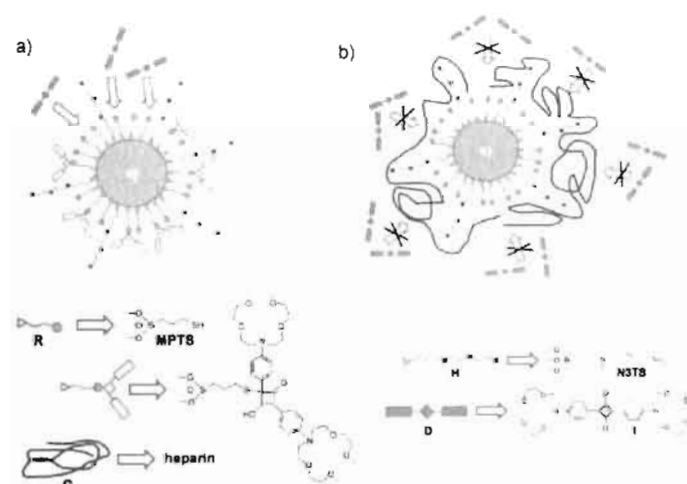


**Figure 1.7.** a) Absorption spectra of **27**, before and after the addition of BSA. b) Photograph of **27** in the absence and presence of BSA.

A selective chromo-fluorogenic sensor for the detection of heparin was developed by using a squaraine dye and functionalized silica nanoparticles.<sup>43</sup> The new chromo-fluorogenic sensing paradigm in this case is shown in Scheme 1.2. It involves the use of silica nanoparticles decorated with two different moieties: thiol groups (R) and polyamines (H). The role of the group R is to react with the squaraine dye (D) through the nucleophilic attack of the thiol group to the electron deficient, central, four member ring of the squaraine scaffold. This is known to result in the bleaching of the blue squaraine solution. Additionally, 'H' is a suitable host for anion coordination.



**Scheme 1.2.** A colorimetric protocol for heparin signaling. a) Bifunctionalised nanoparticles **N1** without the presence of heparin are able to react with squaraine **I**, and b) heparin coordinated with the polyamines on **N1** inhibiting the thiol-squaraine reaction.

Thus, the optical properties of squaraines are excellent for a wide range of applications especially for the design of molecular probes for the selective detection of analytes. This is possible because, the optical properties of squaraines can be tuned to a great extent by structural modification to suit a specific application. Even though various strategies have been adopted for using squaraine dyes in the design of molecular probes for targeting different biorelevant analytes, there is still a huge scope for this class of dyes in the design of new molecular probes.

### **1.5. Concept of Molecular Logic Operations: From Molecular Probes to Logic Gates**

Molecular level information processing is a common feature of numerous biological systems. All of the regulatory processes in living cells, cellular signaling, and of course all of the neurobiological activities need to process information at the molecular level.<sup>50</sup> Every biochemical bifurcate pathway undergoes Boolean logic rules at the molecular level in a sense that every single molecule can follow only one reaction path. Molecular recognition in biological systems, activation of enzymes by small molecules and signal transduction are also processes based on YES-NOT logic schemes.<sup>51,52,53</sup> Although, the collective response of the complex chemical or biochemical system is continuous (or, in other words, highly linear) on a macroscopic level, on a molecular level, every single step is a discrete process and its apparent linearity results from a

combination (or averaging) of uncountable individual discrete processes of Boolean character.<sup>54</sup>

Two philosophically different approaches have been proposed for information processing at the molecular level.<sup>55</sup> The first one attempts to mimic the operational principles of solid state computers which are presently in use, at the nanometer scale with molecular systems. This approach is based on molecular electronics, in which both input and output signals are electronic in nature (electron fluxes). Molecular photonics based on photon fluxes can be of help for this line of research. The second approach, which takes inspiration from information processing in living organisms, is based on chemionics,<sup>56</sup> in which molecules and ions can be used as input/output signals to process information by using a molecular substrate. Chemionics usually operates in solution and can be complemented by photonics since chemical and light input/output signals can be easily coupled. Within each aspect of molecular electronics, photonics or chemionics, information processing takes place at logic gates and data manipulation relies on the binary digital (bit) nature of these input and output signals that are elaborated by means of the Boolean logic.

When considering molecules to perform Boolean operations, the whole spectrum of input and output data encoding channels is significant (Figure 1.8).<sup>57</sup> Classical electronic devices use electric input/electric output communication but molecules can perform operations with a combination of inputs and outputs.

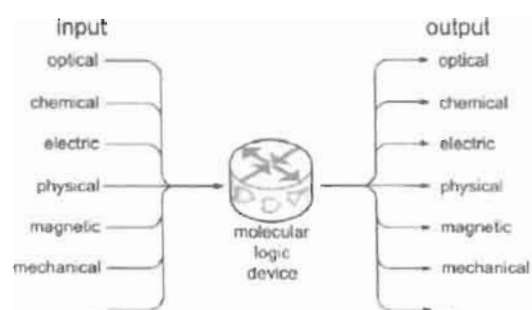


**Figure 1.8.** Input and output channels of molecular logic devices. These devices can be based on classical electronics paradigms (electric input/electric output) or utilize any nonclassical input/output configuration.

Among the various recording media for high density data storage, organic materials have been especially attractive in recent years because of their low cost, simplicity, good stimuli responsive properties, and versatility in molecular design.<sup>58</sup> Therefore, they have been suggested as promising candidates for future application development. In principle, the basic requirements for recording materials are that they should possess at least two distinct stable states via an external stimulus, where each state can represent "0" or "1" of a digital mode, and the states can be clearly distinguished during read-out. In principle, any chemical system that can exist in two quasi-stable states of different chemical or physical properties may be regarded as a molecular switch (or molecular logic gate), provided there are some physical or chemical stimuli that can (reversibly) change the state of the system. The simplest examples are colorimetric pH indicators and compounds that change color upon change in proton concentration.

They function as "YES" or "NOT" logic gates, depending upon the property of the individual indicator and the assignment of input and output channels (e.g., pH values and colors).

There are four possible combinations of input and output values for one-input one-output logic gates (Figure 1.9). The PASS 0 and PASS 1 gates yield outputs "0" and "1" respectively, independently of the input value. The YES gate follows the input value to the output. The gate functions as a simple switch, but in fact is very useful for signal amplification, connecting various devices, and signal transduction. The inverter (NOT gate) performs inversion (complementation) of the input data. It changes one logic level into the opposite: logic 0 (also called the low state, cf. Figure 1.9) is converted into logic 1 (the high state) and vice versa. NOT is one of the principal Boolean operation, and very often, it is concatenated with multiple input gates.

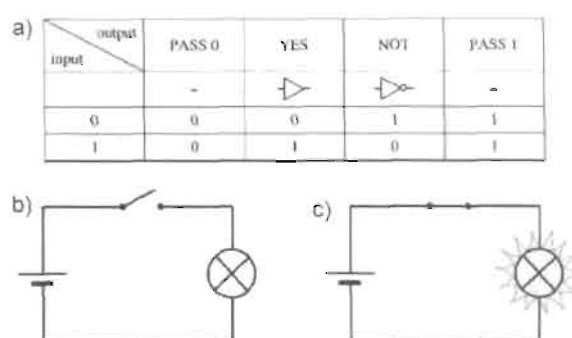


**Figure 1.9.** a) Truth table for single input logic gates. The simplest electric circuits representing the YES (b) and NOT (c) logic gates. Moving the switch (logical 1) turns on the light in the first system (YES gate), but turns it off in the second one (NOT gate).

Apart from these two single input logic gates there are 16 various combinations of input and output signals for two-input logic gates, 8 of which are commonly used in electronics (Table 1): basic OR, AND, and XOR, and gates concatenated with NOT: NOR, NAND, and XNOR. Usually, INHIBIT (INH) and NINH gates are regarded as simple logic gates as well.

Table 1. Truth tables for two input logic gates.

input \ output		OR	AND	XOR	INH	NOR	NAND	XNOR
								
0	0	0	0	0	0	1	1	1
0	1	1	0	1	1	0	1	0
1	0	1	0	1	0	0	1	0
1	1	1	1	0	0	0	0	1

Furthermore, as an ideal recording media, several important performance parameters are required for a memory device which include: 1) chemical stability; 2) film forming properties; 3) storage capacity; 4) transition time (a short transition time between two states is intrinsically indicative of a fast writing); 5) retention ability (the ability to remain in the stored state is necessary for stable and secure recording); and 6) the on-off ratio (a high on-off ratio is crucial for memory devices in order to realize high-resolution and low-error-rate data storage). In

addition, low power consumption, ease of fabrication, and competitive cost are also important for practical application.

### 1.5.1. Chemically Driven Molecular Logic Gates

Chemically driven molecular switches are usually comprised of three main building blocks: receptor moiety, linker (spacer), and the reporter moiety.<sup>59</sup> Receptor moieties are specially designed binding sites for triggering ions or molecules. They should exhibit desirable selectivity and sensitivity toward selected triggers. The linker, in turn, should provide electronic communication between the receptor and reported moieties. There are three main ways of providing sufficient electronic communication: (i) bridge providing overlap of  $\pi$ -systems of both moieties, (ii) short  $\sigma$ -spacer enabling photoinduced electron transfer, or (iii) arrangement of receptor and reporter, using supramolecular interactions to provide perturbation of electronic structure of the reported moiety.<sup>60</sup> The reporter moieties in turn should significantly change their photophysical, electrochemical, magnetic, or chemical properties to yield an easily recognizable signal. The most common are the systems where the interaction between the trigger and the receptor results in the change of photophysical properties: changes in absorption and/or emission characteristics of the reporter moiety. It may also result in changes of redox potentials, translocation of molecular fragment within the supramolecular assembly (which may be also associated with changes in

optical or electrochemical properties as well), chemical reactivity, or magnetic properties.

Even though a large number of reports were published before 1993 based on analyte induced changes in the properties of organic molecules, it was de Silva and coworkers who exploited the use of Boolean operations to define the relations between chemical inputs and readable outputs. In Nature magazine in the year 1993, they have illustrated the use of a simple PET based anthracene fluorophore (**28**) to define a molecular photonic two input AND gate with chemical inputs such as  $H^+$  and  $Na^+$  for the first time (Chart 1.6).<sup>61</sup>

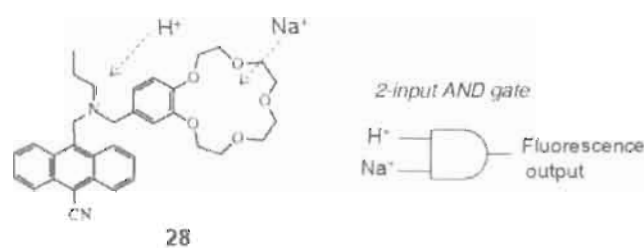


**Chart 1.6.** A molecular photonic AND gate **28** and the corresponding logic diagram.

After this report, a large number of organic fluorophores have been reported which can perform various Boolean operations independently with respect to chemical inputs.<sup>62-65</sup> Basic Boolean operations AND, OR, XOR, INH, NOR and NAND were demonstrated in molecules with different inputs including chemical, electrochemical, photochemical and enzyme action etc. A few

representative examples of molecules which can perform various Boolean operations with respect to chemical inputs are discussed below.

The molecular logic gate **29** responds to various inputs based on PET mechanism. The tricarboxylate receptor part can successfully bind magnesium and calcium ions.<sup>66</sup> This nonselectivity constitutes the basis of OR operation. When metal ions bind to the respective sites, the electronic structure of the molecule rearrange and fluorescence of the fluorophore is switched on. Similarly, in the case of the monomolecular europium (III) complex **30**, a strong fluorescence was observed within the pH range of 4-7. Deprotonation of the ligand and/or the amide linker results in a change in photochemical properties of the complex. Instead of efficient electronic energy transfer from phenanthroline antenna, an electron transfer occurs and a nonfluorescent Eu(II) complex is formed (Chart 1.7).<sup>67</sup>

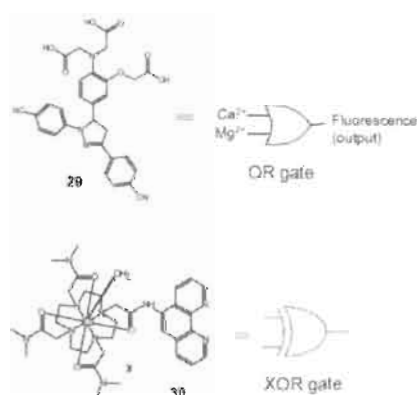


**Chart 1.7.** Molecular photonic OR gate **29** and XOR gate **30** with corresponding logic diagrams.

Perez-Inestrosa et al. have reported a modified 1-benzylisoquinoline *N*-oxide (**31**) that could perform an INHIBIT logic operation with respect to chemical inputs such as  $H^+$  and  $K^+$ .<sup>68</sup> Addition of TFA or alkali metal ions generates the emission at 550 nm in INHIBIT relation.

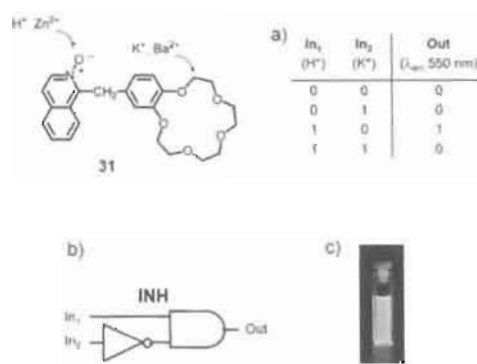


**Figure 1.10.** a) Truth tables for two input INHIBIT logic gate using **31**. b) Logic representation of INHIBIT gate. c) Photograph of emission at 550 nm from **31**.

Performance of arithmetic operation (addition/subtraction) requires the connection of several basic logic gates.<sup>63,64</sup> Binary addition of digits can be achieved by a combination of XOR and AND gates, usually called as “half-adders”. On the other hand, a combination of XOR and INHIBIT gates can perform subtraction, known as “half-subtractors”. There are numerous reports for the implementation of binary half-adders and half-subtractors using molecules. Two representative examples are included in the following discussion.

A molecular binary half-adder based on a photochromic ligand **32** was reported by Zhu et al. On irradiation with UV light (365 nm), the spiropyran

moiety undergoes ring opening, yielding the colored merocyanine form ( $\lambda_{\text{max}} = 590$  nm). It can further react with  $\text{Fe}^{3+}$  ions to form a stable complex characterized by a strong absorption at 430 nm. The ligand **32** reacts also with  $\text{Fe}^{3+}$  in closed spiropyran form which yields a colored cation radical, characterized by a strong absorption at 500 nm. Absorbance at 430 nm, thus corresponds to the AND operation with UV light and  $\text{Fe}^{3+}$  as inputs, while the absorbance at 550 nm (halfway between merocyanine and spiropyran cation radical) corresponds to the XOR function of the same input data.

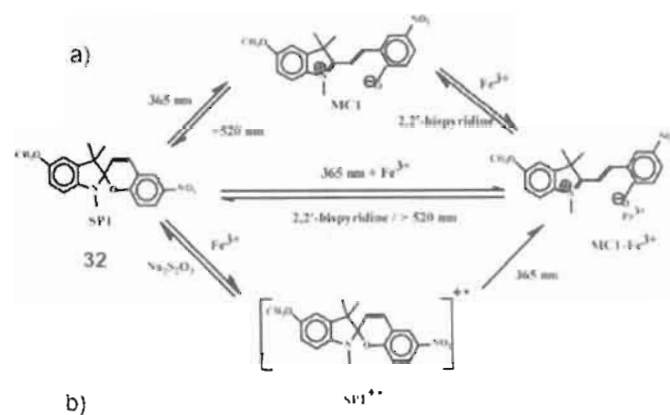


**Figure 1.11.** a) Interconversion network of four states of **32** (SP: Spiropyran, MC: Merocyanin). b) Truth table for half-adder derived from **32**.

Akkaya et al., have reported the switching of emission from a BODIPY based system to define a molecular half-subtractor based on the combined effect of emission modulation by PCT and PET (Figure 1.12). A half-subtractor is a combination of XOR and INHIBIT operations. The molecule **33** under deprotonation of the phenolic -OH group display a quenching in the emission maximum at 660 nm. The quenching in emission is due to a PET process from the phenolate unit of **33**. Addition of TFA (trifluoroacetic acid) generates a hypsochromic shift in both absorbance (~40 nm) and emission bands (~100 nm) of **33**. This shift is due to the modulation in ICT emission due to the protonation of the dialkyl amino moiety of **33**. The three emission responses generated from **33** allow defining a half-subtractor with respect to the chemical inputs such as acid and base.

A survey of the recent literature reveals that a variety of fluorophores have been synthesized and used as either probes for analyte detection or as logic gates. Analyte detection and logic operation are therefore the two sides of the same coin. Depending upon the requirements and nature of the fluorophores, one can use them as chemosensors or molecular switches for logic operations. This area continues to be interesting for chemists and as a result large number of new molecules are being synthesized and studied.

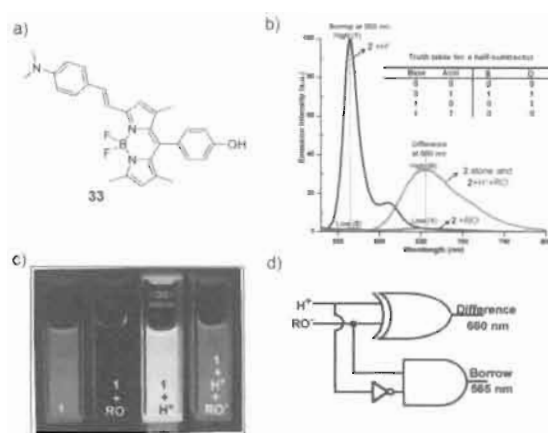


**Figure 1.12.** a) Structure of the BODIPY derivative **33**. b) Emission spectra of **33** in THF in presence of various chemical inputs. Inset shows the truth table for a half-subtractor; outputs are borrow (B) and difference (D). c) Solution of **33** ( $5 \times 10^{-6}$  M) in THF illuminated with a UV lamp at 360 nm. d) Logic diagram of a half-subtractor. The difference and borrow outputs were collected at two different wavelengths at 660 nm and 565 nm.

## 1.6. Objectives of the Present Investigation

Inspired by the recent progress in the design and study of functional organic molecules, we have planned to explore the possibility of designing a few fluorophores for the development of new molecular probes and logic gates. The fluorophores are designed in such a way to have the donor- $\pi$ -acceptor- $\pi$ -donor (D- $\pi$ -A- $\pi$ -D) type structure. Our first aim was to design a  $\pi$ -extended squaraine dye of a fluorophore with strong near-IR absorption for the purpose of detecting biorelevant thiols. We have chosen a 1,4 divinyl (aryl) bridged bispyrrole for the synthesis of a  $\pi$ -extended squaraine dye. Another objective of the present investigation was to develop molecular probes for  $Zn^{2+}$  ions. By incorporating a

bipyridine receptor in the bispyrrole structure. we anticipated the modulation of fluorescence upon binding with a suitable cation. Finally, we have planned the design of a molecular logic gate using a  $\pi$ -conjugated donor-acceptor-donor type molecule containing three receptor sites suitable for different external chemical inputs. Careful modulation of the photophysical properties of these molecules was expected to generate different outputs to address molecular logic operations. The present thesis is a systematic investigation on the synthesis and study of a few of D- $\pi$ -A- $\pi$ -D based molecules as mentioned above and their use as molecular probes and logic gates.

### 1.7. References

1. P. D. Beer in *Chemical Sensors*, T. E. Edmonds; Chapman and Hall, New York, **1988**.
2. J. R. Lakowicz (ed.), *Probe Design and Chemical Sensing. Topics in Fluorescence Spectroscopy*, vol. 4, Plenum, New York, **1994**.
3. R. A. Bissel, A. P. de Silva, H. Q. N. Gunaratne, P. L. M. Lynch, G. E. M. Maguire, K. R. A. S. Sandanayake, *Chem. Soc. Rev.* **1992**, 187.
4. A. P. de Silva, H. Q. N. Gunaratne, T. Gunnlaugsson, A. J. M. Huxley, C. P. McCoy, J. T. Rademacher, T. E. Rice, *Chem. Rev.* **1997**, 97, 1515.
5. B. Valeur, I. Leray, *Coord. Chem. Rev.* **2000**, 205, 3-40.
6. J. -P. Desvergne, A. W. Czarnik, "Chemosensors for Ion and Molecular Recognition" *NATO ASI Ser.* **1997**, 492, 189-194.

7. J. J. R. Frausto da Silva, R. J. P. Williams, *The Biological Chemistry of the Elements*; Oxford University Press: Oxford, **1991**.
8. E. L. Que, D. W. Domaile, C. J. Chang, *Chem. Rev.* **2008**, *108*, 1517.
9. C. J. Frederickson, *Int. Rev. Neurobiol.* **1989**, *31*, 145.
10. J. M. Berg, Y. Shi, *Science* **1996**, *271*, 1081.
11. P. Jiang, Z. Guo, *Coord. Chem. Rev.* **2004**, *248*, 205.
12. N. C. Lim, H. C. Freake, C. Brückner, *Chem. Eur. J.* **2005**, *11*, 38.
13. M. P. Cuajungco, G. J. Lees, *Neurobiol. Dis.* **1997**, *4*, 137.
14. M. de Onis, E. A. Frongillo, M. Blössner, *Bull. W. H. O.* **2000**, *78*, 1222.
15. S. J. Lippard, J. M. Berg, *Principles of Bioinorganic Chemistry* 139–175 (University Science Books, Mill Valley, California, USA, **1994**).
16. S. Y. Assaf, S. -H. Chung, *Nature* **1984**, *308*, 734.
17. E. Kimura, T. Koike, *Chem. Soc. Rev.* **1998**, *27*, 179.
18. D. W. Domaile, E. L. Que, C. J. Chang, *Nat. Chem. Biol.* **2008**, *4*, 168.
19. A. W. Czarnik, *Acc. Chem. Res.* **1994**, *27*, 302.
20. A. P. de Silva, D. B. Fox, H. J. M. Huxley, T. S. Moody, *Coord. Chem. Rev.* **2000**, *205*, 41.
21. S. A. de Silva, A. Zavaleta, D. E. Baron, O. Allam, E. V. Isidor, N. Kashimura, J. M. Percarpio, *Tetrahedron Lett.* **1997**, *38*, 2237.
22. R. P. Haugland, *Handbook of Fluorescent Probes and Research Products*, ninth ed. Molecular Probes Inc., **2002**.

23. J. R. Lakowicz, *Principles of Fluorescence Spectroscopy*, 2nd ed., Kluwer Academic/Plenum, New York, **1999**.
24. K. R. Gee, Z. L. Zhou, D. Ton-That, S. L. Sensi, J. H. Weiss, *Cell Calcium* **2002**, *31*, 245.
25. S. Maruyama, K. Kikuchi, T. Hirano, Y. Urano, T. Nagano, *J. Am. Chem. Soc.* **2002**, *124*, 10650.
26. M. M. Henary, C. J. Fahmi, *J. Phys. Chem. A* **2002**, *106*, 5210.
27. C. C. Woodrooffe, S. J. Lippard, *J. Am. Chem. Soc.* **2003**, *125*, 11458.
28. M. Taki, J. L. Wolford, T. V. O'Halloran, *J. Am. Chem. Soc.* **2004**, *126*, 712.
29. C. J. Chang, J. Jaworski, E. M. Nolan, M. Sheng, S. J. Lippard, *Proc. Natl. Acad. Sci. USA* **2004**, *101*, 1129.
30. K.-Y. Law, *Chem. Rev.* **1993**, *93*, 449-486.
31. A. H. Schmidt, *Synthesis* **1980**, 961.
32. C. R. Chenthamarakshan, A. Ajayaghosh, *Tetrahedron Lett.* **1998**, *39*, 1795.
33. C. R. Chenthamarakshan, J. Eldo, A. Ajayaghosh, *Macromolecules* **1999**, *32*, 5846.
34. M. C. Basheer, S. Alex, K. G. Thomas, C. H. Suresh, S. Das, *Tetrahedron* **2006**, *62*, 605.
35. A. Ajayaghosh, *Acc. Chem. Res.* **2005**, *38*, 449.
36. J. V. Ros-Lis, R. Martínez-Mañez, J. Soto, *Chem. Commun.* **2002**, 2248.
37. J. V. Ros-Lis, B. Garcý'a, D. Jimenez, R. Martínez-Mañez, F. Sancenón, J.

- Soto, F. Gonzalvo, M. C. Valdecabres, *J. Am. Chem. Soc.* **2004**, *126*, 4064.
38. U. Oguz, E. U. Akkaya, *Tetrahedron Lett.* **1997**, *38*, 4509.
39. S. Das, K. G. Thomas, K. J. Thomas, P. V. Kamat, M. V. George, *J. Phys. Chem.* **1994**, *98*, 9291.
40. E. U. Akkaya, S. Turkyilmaz, *Tetrahedron Lett.* **1997**, *38*, 4513.
41. G. Dilek, E. U. Akkaya, *Tetrahedron Lett.* **2000**, *41*, 3721.
42. C. R. Chenthamarakshan, A. Ajayaghosh, *Tetrahedron Lett.* **1998**, *39*, 1795.
43. C. R. Chenthamarakshan, J. Eldo, A. Ajayaghosh, *Macromolecules* **1999**, *32*, 5846.
44. A. Ajayaghosh, E. Arunkumar, J. Daub, *Angew. Chem., Int. Ed.* **2002**, *41*, 1766.
45. E. Arunkumar, P. Chithra, A. Ajayaghosh, *J. Am. Chem. Soc.* **2004**, *126*, 6590.
46. P. T. Snee, R. C. Somers, G. Nair, J. P. Zimmer, M. G. Bawandi, D. G. Nocera, *J. Am. Chem. Soc.* **2006**, *128*, 13320.
47. V. S. Jisha, K. T. Arun, M. Hariharan, D. Ramaiah, *J. Am. Chem. Soc.* **2006**, *128*, 6024.
48. Y. Suzuki, K. Yokoyama, *Angew. Chem. Int. Ed.* **2007**, *46*, 4097.
49. E. Climent, P. Calero, D. Marcos, R. Martínez-Mañez, F. Sancenón, J. Soto, *Chem. Eur. J.* **2009**, *15*, 1816.
50. *Principles of Neural Science*, 3rd ed. (Eds.: E. R. Kandel, J. H. Schwartz, T.

- M. Jessel), Elsevier, New York, 1991.
51. D. Bray, *Nature* **1995**, 376, 307.
  52. J. Stock, S. Da Re, *Curr. Biol.* **2000**, 10, R420.
  53. M. -A. Gilles-Gonzalez, G. Gonzalez, *J. Inorg. Biochem.* **2005**, 99,1.
  54. A. P. de Silva, N. D. McClenaghan, *Chem. Eur. J.* **2004**, 10, 574.
  55. G. Jiang, Y. Song, X. Guo, D. Zhang, D. Zhu, *Adv. Mater.* **2008**, 20, 2888.
  56. R. Ballardini, P. Ceroni, A. Credi, M. T. Gandolfi, M. Maestri, M. Semararo, M. Venturi, V. Balzani, *Adv. Funct. Mater.* **2007**, 17, 740.
  57. G. Milburn, *The Feynman Processor. An Introduction to Quantum Computation*; Perseus Books: Boulder, CO, **1998**.
  58. A. P. deSilva, S. Uchiyama, *Nat. Nanotech.* **2007**, 2, 399.
  59. V. Balzani, A. Credi, M. Venturi, *Molecular Devices and Machines*, Wiley-VCH, Weinheim, **2003**.
  60. A. P. de Silva, G. D. McClean, T. S. Moody, *Encyclopedia of Supramolecular Chemistry* Mirel Dekker Inc. New York, **2004**.
  61. A. P. de Silva, H. Q. N. Gunaratne, C. P. McCoy, *Nature*, **1993**, 364, 42.
  62. A. P. de Silva, S. Uchiyama, T. P. Vance, B. Wannalorse, *Coord. Chem. Rev.* **2007**, 251, 1623.
  63. A. Credi, *Angew. Chem. Int. Ed.* **2007**, 46, 5472.
  64. U. Pischel, *Angew. Chem. Int. Ed.* **2007**, 46, 4026.
  65. F. M. Raymo, *Adv. Mater.* **2002**, 14, 401.

66. A. P. de Silva, S. A. de Silva, A. S. Dissanayake, K. R. A. S. Sandanayake, *J. Chem. Soc., Chem. Commun.* **1989**, 1054.
67. T. Gunnlaugsson, J. P. Leonard, K. Sénéchal, A. J. Harte, *J. Am. Chem. Soc.* **2003**, *125*, 12062.
68. J. -M. Montenegro, E. Perez-Inestrosa, D. Collado, Y. Vida, R. Suau, *Org. Lett.* **2004**, *6*, 2353.
69. X. Guo, D. Zhang, G. Zhang, D. Zhu, *J. Phys. Chem. B* **2004**, *108*, 11942.
70. A. Coskun, E. Deniz, E. U. Akkaya, *Org. Lett.* **2005**, *7*, 5187.

---

### A Near Infrared (NIR) Squaraine Dye for the Detection of Aminothiols Content in Blood Plasma

---

#### 2.1. Abstract

*Squaraine dyes have been extensively investigated as chemosensors and chemodosimeters for various analytes. In the present study, we illustrate a new strategy for the detection of thiols and thiol containing amino acids in human blood plasma using a NIR absorbing squaraine dye, Sq1b. The detection is based on the latent activation of fluorescence of the probe by thiol induced breaking of conjugation of the squaraine backbone in contrast to the usually used color bleaching or fluorescence quenching. The probe, Sq1b selectively responds to thiols and aminothiols which allow their ratiometric detection due to the generation of new, noninterfering absorption and emission bands. Since the detection can be followed through absorption and emission changes due to the analyte specific generation of new chromophores, other impurities do not interfere with sensitivity. Application of the probe is illustrated with the quantitative detection of the total aminothiol content in human blood plasma which has tremendous biological and clinical relevance.*

## **2.2. Introduction**

Design of molecular probes (chemosensors/chemodosimeters) is a priority research topic due to wide ranging fundamental and applied interests in the broad area of chemistry and biology.<sup>1-6</sup> For one time detection of an analyte, chemodosimeters are used which show irreversible fluorescence quenching or color bleaching.<sup>7-10</sup> However, detection based on fluorescence quenching or color bleaching are not the best way of monitoring the response of an analyte due to many reasons. For example, fluorescence in some cases is strongly intercepted by other competing analytes or even by minor impurities. Similarly, bleaching of color can also be due to chemical changes induced by impurities apart from the target molecules. These potential limitations pose serious threats to the sensitivity and selectivity of a given probe. Therefore, molecular probes that generates an intensely absorbing or emitting species upon interaction with an analyte that allow ratiometric probing and imaging at wavelengths different from that of the original probe is of considerable significance. Such probes are particularly useful for the detection of biologically relevant samples, for example blood plasma.

Cysteine and homocysteine (Hcy) are the thiol-containing amino acids present in human blood plasma (HBP).<sup>11</sup> Epidemiological studies have shown that an excess of Hcy in blood plasma can create a higher risk of coronary heart disease, stroke and peripheral vascular diseases.<sup>12-16</sup> Other evidence suggest that Hcy may have an effect on atherosclerosis by damaging the inner lining of arteries

and promoting blood clots.<sup>17,18</sup> The atherogenic property of tobacco smoking is connected with its influence on Hcy and thereby the total aminothiols concentration in HBP.<sup>19-21</sup> Apart from this, glutathione which is the most abundant intracellular nonprotein thiol (1-10 mM), has a pivotal role in maintaining the reducing environment in cells. Glutathione also acts as a redox regulator because cellular thiols exist between sulfhydryl and disulfide forms.<sup>22-25</sup> Intracellular thiol levels change dramatically in response to oxidative stress.<sup>26,27</sup> Among the reported methods for detecting thiols, the use of fluorescent probes had its apparent advantages over other methods in sensitivity and, most importantly, in imaging thiols *in vivo*, even in single living cells. Although high-performance liquid chromatography (HPLC) combined with Ellman's reagent (DTNB) is widely used for detecting thiols in a chemical system,<sup>28-30</sup> the method is inconvenient to operate and unsuitable for intracellular thiol detection. Therefore, detection of thiol containing amino acids in biological fluids as well as cellular environments is important. In this context, the development of new, simple and efficient methods for the determination of the thiol containing amino acids in physiological conditions has considerable significance.

Huang and coworkers have reported a new strategy for the detection of cysteine and homocysteine which is based on colorimetric as well as fluorescence changes.<sup>31</sup> Addition of thiol containing molecules to the probe **1** results in a thiol adduct **2** with a characteristic green to red color change followed by the

enhancement in the emission at 600 nm (Figure 2.1). The probe 1 was further utilized to image intracellular free thiols using confocal and twophoton microscopic imaging techniques.

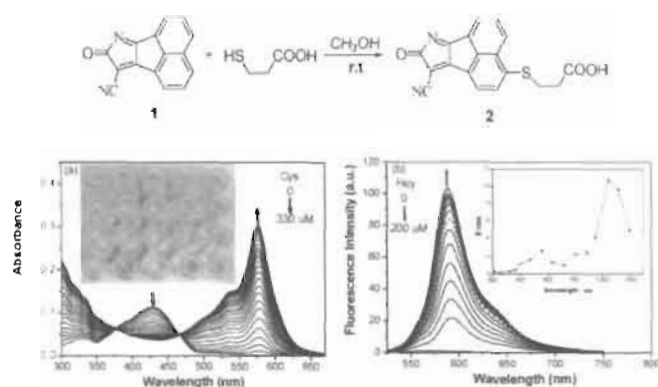


**Figure 2.1.** a) Absorption spectral change of 1 (10 μM) upon addition of cysteine (0-330 μM). Inset shows photograph showing the color change in the absence and presence of aminoacids and peptides. b) Fluorescence spectral changes of 1 upon addition of Hcy (0-200 μM). Inset shows two-photon absorption spectra of 1 upon addition of 40 equivalents of Hcy

BODIPY based fluorescent probe 3 is reported to be useful for the detection of thiol containing aminoacids.<sup>7</sup> The fluorescence of the probe is strongly quenched by photoinduced electron transfer (PET) from BODIPY to the maleimide moiety. After reaction with thiols, the fluorescence of BODIPY is restored with a 350 fold enhancement in the emission intensity (Figure 2.2).

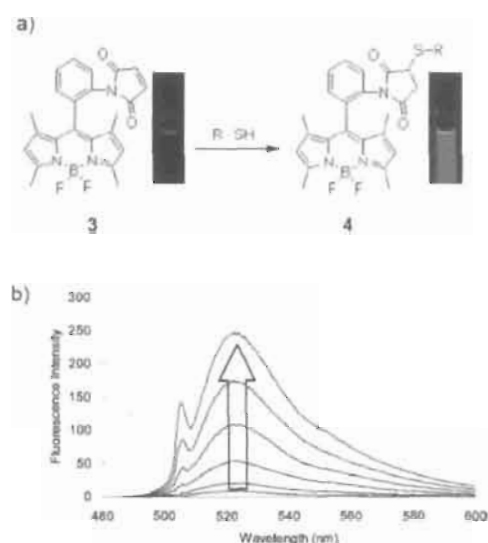


**Figure 2.2.** a) Reaction scheme showing thiol detection. b) Enhancement in the emission intensity of **3** with increasing amounts of cysteine.

In a recent report, Xi et al. have described the use of a coumarin derivative **5** for the detection of thiol containing aminoacids.<sup>33</sup> They have demonstrated the use of this probe as a high through put fluorescent assay for glutathione reductase. The quenching of the emission of **5** due to PET was prevented by the thiol addition to the acceptor moiety. The enhanced emission from the coumarin moiety corresponds to the concentration of the thiol containing amino acids in the sample. The methodology was further utilized for investigating the catalytic role of glutathione reductase enzyme during NADPH reduction of glutathione homodimer to glutathione.

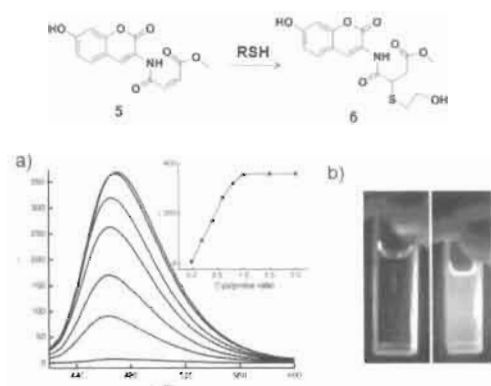


**Figure 2.3.** Reaction scheme showing thiol detection by PET a) Fluorescence spectra of **5** (1.0  $\mu\text{M}$ ) in tris-HCl (pH 7.4, 50 mM) buffer in the presence of different concentrations of GSH (0.2, 0.4, 0.6, 0.8, 1.0, 1.5, and 2.0  $\mu\text{M}$ ). Inset : fluorescence intensity at 465 nm as a function of GSH concentration. b) Fluorescence photograph of **5** (10  $\mu\text{M}$ ) in the absence (left) and presence (right) of  $\beta$ -mercaptoethanol (10  $\mu\text{M}$ ) in tris-HCl buffer under irradiation of a 365 nm UV lamp.

Ros-Lis *et al.* have reported the use of *N,N*-Dialkylaniline derived squaraine dyes **7** and **8** as dosimeters for the detection of  $\text{CN}^-$  ions.<sup>54</sup> The same squaraines have been found useful as fluoro- and chromogenic dosimeters for the detection of thiol containing compounds, particularly, biorelevant thiols such as cysteine.<sup>55</sup> In this strategy, squaraines were used as molecular probes by utilizing the susceptibility of the electron deficient central cyclobutene ring towards nucleophilic attack. The electron deficient central cyclobutene ring of squaraine dyes is vulnerable for nucleophilic attack which will break the conjugation of the dye, resulting in drastic changes in the optical properties of the dye (Figure 2.4).

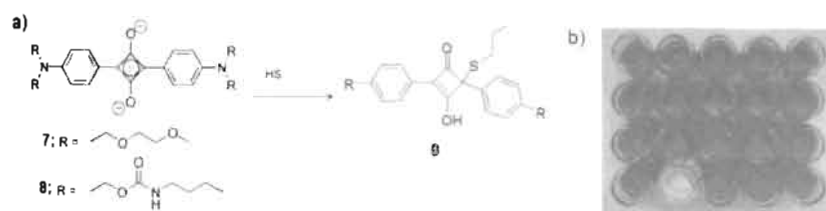


**Figure 2.4.** a) Scheme showing the reaction of thiol to squaraine dye. b) Photograph showing the color change in acetonitrile/water, 20:80 v/v, at pH 6 (MES  $0.01 \text{ mol dm}^{-3}$ ) of the squaraine 7 ( $[7] 1.21 \times 10^{-5} \text{ mol dm}^{-3}$ ) in presence of 10 equivalents of certain amino acids. From left to right and top to bottom: no amino acid, phenylalanine, threonine, arginine, histidine, asparagine, leucine, alanine, proline, valine, glycine, lysine, glutamine, methionine, isoleucine, serine, cysteine, tryptophan, glutamic acid, and aspartic acid.

In the above case, the presence of thiol is detected either by bleaching of the color or decrease in the fluorescence of the dye. However, since the absorption and emission properties of squaraine dyes are strongly influenced by acidic and basic impurities, or by any redox active species, it is desirable to have a probe that is stable and produces a strongly absorbing or emitting species in the visible/NIR region upon interaction with a specific analyte, rather than the usually used color bleaching or fluorescence quenching strategies.

In the present study, we have investigated the use of  $\pi$ -extended squaraine dyes that exhibit remarkable absorption and emission changes in the presence of aliphatic thiols and demonstrate its applications in the detection of low molecular weight amino thiols such as cysteine and homocysteine in human blood plasma (HBP).

## **2.3. Results and Discussion**

### **2.3.1. The Design Strategy**

Since the photophysical properties of most squaraine derivatives are strongly influenced by acidic and basic impurities, polarity and the pH of the medium, specific sensing of an analyte using the fluorescence quenching of conventional squaraine dyes is often difficult. Due to this reason, it is desirable to design new dyes which are stable and generate new emitting species upon specific interaction of an analyte. We have chosen fluorescent bispyrroles as the monomers for designing  $\pi$ -extended squaraine dyes, which strongly absorb in the near-IR region with weak emission. Upon a specific analyte attack to the squaraine, the probe becomes strongly fluorescent. We have exploited the vulnerability of the squaraine cyclobutene ring for thiol attack thereby breaking the conjugation of the dye. Thus, the present strategy involves the chemical activation of a weakly fluorescent NIR probe through a conjugation break associated with the nucleophilic attack by a thiol to generate a strongly emitting fluorophore. For this purpose, we have prepared two bispyrrole appended squaraine dyes with different side chains **Sq1a** and **Sq1b**. The squaraine dye **Sq1b** with glycol side chain was prepared in order to make it more compatible with the aqueous environments.

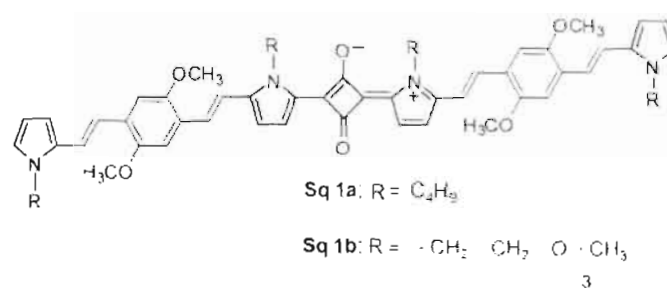
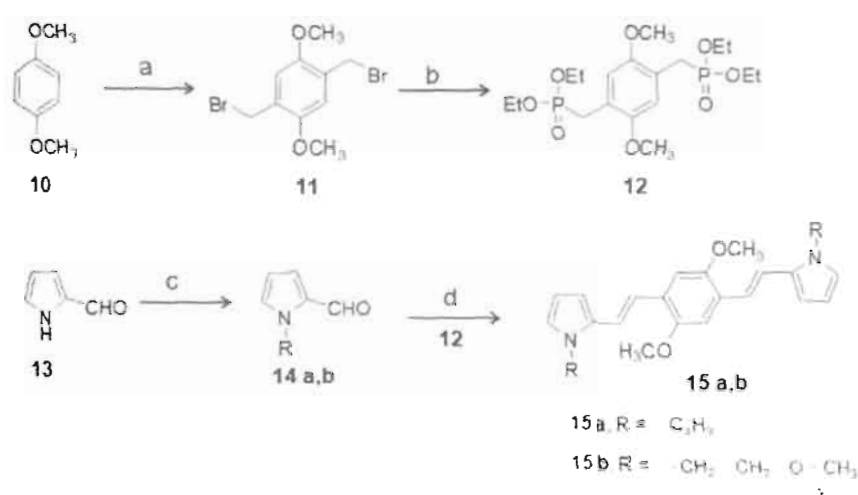


Chart 2.1. Structure of the squaraine derivatives Sq1a and Sq1b.

### 2.3.2. Synthesis of the Squaraine based Probes Sq1a and Sq1b

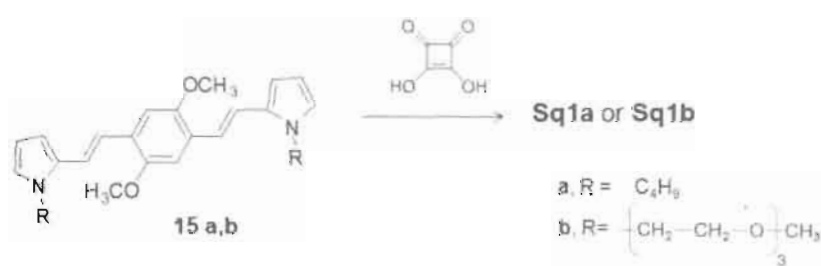
The squaraine based probes **Sq1a** and **Sq1b** were synthesized from the corresponding bispyrroles **15a** and **15b** which were prepared according to known procedures. The 1, 4 dimethoxybenzene (**10**) on bromomethylation using paraformaldehyde and HBr in acetic acid provided the bisbromomethyl derivative (**11**) in 90% yield. The bisbromomethyl derivative on reaction with triethyl phosphate gave the corresponding bisphosphonate (**12**) in 86% yield. The Wittig-Homer reaction of the pyrrole carbaldehydes **14a,b** with the bisphosphonate **12** using NaH in THF gave the bispyrroles **15a,b** in 58 and 63% yields, respectively (Scheme 2.1).



Scheme 2.1. Reagents and conditions: a) Paraformaldehyde, 33% HBr in acetic acid, glacial acetic acid, sonication 4 h (90%); b) P(OEt)<sub>3</sub>, 100°C, 12 h (90-95%); c) 1-bromo-2-(2-(2-methoxyethoxy)ethoxy)ethane, potassium *t*-butoxide, THF, 27°C, 21 h (78%); d) NaH, THF, 70°C, 12 h (45%).

Reaction of the required bispyrroles **15a** or **15b** (4 mmol) with squaric acid (2 mmol) in 1:3 butanol/benzene mixture (80 mL) under azeotropic conditions gave the squaraine dyes **Sq1a** and **Sq1b**, respectively (Scheme 2.2). The progress of the reaction was monitored through UV-visible absorption spectra at intervals of the reaction. The reaction was stopped when higher homologues started appearing. Repeated precipitation using petroleum ether gave the dye **Sq1a** and **Sq1b** in 26-32 % yields. The compounds were characterized by <sup>1</sup>H NMR, <sup>13</sup>C NMR, IR and HRMS (FAB). Significant amount of polymeric dyes were also formed which were removed by precipitation and column chromatography. **Sq1a**

and **Sq1b** showed strong peak between 1625-1620  $\text{cm}^{-1}$  region, which corresponds to the C-O stretching frequency of the cyclobutenediylum-1-3-diolate moiety.  $^1\text{H}$  NMR spectra of the dyes showed strong *trans* coupling for the vinylic linkages, which was in agreement with the structure assigned to the dye. The N-CH<sub>2</sub> protons were observed as triplets around  $\delta$  4.8 and 4.1 ppm indicating strong resonance stabilization in the dyes. The -OCH<sub>3</sub> protons of the phenyl ring were observed at  $\delta$  3.9 ppm as a multiplet along with N-CH<sub>2</sub> protons. The -OCH<sub>3</sub> protons of the glycol side chains appeared as a singlet at  $\delta$  3.3 ppm.



**Scheme 2.2.** Synthesis of **Sq1a** and **Sq1b**. Reagents and conditions: i) Squamic acid (0.5 equiv.) (1:3 butanol/benzene azeotropic mixture), 80°C, 1 h.

### 2.3.3 Absorption and Emission Spectra of the Bispyrroles **15a** and **15b**

The absorption and emission spectra of **15a** and **15b** were recorded in acetonitrile. These bispyrroles showed absorption maximum at 414 nm with a broad emission band at 482 nm. The fluorescence quantum yields ( $\Phi_f$ ) of



bispyrroles in acetonitrile were determined using quinine sulphate as standard. **15a** and **15b** shows high quantum yield of 0.43 and 0.4, respectively. The detailed photophysical properties of **Sq1a** and **Sq1b** are discussed in the following section.

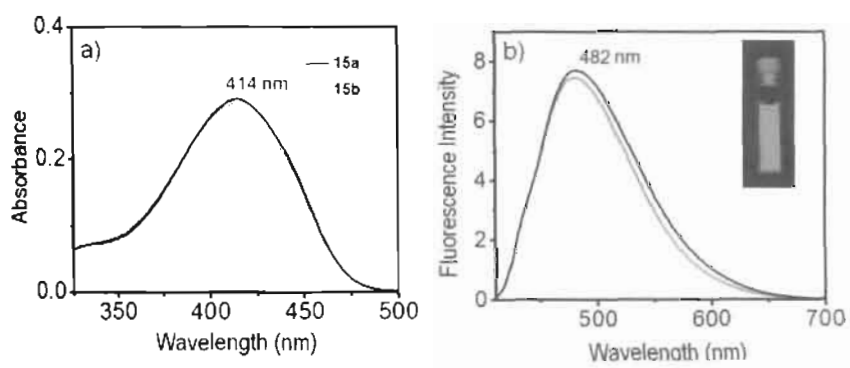


**Figure 2.5.** a) Absorption and b) emission ( $\lambda_{ex} = 400$  nm) spectra of **15a** and **15b** in acetonitrile ( $6 \times 10^{-6}$  M). Inset photograph shows the fluorescence of **15b** in acetonitrile (under 365 nm UV light).

### 2.3.4. Absorption and Emission Studies of **Sq1a** and **Sq1b**

The dyes **Sq1a** and **Sq1b** showed intense absorption band around 750 nm ( $\epsilon \approx 4 \times 10^5$ ) and a shoulder at 670 nm in acetonitrile ( $6 \times 10^{-6}$  M) (Figure 2.6). This shoulder band is common to many squaraine dyes and could be attributed to the excitonic interaction. The emission spectrum of **Sq1a** showed a weak band in the range of 750-850 nm with maximum centered at 800 nm. Detailed photophysical properties of **Sq1b** were investigated in a 1:1 solvent mixture of acetonitrile and water (CHES, buffer, 0.01M, pH 9.6).

CO 543-291 PG

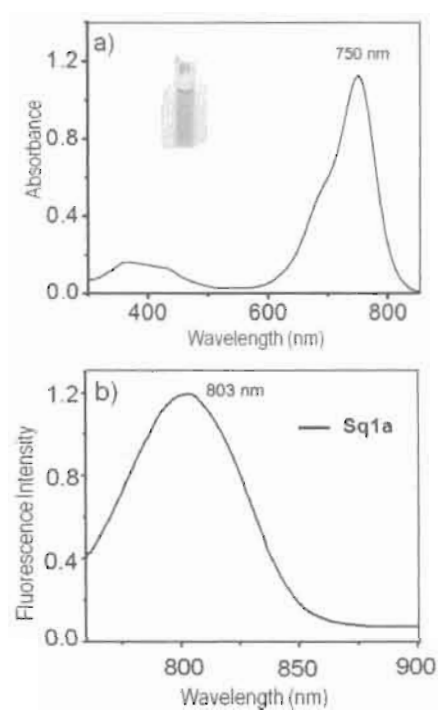


**Figure 2.6.** a) Absorption and b) emission ( $\lambda_{ex} = 730$  nm) spectra of **Sq1a** in acetonitrile ( $6 \times 10^{-6}$  M). Inset photograph shows the color of **Sq1a** in acetonitrile.

Absorption and emission spectra of **Sq1b** ( $6 \times 10^{-6}$  M) in acetonitrile/water (1:1 CHES buffer, 0.01M, pH 9.6) is shown in Figure 2.7. The dye exhibits a strong absorption maximum around 750 nm ( $\epsilon = 1.8 \times 10^5$ ) and a shoulder at 363 nm. The fluorescence emission spectrum of **Sq1b** showed a broad band with a maximum at 800 nm ( $\lambda_{ex} = 730$  nm). The effect of pH on the photophysical properties of **Sq1b** were investigated by varying the pH from 6.8-9.8. The

absorption and emission properties of **Sq1b** did not show much change in this pH window. The dye was found to be unstable below pH 6.8.

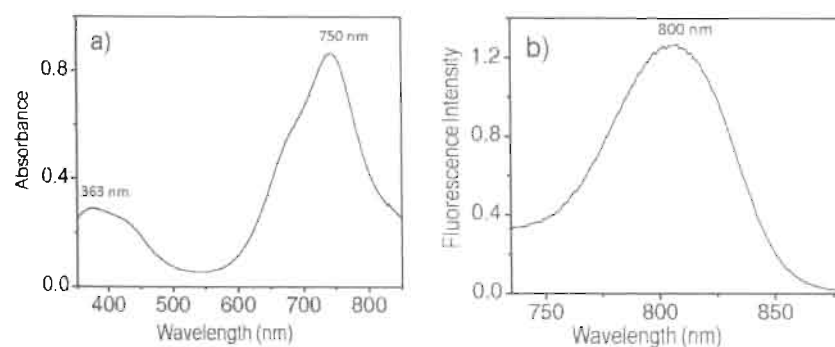
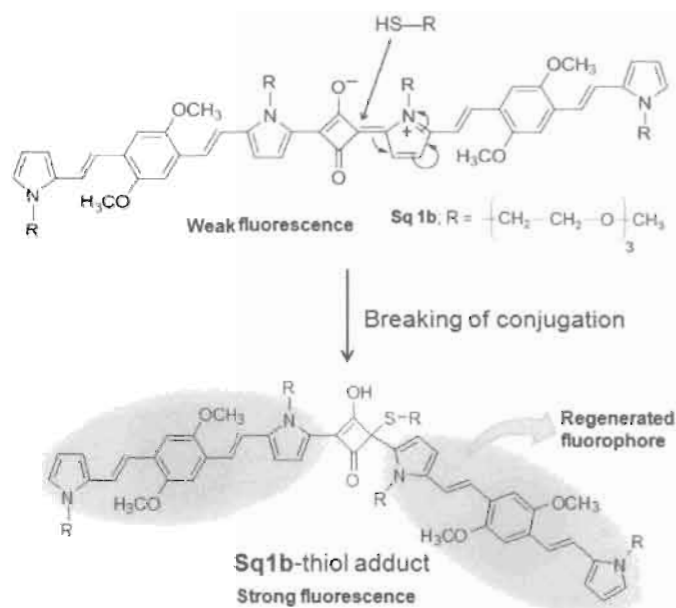


**Figure 2.7.** a) Absorption and b) emission ( $\lambda_{\text{ex}} = 730 \text{ nm}$ ) spectra of **Sq1b** ( $6 \times 10^{-6} \text{ M}$ ) in acetonitrile/water (1:1 CHES buffer, 0.01M) at pH 9.6.

### 2.3.5. Thiol Detection

It is known that the electron deficient cyclobutene ring of squaraine dyes are amenable for nucleophilic attack.<sup>34-36</sup> For example, *N,N*-dialkyl aniline derived squaraine dyes, upon addition of alkyl thiols undergo decoloration and fluorescence quenching due to the thiol addition and conjugation break. In analogy to these reports, we speculated that aliphatic thiols may open up the double bond that connects the cyclobutene ring with the pyrrole moiety in **Sq1b**. In such a case, the electronic communication between the two bispyrrole moieties will be broken leading to significant changes in the optical properties of the probe. In particular, the fluorescence emission of the probe may be considerably enhanced due to the formation of two different chromophores as shown in Scheme 2.3.



**Scheme 2.3.** Chemical activation of weak fluorophore **Sq1b** to an active fluorophore through thiol group attack. The background color indicates the fluorescence color of the molecules.

The above hypothesis was established by the addition of aliphatic thiols or a thiol containing  $\alpha$ -amino acid, cysteine ( $0 - 4.9 \times 10^{-4}$  M) to **Sq1b** ( $6 \times 10^{-6}$  M) in 1:1 acetonitrile/water (CHES buffer, pH 9.6) which resulted in a reduction in the intensity of the absorption band at 750 nm, with concomitant formation of a new band at 440 nm. The corresponding change in the absorption spectrum is shown in Figure 2.8a. The thiol interaction can be visually followed by a color change from green to light yellow (Figure 2.8a insets).

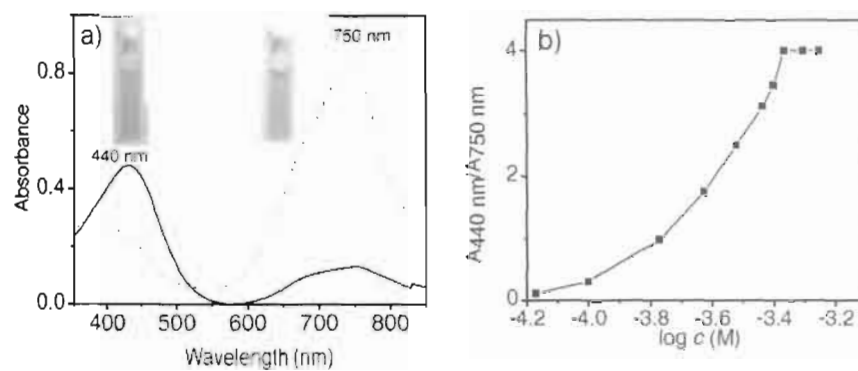


**Figure 2.8.** a) UV/Vis spectra of **Sq1b** ( $6 \times 10^{-6}$  M) before (---) and after (—) addition of cysteine in acetonitrile/water (1:1, CHES buffer (0.01 M), pH 7.4) (Inset shows the photograph of the visible color change of **Sq1b** with and without the addition of cysteine) b) Ratiometric plot based on the change in the absorption spectrum of **Sq1b** at 440 nm and 750 nm against concentration of cysteine.

The emission properties of **Sq1b** showed a dramatic change upon addition of cysteine. When excited at 410 nm, **Sq1b** exhibited a new band at 592 nm with a bright orange fluorescence (Figure 2.9) whereas upon 730 nm excitation, a decrease in the intensity of the weak NIR emission at 800 nm with increasing concentration of cysteine is observed (Figure 2.9). These changes in the absorption and emission spectra are attributed to the addition of the thiol group to the cyclobutene ring, resulting in new UV-Vis absorbing chromophores with strong fluorescence.

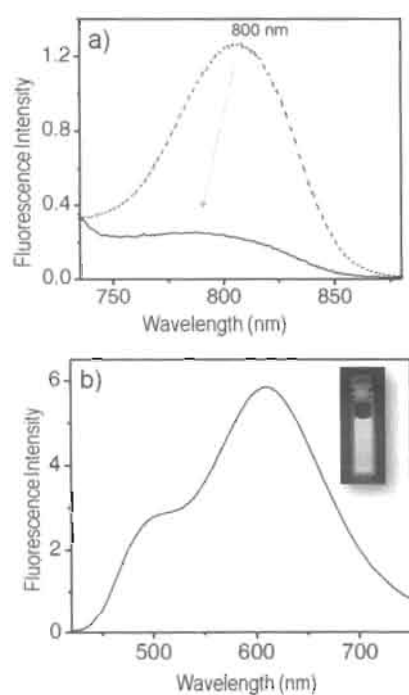


**Figure 2.9.** a) Emission spectra of **Sq1b** ( $6 \times 10^{-6}$  M) before (---) and after (—) addition of cysteine in acetonitrile/water (1:1, CHES buffer (0.01 M), pH, when excited at 730 nm; b) Emission spectra of **Sq1b**-cysteine adduct when excited at 410 nm (Inset shows the photograph of the visible fluorescence of the **Sq1b**-cysteine adduct when illuminated in a 365 nm UV light)

Variations in the emission at 592 nm and 800 nm against the concentration of cysteine and the corresponding ratiometric plot are shown in Figure 2.10a and b, respectively. The noninterfering absorption bands with large wavelength shift ( $\Delta\lambda = 310$  nm) and the possibility to monitor two emission maxima at dual wavelength excitation make the **Sq1b** a unique ratiometric probe (Figure 2.10b).

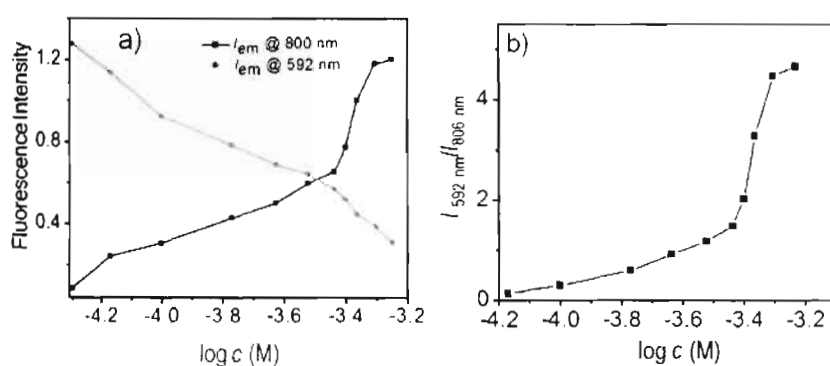


**Figure 2.10.** a) Changes in the emission spectra of **Sq1b** ( $6 \times 10^{-6} \text{ M}$ ) at 592 nm and 805 nm upon addition of cysteine ( $0-4.9 \times 10^{-4} \text{ M}$ ) in 1:1 acetonitrile/water solution buffered at pH 9.6 (CHES 0.01M). b) A ratiometric plot of the emission intensity changes at 592 nm and 806 nm against the concentration of cysteine.

The changes in the absorption and emission spectra of **Sq1a** and **Sq1b** could be due to the addition of thiol moiety to the probe resulting in the formation of the corresponding adduct. This is confirmed by high resolution mass spectroscopy (HRMS) analysis of **Sq1a** after the addition of butane thiol. The dye-thiol adduct was prepared by stirring **Sq1a** and butane thiol in acetonitrile/water 9:1 mixture buffered at pH 9.6 for 15 minutes. The formation of **Sq1a**-thiol adduct was confirmed by UV-NIR spectral changes. The resulting yellow solution was analyzed using HRMS. A mass corresponding to **Sq1a**-thiol adduct was obtained at  $m/z$  1033.33 (Figure 2.11).

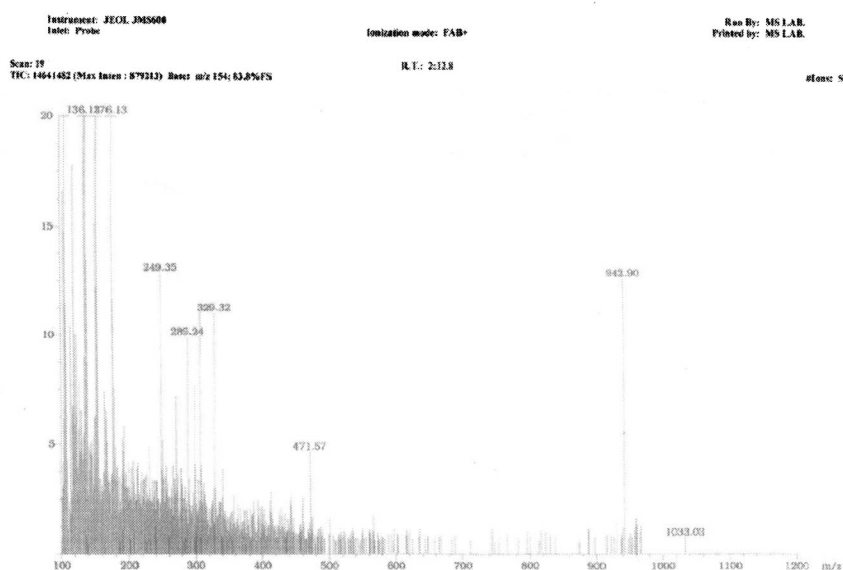


**Figure 2.11.** High Resolution Mass Spectrum (HRMS) corresponding to **Sq1a**-butanethiol adduct ( $m/z$  1033.33) in acetonitrile/water (9:1 v/v) solution at pH 9.6 (CHES 0.01M).

Addition of different amino acids without thiol groups to **Sq1b** did not alter the absorption or emission properties, which indicated the selective interaction of the thiol group of cysteine with the cyclobutene ring of the dye. Equal volume of (60  $\mu$ L,  $4.9 \times 10^{-4}$  M) amino acids such as phenylalanine (Phe), glycine (Gly), tryptophan (Trp), leucine (Leu), cystine, cysteine (Cys) and glutathione (GSH) were added to **Sq1b** ( $6 \times 10^{-6}$  M). The emission spectrum of **Sq1b** at 592 nm is monitored by exciting at 410 nm with each addition. Figure 2.12 shows plots of the intensity of emission at 592 nm against the corresponding amino acids. Thus, the two noninterfering absorption bands and the possibility of monitoring the

emission at two different excitation wavelengths extend the scope of **Sq1b** as a suitable ratiometric probe for the detection of thiol containing amino acids in biological samples especially in human blood plasma (HBP).

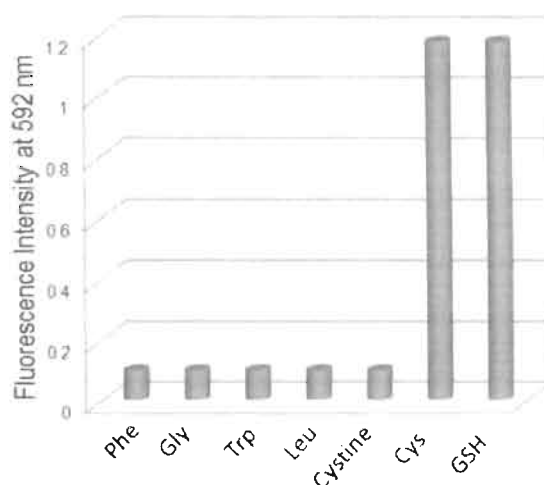


**Figure 2.12.** Plots of the response of **Sq1b** ( $6 \times 10^{-6}$  M) to different amino acids and to a tripeptide glutathione (GSH). The emission intensity is monitored at 592 nm in 1:1 acetonitrile/water solution buffered at pH 9.6 (CHES 0.01M). Amino acids without a thiol moiety as well as cysteine (two cysteine molecules joined by disulphide bond) did not show any response.

### 2.3.6. Human Blood Plasma Analysis

The thiol containing amino acids such as cysteine and homocysteine in human blood plasma (HBP) are in the disulphide form, bound either to the proteins or to low molecular mass thiols. Estimation of the aminothiols level in blood plasma is essential for understanding the role of these groups in the

pathogenesis of vascular diseases. In this context, we have investigated the use of **Sq1b** in the evaluation of the total content of amino thiols under different conditions. Fresh human blood samples (5 mL) with added ethylene diamine tetra acetic acid (EDTA) were centrifuged in a vacutainer tube at 3000 rpm for 15 min. The supernatant solution (plasma), which contains proteins and amino acids, was collected and used as such for further studies. For a healthy human adult, blood is composed of about 43-56% blood plasma. 500  $\mu$ L of the collected plasma was reduced using dilute HCl in the presence of triphenylphosphine as the catalyst. Proteins present in the sample after reduction were precipitated by the addition of acetonitrile, followed by centrifugation (6000 rpm) of the sample for 20 min. The supernatant liquid which contained amino thiols in blood plasma was filtered through a nylon filter and diluted to 2 mL with water/acetonitrile (1:1) and used as such for analysis.

Addition of aliquots (10, 20, 30 and 40  $\mu$ L) of the reduced HBP to **Sq1b** (in water/acetonitrile 1:1, pH 9) resulted in the decrease of the absorption band at 750 nm with the formation of new band at 440 nm. Consequently, the intensity of the emission band at 600 nm (Figure 2.13) is enhanced, which indicated the presence of free amino thiols that form fluorescent adducts with the probe.

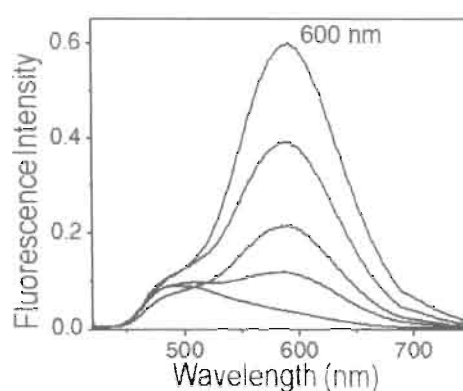


**Figure 2.13.** Increase in the emission intensity of **Sq1b** ( $6 \times 10^{-6}$  M) at 600 nm ( $\lambda_{em} = 410$  nm) upon addition of aliquots (0, 20, 30, 40  $\mu$ L) of human blood plasma after reduction.

Micro test assay experiments for the detection of thiol containing amino acids and low molecular weight amino thiols in HBP were conducted in microwell containers, each filled with 200  $\mu$ L of a solution of **Sq1b** in water /acetonitrile (1:1) at pH 9.6 (CHES buffer (0.01M)). Equal volumes of different amino acids were separately added to the wells (A-C). The samples in the microwells were illuminated from underneath by 365 nm UV light in a gel documentation apparatus. Interestingly, only *L*-cysteine (C1) and the reduced glutathione (C3) exhibited intense emission (orange) at 600 nm (Figure 2.14). The fourth row (D) shows the response of **Sq1b** to aliquots of HBP under different conditions. The bright orange emission indicating the presence of amino thiols was obtained only in microwells D5-D8, which contained different HBP samples after reduction.

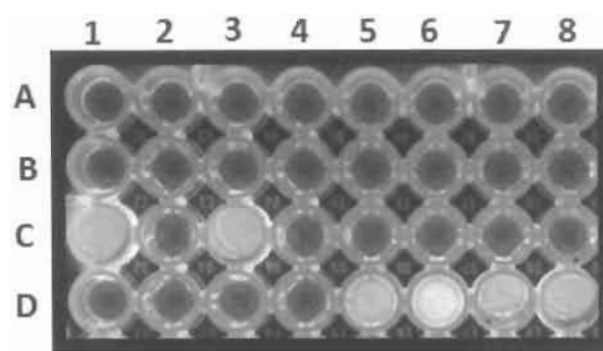


**Figure 2.14.** Detection of aminothiols in human blood plasma using a micro well test assay. Contents of wells (each contain **Sq1b**): Well A1 (blank, Sq1 alone), A2 (phenylalanine), A3 (threonine), A4 (arginine), A5 (histidine), A6 (asparagine), A7 (leucine), A8 (alanine), B1 (proline), B2 (valine), B3 (glycine), B4 (lycine), B5 (serine), B6 (methionine), B7 (isoleucine), B8 (glutamine), C1 (L-cysteine), C2 (cystine), C3 (glutathione), C4 (tryptophan), C5 (glutamic acid), C6 (aspartic acid), C7 (aqueous buffer at pH 6), C8 (aqueous buffer at pH above 10), D1 (Sq1 alone), D2 (20  $\mu$ L HBP before reduction), D5-D8 (different HBP samples after reduction).

The practical application of **Sq1b** is demonstrated by the quantitative estimation of aminothiols in HBP. It is known that the total aminothiol content in blood plasma varies for many reasons. For example, aminothiol concentration during fasting and after food is known to vary significantly. Similarly, the total aminothiol content in the blood of chain smokers are known to be very high, which is one of the reasons for the health risk associated with the thickening of the blood vessels. Therefore, quantitative determination of free aminothiols in blood plasma is of great analytical importance.

Analysis of HBP samples collected under three different physiological conditions revealed significant variation in the amino thiol content. The unknown concentrations of amino thiols were determined by the standard addition method using cysteine as the standard. To 300  $\mu$ L of the unknown plasma sample, known concentrations of the aqueous solution of cysteine were added and prepared the solution to a definite volume (1 mL) in separate standard flasks. A blank was prepared using 300  $\mu$ L plasma by diluting to 1 mL. Equal volume (60  $\mu$ L) from each standard flasks were added to **Sq1b** ( $6 \times 10^{-6}$  M) in 1:1 (v/v) acetonitrile/water mixture buffered at pH 9.6 and the emission was monitored at 600 nm. A graph was plotted using concentration of known amount of cysteine in the x-axis and emission at 600 nm in the y-axis. Concentration of the unknown amino thiols in 300  $\mu$ L of the plasma sample was calculated from the slope of the straight line obtained.

For comparison of the total amino thiol concentration in variation with dietary intake, blood samples of a healthy person was collected before breakfast (BBF) and after breakfast (ABF) and analyzed by the standard addition method (Figure 2.15).<sup>37</sup> To study the effect of tobacco smoking on amino thiol production, a third sample was taken from a person who smokes 8-10 cigarettes per day (AS) (Figure 2.16). HBP collected before breakfast which was taken as the standard for comparison with the other samples after reduction of the protein bound amino thiols.

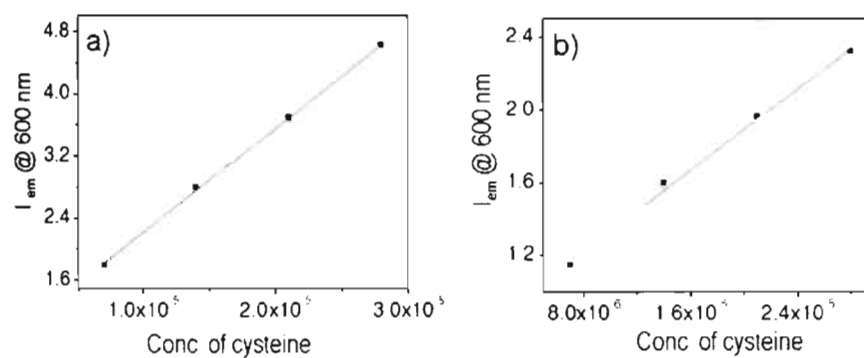


**Figure 2.15.** Standard addition plots for the determination of aminothiol concentration in human blood plasma. a) from an overnight fasting person (BBF) b) from the same person after breakfast (ABF). **Sq1b** ( $6 \times 10^{-6}$  M) was taken in 1:1 (v/v) water/acetonitrile mixture buffered at a basic pH. Intensity of enhanced emission at 600 nm was plotted against concentration of the known amount of the cysteine added. Unknown concentration was determined from the slope of the straight lines.

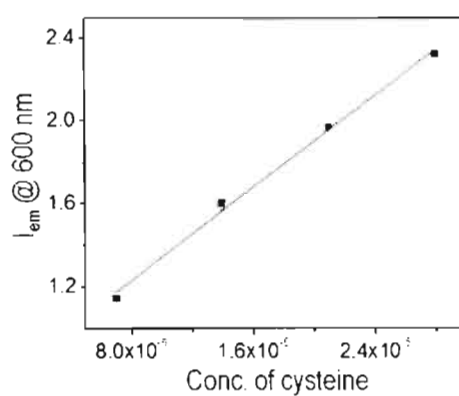


**Figure 2.16.** Standard addition plot for the determination of aminothiol concentration in the blood plasma of a person who smokes 8-10 cigarettes per day. **Sq1b** ( $6 \times 10^{-6}$  M) was taken in 1:1 (v/v) water/acetonitrile mixture buffered at a basic pH. Intensity of enhanced emission at 600 nm was plotted against concentration of known amount of cysteine added. Unknown concentration was determined from the slope of the straight lines.

**Table 2.1.** Summary of the determined aminothiol concentrations using **Sq1b** in human blood plasma at three different conditions. BBF (before breakfast), ABF (after breakfast), AS (after smoking). Recovery (%) can be calculated using the equation  $R = (Q_M - Q_E/Q_A) \times 100$ , where  $Q_M$  is the amount of unknown with added standard (cysteine),  $Q_E$  is the amount of unknown without the added standard and  $Q_A$  is the amount of standard added to the unknown.

HBP Samples	Amount of amino thiols determined in $10^{-6}$ g/L	Amount of cysteine added in $10^{-6}$ g/L	Recovery, %
<b>BBF</b>	254	105 210	102.7 101.3
<b>ABF</b>	352	105 210	101.7 100.8
<b>AS</b>	545	105 210	102 101.8

Analysis of reduced HBP using **Sq1b** revealed that the amount of total aminothiol concentration in plasma sample before breakfast is 245  $\mu\text{g/L}$  and is high in the HBP after breakfast (352  $\mu\text{g/L}$ ). The higher concentration of thiol after breakfast arises from the physiological processes associated with dietary intake (Table 2.1) which will be decreased with time. However, the plasma sample (300  $\mu\text{L}$ ) obtained after smoking showed very high aminothiol content of 545  $\mu\text{g/L}$  (Figure 2.17). This level of amino thiols may remain high in the case of chain

smokers who smoke at intervals which could be the reason for higher risk of coronary heart diseases.

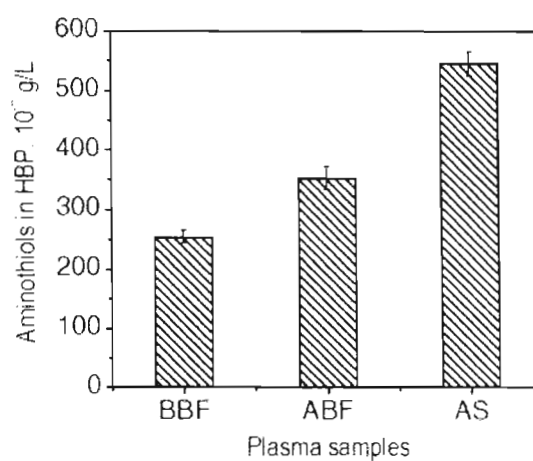


**Figure 2.17.** Plot showing the variation in the amount of total aminothiol concentrations in 300  $\mu\text{L}$  HBP obtained at three different conditions. BBF (HBP from a person after breakfast), ABF (HBP from a person after breakfast), and AS (HBP from a person after smoking).

Thus, the utility of **Sq1b** as a suitable molecular probe for the detection and estimation of the total aminothiol level in HBP is clearly demonstrated.

## 2.4. Conclusions

We have demonstrated a novel strategy for the detection of low molecular weight aminothiols using a  $\pi$ -extended squaraine dye that exhibits a NIR/Vis electronic transition. **Sq1b** is a novel ratiometric probe which is different from other known probes, since the detection is based on the generation of a new fluorophore that emits at a different wavelength through an analyte induced

breaking of  $\pi$ -conjugation. This is particularly important in biolabeling and imaging applications since the presence of any unchanged probe does not interfere with the measurement as the native dye is nearly nonfluorescent. The present system is also reliable as a chromogenic probe because the analyte interaction leads to a color formation rather than a color bleaching. The probe was successfully used for the detection and estimation of amino thiols in human blood plasma and confirmed the presence of the increased level of amino thiols in blood plasma of chain smokers. Due to the crucial role of free amino thiols present in blood plasma to the development of coronary heart diseases, stroke and peripheral vascular diseases, the current fluorescence based technique has significant biological and clinical relevance.

## **2.5. Experimental Section**

### **2.5.1. Synthesis and characterization**

Unless otherwise stated, all starting materials and reagents were purchased from commercial suppliers and used without further purification. The solvents and the reagents were purified and dried by usual methods prior to use. Melting points were determined with a Mel-Temp-II melting point apparatus.  $^1\text{H}$  and  $^{13}\text{C}$  NMR spectra were recorded on a 300 MHz Bruker Avance DPX Spectrometer. High Resolution Mass Spectra were recorded using JEOL JMS600. FT-IR spectra were recorded on a Shimadzu IR Prestige-21 Fourier Transform Infrared

Spectrophotometer. Electronic absorption spectra were recorded on a Shimadzu UV-3101 PC NIR Scanning spectrophotometer and the emission spectra were measured on a SPEX-Fluorolog F112X spectrofluorimeter. Microtest assay experiments were performed using a gel documentation apparatus.

### **2.5.2. Preparation of 1,4-bis(bromomethyl)-2,5-dimethoxybenzene (11)**

To a suspension of the appropriate hydroquinone dialkyl ether, **10** (10 mmol) in glacial acetic acid (35 mL), paraformaldehyde (30.25 mmol) was added and sonicated for 10 min. To this mixture, 33% of HBr in acetic acid (31.12 mmol) was added and sonicated for 3 h. After a further addition of 5 mL acetic acid followed by sonication for 30 min, the reaction mixture was poured into cold water. The precipitated product was filtered and dried.

Yield 92%; mp 203-204 °C; <sup>1</sup>H NMR (CDCl<sub>3</sub>, 300 MHz) δ (ppm): 6.81 (s, 2H, aromatic), 4.60 (s, 4H, CH<sub>2</sub>Br), 3.80 (s, 6H, OCH<sub>3</sub>); <sup>13</sup>C NMR (CDCl<sub>3</sub>, 75.4 MHz) δ (ppm): 150.72, 127.51, 114.62, 56.20, 29.65.

### **2.5.3. Preparation of tetraethyl (2-methoxy-5-methyl-1,4-phenylene)bis(methylene)diphosphonate (12)**

The bisphosphonate (**12**) was prepared by the reaction of the bisbromomethyl derivative (**11**) (643 mg, 2 mmol) with 3 mL of triethyl phosphite at 80-85 °C for 10-12 h followed by the removal of the unreacted triethyl phosphite under

vacuum. Yield 90-95%;  $^1\text{H}$  NMR ( $\text{CDCl}_3$ , 300 MHz)  $\delta$  (ppm): 6.7 (2H, aromatic), 4.19 (m, 8H,  $\text{OCH}_2$ ), 3.83 (s, 6H,  $\text{OCH}_3$ ), 3.03 (s, 4H,  $\text{CH}_2\text{P}$ ).

#### 2.5.4. General procedure for the preparation of *N*-butyl (14a) and *N*-glycol (14b) pyrrole-2-carbaldehydes

To a solution of potassium *tert*-butoxide (11 g, 100 mmol) in 100 mL dry THF, pyrrole-2-carbaldehyde (13) (9 g, 95 mmol) was added and stirred at 30 °C for 3 h. To the potassium pyrrole solution, 18-crown-6 (9 mmol) was added and stirred for 15 min. To the reaction mixture, 1-bromoalkyl (24 g, 108 mmol) was added drop wise and the stirring was continued for 18 h. The precipitated inorganic salt was filtered off and the solvent was removed under reduced pressure. The residue was extracted with dichloromethane. The combined organic extracts were washed with brine followed by water and dried over sodium sulfate. The solvents were removed and the crude product was purified by column chromatography over silica gel using petroleum ether to give the pure products **14a** and **14b**. Details of the characterization data are given below.

**14a**, Yield 70%;  $^1\text{H}$  NMR ( $\text{CDCl}_3$ , 300 MHz)  $\delta$  (ppm): 9.5 (s, 1H, aldehyde), 6.8 (m, 2H, aromatic), 6.1 (t, 1H, aromatic), 4.2 (t, 2H,  $\text{NCH}_2$ ), 1.1-1.8 (m, 4H,  $\text{CH}_2$ ), 0.7-0.9 (t, 3H,  $\text{CH}_3$ );  $^{13}\text{C}$  NMR ( $\text{CDCl}_3$ , 75.4 MHz)  $\delta$  (ppm): 179.10, 131.8, 131.0, 124.6, 111.30, 71.6, 70.6, 59.3.

**14b**, Yield 58%;  $^1\text{H}$  NMR ( $\text{CDCl}_3$ , 300 MHz)  $\delta$  (ppm): 9.5 (s, 1H, aldehyde), 6.8 (m, 2H, aromatic), 6.1 (t, 1H, aromatic), 4.2 (t, 2H,  $\text{NCH}_2$ ), 3.54 (m, 8H,  $\text{CH}_2$ ), 3.3 (t, 3H,  $-\text{OCH}_3$ );  $^{13}\text{C}$  NMR ( $\text{CDCl}_3$ , 75.4 MHz)  $\delta$  (ppm): 179.10, 131.8, 131.0, 124.6, 111.30, 71.6, 70.6, 59.3.

### 2.5.5. General procedure for the preparation of bispyrroles (15a,b)

A suspension of sodium hydride (720 mg, 30 mmol) in THF was added slowly to a solution of the corresponding bisphosphonate (2 g, 5 mmol) and the respective *N*-alkyl or glycolated pyrrole-2-carboxaldehyde (2.4 g, 10 mmol) in THF. After refluxing for 10 h, the reaction mixture was cooled and THF was removed under reduced pressure to give a pasty residue. The residue was suspended in water and extracted with dichloromethane. The organic layer was washed with brine, dried over  $\text{Na}_2\text{SO}_4$  and concentrated to give the crude product. Further purification was done either by precipitation using methanol from a dichloromethane solution or by column chromatography over silica gel using 5% ethyl acetate-petroleum ether mixture.

**15a**, Yield 63%; mp 141 °C;  $^1\text{H}$  NMR (300 MHz,  $\text{CDCl}_3$ )  $\delta$  (ppm): 7.08 (d, 2H, vinylic,  $J = 16.26$  Hz), 7.00 (d, 2H, vinylic,  $J = 16.30$  Hz), 6.91 (s, 2H, aromatic), 6.56 (s, 2H, aromatic), 6.42 (m, 2H, aromatic), 6.09 (t, 2H, aromatic), 4.2 (t, 2H,  $\text{NCH}_2$ ), 1.1-1.8 (m, 4H,  $\text{CH}_2$ ), 0.7-0.9 (t, 3H,  $\text{CH}_3$ );  $^{13}\text{C}$  NMR (75.4 MHz,  $\text{CDCl}_3$ )  $\delta$  (ppm): 150.93, 132.87, 126.56, 123.44, 121.46, 117.56, 110.95, 108.23, 106.63, 69.12, 34.15, 31.66, 19.47, 13.91; IR (KBr)  $\nu_{\text{max}}$ : 2949, 2868, 1462, 1417, 1327,

1197, 1039, 1012, 954, 707  $\text{cm}^{-1}$ ; HRMS calcd for  $\text{C}_{28}\text{H}_{36}\text{N}_2\text{O}_2$  ( $\text{M}^+$ ): 432.27, found 432.27.

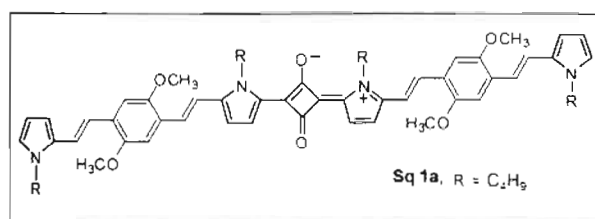
**15b**, Yield 58%; mp 141  $^{\circ}\text{C}$ ;  $^1\text{H}$  NMR (300 MHz,  $\text{CDCl}_3$ )  $\delta$  (ppm): 7.08 (d, 2H, vinylic,  $J=16.28$  Hz), 7.00 (d, 2H, vinylic,  $J = 16.20$  Hz), 6.91 (s, 2H, aromatic), 6.56 (s, 2H, aromatic), 6.42 (m, 2H, aromatic), 6.09 (t, 2H, aromatic), 4.1 (t, 4H, - $\text{NCH}_2$ ), 3.3 (s, 6H, - $\text{OCH}_3$ ), 2.8 (s, 6H);  $^{13}\text{C}$  NMR (75.4 MHz,  $\text{CDCl}_3$ )  $\delta$  (ppm): 150.93, 132.87, 126.56, 123.44, 121.46, 117.56, 110.95, 108.23, 106.63, 69.12, 34.15, 31.66, 19.47, 13.91; IR (KBr)  $\nu_{\text{max}}$ : 2949, 2868, 1462, 1417, 1327, 1197, 1039, 1012, 954, 707  $\text{cm}^{-1}$ ; HRMS calcd for  $\text{C}_{28}\text{H}_{36}\text{N}_2\text{O}_2$  ( $\text{M}^+$ ): 612.75, found 612.34.

### 2.5.6. General procedure for the syntheses of squaraine derivatives

#### **Sq1a and Sq1b**

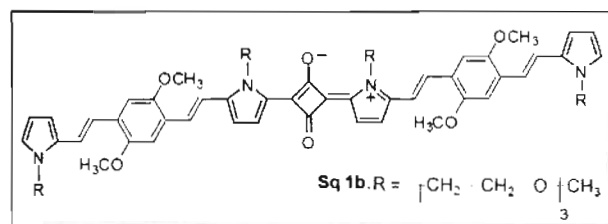
The squaraine dyes **Sq1a** and **Sq1b** were synthesized by condensing the corresponding dialkyloxy benzene bridged bispyrroles **15a** or **15b** (4 mmol) with squaric acid (0.2 g, 2 mmol) in 1:3 butanol/benzene mixture (80 mL) under azeotropic conditions (Scheme 2.2). The progress of the reaction was followed by recording the absorption spectra at interval of the reaction. The reaction was stopped when higher homologues started appearing. Repeated precipitation using petroleum ether gave **Sq1a** and **Sq1b** in moderate yields. Significant amount of polymeric dyes were also formed which were removed by precipitation and

column chromatography in Silica Gel using chloroform/methanol (8:2) solvent mixture.



**Sq1a:** Yield 26%, <sup>1</sup>H NMR (300 MHz, CDCl<sub>3</sub>) δ (ppm): 7.84 (s, 2H, aromatic),

7.53 (d, 2H, vinylic, *J* = 15.91 Hz), 7.19 (m, 6H, vinylic + aromatic), 7.06 (m, 6H, vinylic + aromatic), 6.94 (m, 2H, aromatic), 6.77 (s, 2H, aromatic), 6.17 (s, 2H, aromatic), 4.83 (s, 4H, -NCH<sub>2</sub>), 3.94 (m, 10H, OCH<sub>3</sub>+NCH<sub>2</sub>), 1.63 (m, 8H, CH<sub>2</sub>), 0.94 (m, 12H, CH<sub>3</sub>). <sup>13</sup>C NMR (75 MHz, CDCl<sub>3</sub>) δ (ppm): 193.67, 174.07, 149.67, 135.11, 134.74, 134.40, 132.44, 130.05, 129.72, 129.33, 129.16, 128.96, 128.86, 128.80, 128.65, 128.36, 96.37, 83.76, 77.65, 76.80, 28.41, 28.37, 28.09. FT-IR (KBr) ν<sub>max</sub>: 704, 956, 1093, 1296, 1384, 1502, 1620, 2954 cm<sup>-1</sup>; HRMS-FAB calcd for C<sub>61</sub>H<sub>71</sub>N<sub>4</sub>O<sub>6</sub> (M<sup>+</sup>): 942.53 found: 942.30.



**Sq1b:** Yield 32%, <sup>1</sup>H NMR (300 MHz, CDCl<sub>3</sub>) δ (ppm): 7.6(d, 2H, vinylic, *J* = 15.82 Hz), 7.15

(m, 5H, vinylic + aromatic), 7.01 (m, 5H, vinylic + aromatic), 6.76 (s, 2H, aromatic), 6.55 (s, 2H, aromatic), 6.17 (s, 2H, aromatic), 4.1 (t, 8H, -NCH<sub>2</sub>), 3.3

(s, 12H, -OCH<sub>3</sub>), 2.8 (s, 12H); <sup>13</sup>C NMR (75 MHz, CDCl<sub>3</sub>) δ (ppm): 178.611, 176.83, 152.12, 148.24, 131.91, 129.53, 120.36, 110.67, 106.69, 70.64, 70.34, 58.83, 58.73, 56.13, 46.59, 29.52; FT-IR (KBr) ν<sub>max</sub>: 954, 1034, 1094, 1207, 1278, 1382, 1465, 1497, 1618, 1742, 2851, 2923 cm<sup>-1</sup>; HRMS-FAB calcd for C<sub>72</sub>H<sub>94</sub>N<sub>4</sub>O<sub>18</sub> (M<sup>+</sup>): 1302.66 found: 1302.53.

### 2.5.7. Details of Blood Plasma Analysis

Fresh human blood samples (5 mL) containing added EDTA were centrifuged in a vacutainer tube at 3000 rpm for 15 min. The supernatant solution called 'plasma' which contains proteins and amino acids was collected and used as such for further studies. Blood samples were collected from different volunteers for analysis. For the comparison of variation in the total amino thiol content before and after dietary intake, blood samples from the same person were analyzed before and after breakfast. In order to study the effect of tobacco smoke on the level of amino thiols, blood samples were collected from a volunteer who smokes 8-10 cigarettes per day. Each collected samples were reduced using similar procedure as explained. In the case of a healthy adult, 5 mL of the blood is composed of about 43-56% human blood plasma. 500 μL of the collected plasma was reduced using dilute HCl in presence of triphenylphosphine as a catalyst. Proteins present in the sample after reduction was precipitated using acetonitrile which was followed by centrifugation (6000 rpm) of the sample for 20 minutes. The supernatant liquid which contains amino thiols in blood was filtered through a

nylon filter and diluted to 2 mL with water/acetonitrile and used as such for analysis. Aliquot of the plasma sample was added to solutions of **Sq1b** ( $6 \times 10^{-6}$  M) in 1:1 acetonitrile/water (CHES buffer 0.01M, pH 9.6) and the emission at 600 nm were determined. The unknown amount of aminothiols was estimated using the standard addition method.

## 2.6. References

1. A. P. de Silva, H. Q. N. Gunaratne, T. Gunnlaugsson, A. J. M. Huxley, C. P. McCoy, J. T. Rademacher, T. E. Rice, *Chem. Rev.* **1997**, *97*, 1515.
2. J.-P. Desvergne, A. W. Czarnik, in *Chemosensors for Ion and Molecular Recognition*; NATO series, Vol 492, Kluwer Academic Press; **1997** pp. 189-194.
3. S. L. Wiskur, H. A. Haddou, J. J. Lavigne, F. V. Anslyn, *Acc. Chem. Res.* **2001**, *34*, 963.
4. K. Rurack, U Genger, *Chem. Soc. Rev.* **2002**, *31*, 116.
5. R. Martínez-Máñez, F. Sancenón, *Chem. Rev.* **2003**, *103*, 4419.
6. R. Martínez-Máñez, F. Sancenón, *Coord. Chem. Rev.* **2006**, *250*, 3081.
7. O. S. Wolfbeis, in *Fiber Optic Chemical Sensors and Biosensors*, Vol. 1, CRC Press, Boca Raton, FL, **1991**, p 2.
8. V. Dujols, F. Ford, A. W. Czarnik, *J. Am. Chem. Soc.* **1997**, *119*, 7386.
9. F. Sancenón, R. Martínez-Máñez, M. A. Miranda, M. -J. Segui, J. Soto, *Angew. Chem. Int. Ed.* **2003**, *42*, 647.
10. A. M. Costero, S. Peransi, S. Gli, *Tetrahedron Lett.* **2006**, *47*, 6561.

11. S. Melnyk, M. Pogribna, I. Pogribny, R. J. Hine, S. J. James, *J. Nutr. Biochem.* **1999**, *10*, 490.
12. O. Nekrassova, N. S. Lawrence, R. G. Compton, *Talanta* **2003**, *60*, 1085.
13. W. G. Christen, U. A. Ajani, R. J. Glynn, C. H. Hennekens, *Arch. Intern. Med.* **2000**, *160*, 422.
14. M. T. Heafield, S. Fearn, G. B. Stevenson, R. H. Waring, A. C. Williams, S. G. Sturman, *Neurosci. Lett.* **1990**, *110*, 216.
15. H. Refsum, P. M. Ueland, O. Nygard, S. E. Vollset, *Annu. Rev. Med.* **1998**, *49*, 31.
16. J. Selhub, *Annu. Rev. Nutr.* **1999**, *19*, 217.
17. M. R. Malinow, F. J. Nieto, M. Szklo, L. E. Chambless, G. Bond, *Circulation* **1993**, *87*, 1107.
18. M. Soinio, J. Marniemi, M. Laakso, S. Lehto, T. Ronnema, *Ann. Intern. Med.* **2000**, *140*, 94.
19. A. Sobczak, *Addict. Biol.* **2003**, *8*, 147.
20. P. M. Ueland, H. Refsum, S. A. Beresford, S. E. Vollset, *Am. J. Clin. Nutr.* **2000**, *72*, 324.
21. C. Chrysohoou, D. B. Panagiotakos, C. Pitsavos, A. Zimbeke, A. Zampelas, L. Papademetriou, C. Masoura, C. Stefanadis, *Vasc. Med.* **2004**, *9*, 117.
22. A. Meister, M. E. Anderson, *Annu. Rev. Biochem.* **1983**, *52*, 711.
23. I. Rahman, W. MacNee, *Free Radical Biol. Med.* **2000**, *28*, 1405.

24. P. K. Pullela, T. Chiku, M. J. Carvan, D. S. Sem, *Anal. Biochem.* **2006**, 352, 265.
25. F. Tietze, *Anal. Biochem.* **1969**, 27, 502.
26. R. E. Basford, F. M. Huennekens, *J. Am. Chem. Soc.* **1955**, 77, 3873.
27. S. Y. Zhang, C. -N. Ong, H. -M. Shen, *Cancer Lett.* **2004**, 208, 143.
28. G. L. Ellman, *Arch. Biochem. Biophys.* **1959**, 82, 70.
29. J. Reeve, J. Kuhlenkamp, N. Kaplowitz, *J. Chromatogr.* **1980**, 194, 424.
30. C. Komuro, K. Ono, Y. Shibamoto, T. Nishidai, M. Takahashi, M. Abe, *J. Chromatogr.* **1985**, 338, 209.
31. M. Zhang, M. Yu, F. Li, M. Zhu, M. Li, Y. Gao, L. Li, Z. Liu, J. Zhang, D. Zhang, T. Yi, C. Huang, *J. Am. Chem. Soc.* **2007**, 129, 10322.
32. T. Matsumoto, Y. Urano, T. Shoda, H. Kojima, T. Nagano, *Org. Lett.* **2007**, 9, 3375.
33. L. Yi, H. Li, L. Sun, L. Liu, C. Zhang, Z. Xi, *Angew. Chem. Int. Ed.* **2009**, 48, 4034.
34. J. V. Ros-Lis, R. Martínez-Máñez, J. Soto, *Chem. Commun.* **2002**, 2248.
35. J. V. Ros-Lis, B. Garcyá, D. Jiménez, R. Martínez-Máñez, F. Sancenón, J. Soto, F. Gonzalvo, M. C. Valldecabres, *J. Am. Chem. Soc.* **2004**, 126, 4064.
36. V. Ros-Lis, M. D. Marcos, R. Martínez-Máñez, K. Rurack, J. Soto, *Angew. Chem. Int. Ed.* **2005**, 44, 4405.
37. A. Küster, I. Tea, S. Sweeten, J. C. Rozé, R. J. Robins, D. Darmaun, *Anal. Bioanal. Chem.* **2008**, 390, 1403.

---

### Bipyridine based Fluorophores for the Detection of Zinc Ions under Cellular and Aqueous Environments

---

#### 3.1. Abstract

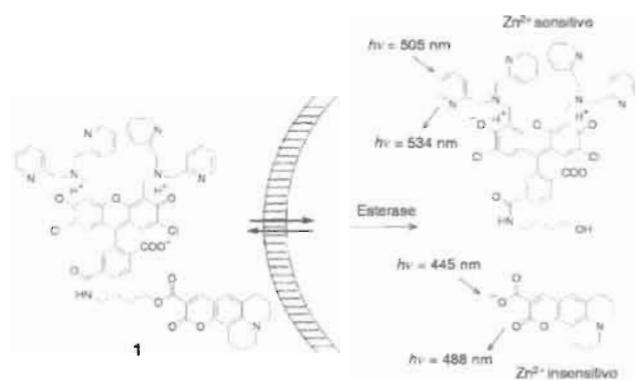
*Detection and imaging of  $Zn^{2+}$  in biological as well as analytical samples are of paramount importance due to the role of this cation in physiological functions. In this chapter, we discuss the synthesis, biological as well as analytical applications of bipyridine conjugated bispyrrole derivatives. The fluorescent water soluble derivative, **GBP**, containing glycol side chains is used for imaging  $Zn^{2+}$  in **MCF-7** (Human breast cancer) cell lines. **GBP** showed a characteristic green emission around 540 nm ( $\Phi_f = 0.51$ ) in aqueous environments. The emission of **GBP** was significantly quenched by other transition metal cations such as  $Cu^{2+}$ ,  $Ni^{2+}$ ,  $Hg^{2+}$ ,  $Co^{2+}$  and  $Mn^{2+}$  whereas the titration of  $Zn^{2+}$  ions resulted in a strong red emission around 640 nm. The maximum change in the fluorescence intensity was observed in the pH window of 6.8-7.4 which is suitable for the detection of  $Zn^{2+}$  in cellular environments. A bispyrrole ligand, **CBP**, with chiral side chains, showed high solid state fluorescence which allowed the fabrication of a reusable dipstick for the detection of  $Zn^{2+}$  ions in aqueous solutions. Details of the synthesis and the optical properties of **GBP** and **CBP** and their use in the detection and imaging of  $Zn^{2+}$  are discussed.*

### 3.2. Introduction

Detection of heavy metal cations is a topic of numerous studies motivated by human health related problems as well as environmental concerns.<sup>1</sup> In this context, organic molecular probes that exhibit metal ion induced changes in photophysical properties especially, changes in fluorescence are very attractive due to high sensitivity of detection at a low analyte concentration.<sup>2</sup> Fluorescent probes displaying “turn-on” ratiometric fluorescent signaling are particularly valuable since the signal transduction is less likely to be biased by nonspecific interactions with background impurities and offer an improved signal to noise ratio.<sup>3</sup> Among the different heavy metal cations, detection of spectroscopically silent  $Zn^{2+}$  ions is significantly important.<sup>4-6,8</sup> In the usual case, a  $Zn^{2+}$  specific chemosensor consists of a multi-dendate ligand tethered to a fluorophore. For example, 2, 2' bis(2-picolyl) amino derivatives (DPA) attached to various chromophores are the ligands of choice for  $Zn^{2+}$ .<sup>7,8</sup> Although, highly effective, such sensors often require laborious multistep organic synthetic protocol for their assembly. Therefore, synthesis of new fluorescent molecular probes for the selective detection and imaging of  $Zn^{2+}$  has been of continued interests to chemists.<sup>9,10</sup>

A wide range of reports are available for detecting  $Zn^{2+}$  ions in cellular environments.<sup>11</sup> Most of the reported molecules rely on the specific binding affinity of  $Zn^{2+}$  to dipicolyl amine derivatives. Lippard and coworkers have made significant contributions to the development of  $Zn^{2+}$  probes.<sup>12-15</sup> They have

synthesized a number of ratiometric Zn<sup>2+</sup> probes by attaching DPA-chelating groups to different chromophores. An interesting case is the novel two-fluorophore approach with coumazin-1 (**1**), which is a nonfluorescent prosensor containing a Zn<sup>2+</sup> insensitive coumarin derivative attached to a Zn<sup>2+</sup> sensitive fluorescein moiety.<sup>16</sup> The two fluorophores, when conjugated through an ester linkage, become nonfluorescent. This nonfluorescent compound can be hydrolyzed by esterase (Scheme 3.1), thus separating the Zn<sup>2+</sup> sensitive fluorescein chemosensor from the coumarin part, both of which are fluorescent. Coumazin-1 is a cell-permeable latent fluorophore useful for the biological ratio imaging of Zn<sup>2+</sup> (Figure 3.1). When it is injected into cells, the ester linkage is cleaved by esterase, and the fluorophores are activated. As both fluorophores have characteristic excitation and emission properties, they can be probed ratiometrically. Excitation of the coumarin at 445 nm and measurement of the emission intensity at 488 nm provides information about the cleaved sensor. Excitation of the fluorescein part at 505 nm and monitoring of the emission intensity at 534 nm gives information about the amount of zinc present. In the absence of Zn<sup>2+</sup>, the ratio of the emission intensities  $I_{534}/I_{488}$  was 0.5, which increased to 4.0 upon saturation with Zn<sup>2+</sup>.



Scheme 3.1. Proposed mechanism of activation of coumazin-1

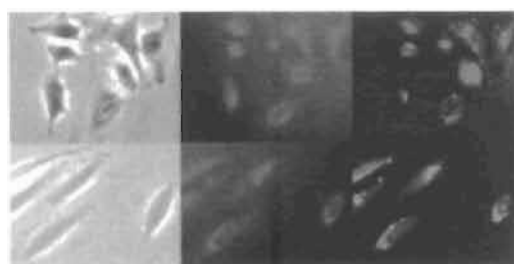
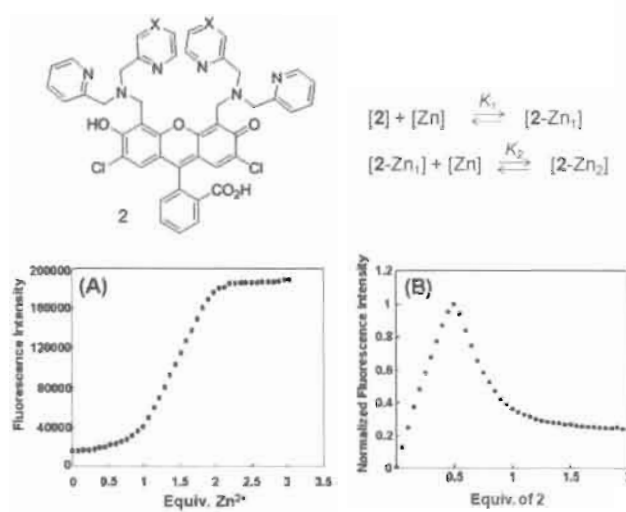


Figure 3.1. Phase contrast (left) and fluorescence (middle, right) microscopy images of HeLa cells incubated for 6 h with **1** (5  $\mu\text{M}$ ), without (top) and with (bottom) the addition of  $\text{ZnCl}_2$  (5  $\mu\text{M}$ ) and sodium pyrithione (45  $\mu\text{M}$ ). Fluorescence images were acquired with excitation at 400–440 nm, band pass of 475 nm (middle) or with excitation at 460–500 nm, band pass of 510–560 nm (right).

Recently, Lippard and co-workers have reported a fluorescein derivative **2** which responds to  $\text{Zn}^{2+}$  in two different ways depending on the binding at different sites.<sup>17</sup> Mode of addition of  $\text{Zn}^{2+}$  to **2** resulted in two different emission responses, which is the result of the formation of two stepwise complexes (Figure 3.2). The

probe **2** was then used for imaging Zn<sup>2+</sup> ions in Min6, an insulin cell line that contain a relatively high concentration of zinc ions (Figure 3.3).



**Figure 3.2.** A zinc ion selective probe **2** and the stepwise equilibria showing binding events. a) Changes in the fluorescence response of **2** (5  $\mu$ M) upon the addition of Zn<sup>2+</sup> (A) and fluorescence titration of Zn<sup>2+</sup> (5  $\mu$ M) upon stepwise addition of **2** (B).



**Figure 3.3.** Live Min6 cells were incubated with **2** (green channel), and cell nuclei were stained with Hoechst 33258 (blue channel). a) DIC image; fluorescence images of b) before and c) after addition of TPEN. Bars are 25  $\mu$ m.

The development of a practical colorimetric or fluorescence based sensor is largely dependent upon unique optical signal transduction resulting from a given analyte.<sup>18</sup> In addition to binding a variety of metal ions more or less indiscriminately, a chemosensor based on a derivatized bipyridyl ligand 'L' may undergo an optical response upon formation of an  $L-M^{n+}$  complex. However, the interpretation of sensor response can be complicated when two or more L units bind to a single metal ion, producing equilibrium mixtures of  $L_n M^{n+}$ ,  $L_{n-1} M^{n+}$ , etc., each of which will exhibit its own optical signature. Consequently, chemosensors tend to employ receptors designed to provide selective binding of the target analyte in a 1:1 ratio through an appropriate combination of size/shape and electronic character.

Bipyridyl derivatives are one of the widely used ligands in co-ordination chemistry.<sup>19</sup> The widespread utility of these ligands stems from their facile preparation/functionalization, stability and ability to bind a wide array of d- and f-block elements. Smith and coworkers have recently reported a molecule **3** having a sterically crowded 5, 5' distyryl bipyridyl moiety that enforces 1:1 metal-to-ligand ratio allowing a selective turn on sensing of  $Zn^{2+}$  in THF.<sup>20</sup> Binding of  $Zn^{2+}$  to the sterically crowded bipyridyl moiety significantly enhances the fluorescence at 500 nm (Figure 3.4).

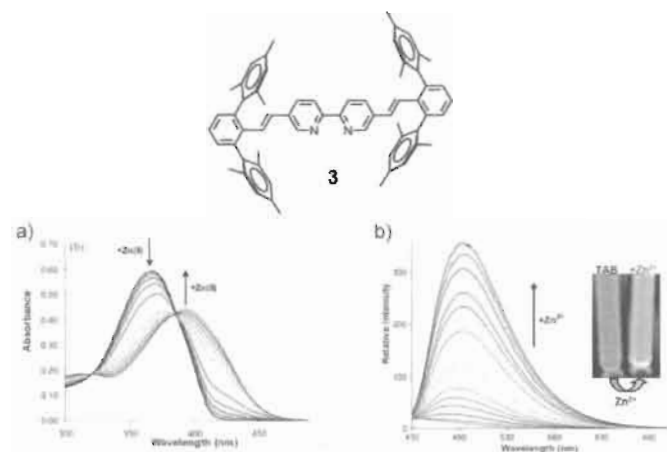


**Figure 3.4.** Changes in the a) absorption and b) emission spectra of **3** with increasing amounts of  $Zn^{2+}$  ions in THF. Inset shows the corresponding fluorescence change.

Liu et al. have reported a 5, 5' bipyridine based fluoroionophore **4** (Figure 3.5) which exhibits fluorescence changes based on both photoinduced charge transfer (PCT) and photoinduced electron transfer (PET) mechanisms.<sup>21</sup> The molecule **4** is nonfluorescent (off) in the absence of  $Zn^{2+}$  ions. Binding of  $Zn^{2+}$  to the high affinity dipicolylamine site prevents PET, thereby generating a concentration dependent fluorescence enhancement at a relatively short wavelength. Co-ordination of  $Zn^{2+}$  with the bipyridine site occurs at a sufficiently high concentration, where planarization of bipyridine triggers the internal charge transfer process (ICT) which ultimately results in bathochromic shift to generate a new emission band.

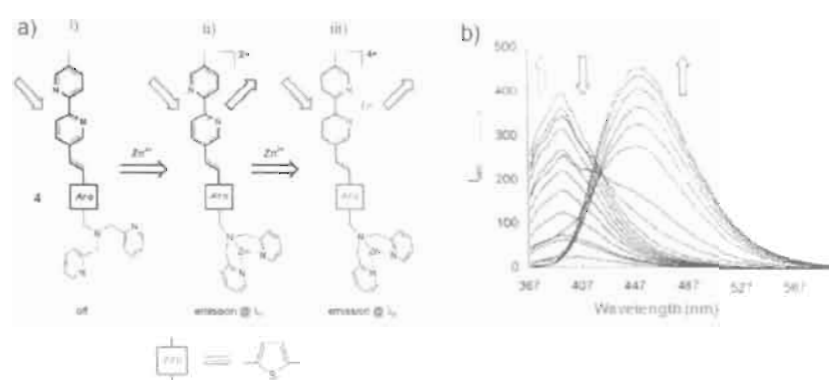
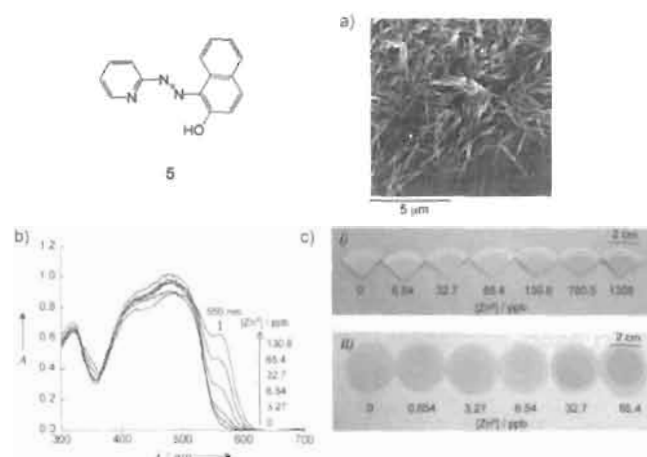


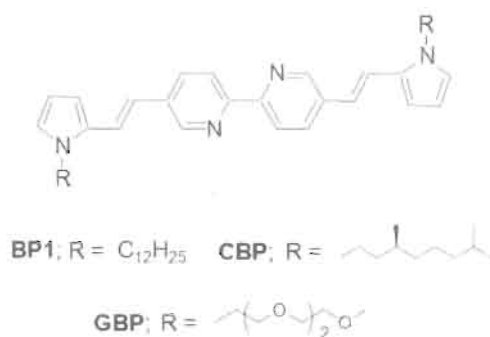
**Figure 3.5.** Changes in the a) absorption and b) emission spectra of **4** with increasing equivalents of Zn<sup>2+</sup> ions in THF.

A wide range of reports on efficient Zn<sup>2+</sup> selective fluorescent molecular probes either by fluorescent enhancement or by fluorescence shift, which can be effectively applied in imaging zinc ions in cellular environments, are available in the literature.<sup>4-10</sup> However, attempts to develop practical strategies to the detection of Zn<sup>2+</sup> under aqueous conditions are not many. For example, analytical test strips for heavy metal ions can provide simple and convenient procedures for the onsite analysis and daily monitoring of water quality without using costly instruments. From this view point, Suzuki and coworkers have developed colorimetric analytical test strips for zinc ion detection in ppm range (Figure 3.6).<sup>22</sup> This was obtained by filtering the dispersion of the hydrophobic indicator azo dyes, 1-(2-pyridylazo)-2-naphthol (**5**) in the form of nanoparticles or nanofibers through

cellulose ester membrane filters, which gave a uniform coating of the dye on the surface. Presence of Zn<sup>2+</sup> could be detected by a color change from yellow to pink.



the chiral side chain (**CBP**) exhibits strong solid state fluorescence which is useful for the detection of  $\text{Zn}^{2+}$  in aqueous conditions. For comparison of the fluorescence properties an achiral derivative **BP1** was also prepared. Details of these studies are presented.

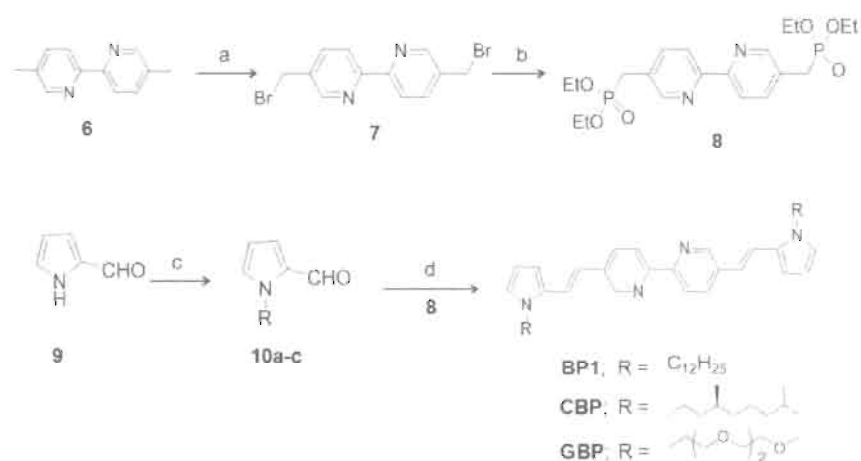


### 3.3. Results and Discussion

#### 3.3.1. Synthesis of $\text{Zn}^{2+}$ Probes

The bispyrroles **BP1**, **CBP** and **GBP** were prepared as shown in Scheme 3.2. Bromination of 5, 5'-dimethyl-2, 2'-bipyridine (**6**) was carried out with *N*-bromosuccinimide. The bisbromomethyl derivative **7** was converted to the corresponding bisphosphonate ester (**8**) by Michaelis-Arbuzov reaction in 70-80% yields. The Wittig-Horner-Emmons olefination reaction of the bisphosphonate ester **8** with the corresponding *N*-alkylpyrrole-2-carboxaldehydes **10a-c** provided the bispyrroles **BP1**, **CBP** and **GBP** in 40-50% yields. The compounds were purified by column chromatography and characterized by FT-IR, NMR and mass

spectral analyses. The all *trans* configuration of the bispyrroles were confirmed from the coupling constants ( $J = 16\text{-}17\text{ Hz}$ ) obtained from their <sup>1</sup>H NMR spectra.



**Scheme 3.2.** Reagents and conditions: a) NBS, CCl<sub>4</sub>, 18 h; b) P(OEt)<sub>3</sub>, 100 °C, 12 h; c) 1-Bromo alkyl chain, potassium *t*-butoxide, THF, 27 °C, 21 h; d) NaH, THF, 70 °C, 10 h.

### 3.3.2. Optical Properties

In polar solvents, the bispyrroles exhibited broad absorption around 350-450 nm without noticeable difference in spectral shape from each other. The absorption maxima in the range of 390-430 nm showed minor shift with polarity of the solvent, whereas the emission spectra showed considerable solvatochromic shift. As representative examples, the solvent dependent absorption and emission properties of **GBP** and **CBP** are shown in Figure 3.7 and 3.8, respectively. For example, in toluene, **GBP** showed an absorption maximum at 412 nm. Change of

the solvent from toluene to acetonitrile resulted in a mere blue shift of 5 nm with absorption maximum around 407 nm (Figure 3.7a). The fluorescence emission spectra of the bispyrroles **BPI**, **CBP** and **GBP** showed intense emission with high fluorescence quantum yields. As the solvent is changed from toluene to acetonitrile, the emission became broad with a red shift. For example, in toluene, **GBP** showed a structured emission with two maxima at 463 nm and 490 nm. In chloroform the absorption is red shifted and a new maximum at 503 nm is observed. When the solvent is changed to acetonitrile, the emission is red shifted to 537 nm (Figure 3.7b).

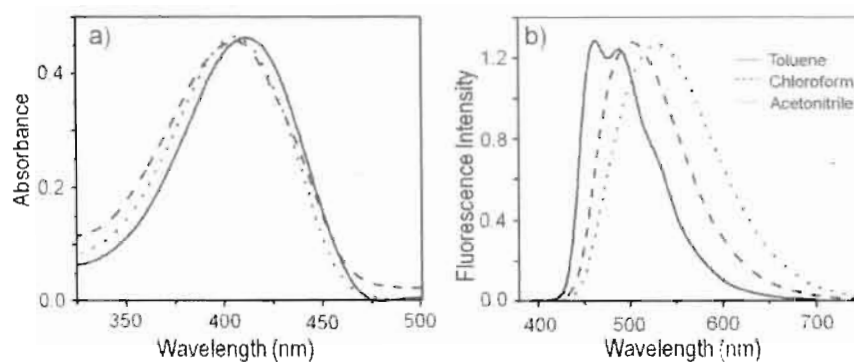


**Figure 3.7.** a) Absorption and b) emission spectra of **GBP** in toluene, chloroform and acetonitrile ( $c = 6 \times 10^{-6}$  M,  $\lambda_{ex} = 415$  nm).

The spectral property of **CBP** is more or less similar to those of **GBP**. In three different solvents ranging from toluene to acetonitrile, only a small blue shift of 3 nm was observed for the absorption maxima of **CBP** around 400 nm (Figure

3.8). As the polarity of the solvent is increased from toluene to acetonitrile, 41 nm red shift in the emission maxima is observed. The **CBP** derivative exhibited an absorption maximum at 408 nm ( $\pi$ - $\pi^*$  transition,  $\epsilon = 4.81 \times 10^4 \text{ M}^{-1} \text{ cm}^{-1}$ ) and an emission maxima at 537 nm ( $\Phi_f = 0.51$ ) (Figure 3.8b) in acetonitrile.

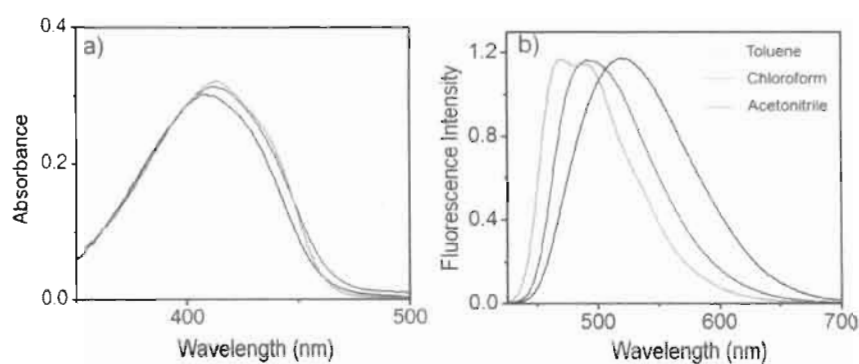


**Figure 3.8.** a) Absorption and b) emission spectra of **CBP** in various solvents like toluene, chloroform and acetonitrile ( $c = 6 \times 10^{-6} \text{ M}$ ,  $\lambda_{ex} = 415 \text{ nm}$ ).

Interestingly, the bispyrrole derivative **CBP** appended with chiral side chains showed strong green emission in the solid state (Figure 3.9 and Table 3.1). This observation is in contrast to the properties of **BPI** and **GBP** which did not show any measurable solid state fluorescence response. This phenomenon has been observed in many other cases. For example, enhanced solid state fluorescence has been reported in some *p*-phenylenevinylene derivatives.<sup>23, 26</sup> Adjustment of the tilt angle between the long axes of the transition dipole of adjacent molecules in the solid state is responsible for the enhanced emission in these molecules. In view of

this observation, the enhanced solid state fluorescence of **CBP** could be ascribed to the asymmetric carbon induced helical twist, resulting in the formation of emissive aggregates. Detailed cation binding properties of **CBP** were conducted in acetonitrile and found that **CBP** is highly selective to  $Zn^{2+}$  ions.<sup>37</sup> The high solid state luminescence of **CBP** is advantageous for the development of a reusable sensor for the practical detection of  $Zn^{2+}$  under aqueous conditions.

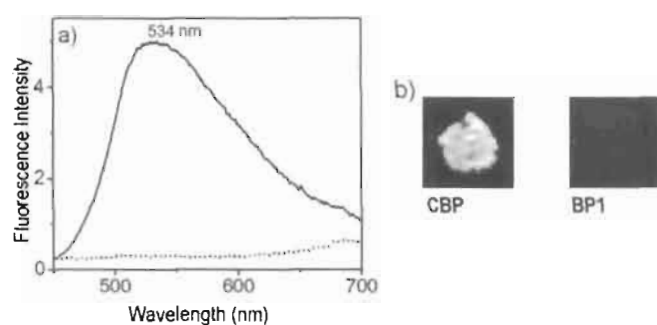


**Figure 3.9.** a) Solid state emission spectra of **CBP** (—) and **BP1** (...) ( $\lambda_{ex}$  = 440 nm). b) Photograph showing solid state fluorescence of **CBP** and **BP1**.

The fluorescence quantum yields ( $\Phi_f$ ) of the bispyrroles in toluene, chloroform and in acetonitrile were determined using quinine sulfate as the standard. The  $\Phi_f$  value in toluene is found to be higher than that in chloroform and acetonitrile. All the bispyrroles under study showed quantum yields above 0.4 in acetonitrile. The fluorescence lifetime measurements in acetonitrile showed a monoexponential decay in all cases. The excited state lifetimes ( $\tau$ ) of **BP1**, **CBP** and **GBP** are found to be high in acetonitrile ( $\tau$  = 1.96, 1.94, 1.86 ns, respectively).

when compared to those values in toluene. The optical characteristics of the bispyrroles under study are listed in Table 3.1.

**Table 3.1.** Photophysical parameters of **BP1**, **CBP** and **GBP** in acetonitrile solution and in the solid state.

Compound	Acetonitrile			Solid-state		
	$\lambda_{\text{abs}}$ (nm) <sup>[a]</sup>	log $\epsilon$	$\lambda_{\text{em}}$ (nm) <sup>[a]</sup>	$\Phi_{\text{f}}$ <sup>[b]</sup>	$\lambda_{\text{em}}$ (nm) <sup>[c]</sup>	$\Phi_{\text{f}}$ <sup>[d]</sup>
<b>BP1</b>	406	4.20	537	0.43	NE <sup>[e]</sup>	NE <sup>[e]</sup>
<b>CBP</b>	408	4.74	537	0.51	534	0.460
<b>GBP</b>	408	4.89	537	0.51	NE <sup>[e]</sup>	NE <sup>[e]</sup>

[a] Determined in spectroscopic grade acetonitrile. [b] Fluorescence quantum yields ( $\pm 5\%$  error) were determined using quinine sulphate as the standard ( $\Phi_{\text{f}} = 0.546$  in 1 N H<sub>2</sub>SO<sub>4</sub>). [c] Solid-state emission ( $\pm 2\%$  error) was recorded using a combination of spectrofluorimeter and integrated sphere. [d] Quantum yield measured using equation 1. [e] No detectable emission.

### 3.3.3. Solid State Quantum Yield Measurements of CBP

Solid state quantum yield of **CBP** was calculated by Horiba Jobin Yvon Quantum Yield Calculator using equation 1.<sup>28,29</sup>

$$\Phi_{\text{f(solid state)}} = E_1(\lambda) - (1 - A)E_2(\lambda) / I_{\text{sc}}(\lambda)A \dots \dots \dots (1)$$

$$\{A \text{ (film absorbance)} = L_{\text{f}}(\lambda) - I_{\text{t}}(\lambda) / I_{\text{a}}(\lambda)\}$$

where  $E_i(\lambda)$  and  $E_{ii}(\lambda)$  are respectively, the integrated luminescence as a result of the direct excitation of the film and as secondary excitation.  $L_0(\lambda)$  and  $L_1(\lambda)$  are integrated excitations when the excited light directly hits the sphere, and when the film is directly excited.  $L_e(\lambda)$  is the integrated excitation profile for an empty sphere (Figure 3.10a).

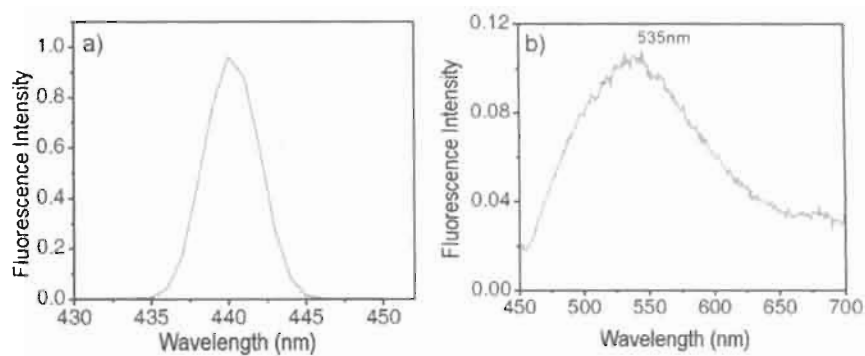


**Figure 3.10.** a) Magnification of excitation lines. Red solid line gives  $L_0$  parameter (integrated excitation when the light directly hits the sphere in the absence of sample film). Dashed line gives  $L_1$  parameter (integrated excitation when the sample film is directly excited). b) Photoluminescence of CBP in PMMA matrix. The fluorescence quantum yield of the emission in the film state is calculated as described above.

### 3.3.4. Circular Dichroism Studies of CBP

As discussed earlier, the chiral center in the side chain of **CBP** can induce chirality to the attached chromophores in the aggregated state. The enhanced solid state emission of **CBP** could be due to the helical twist in the aggregates which may weaken the  $\pi$ -interaction between the molecules. Circular dichroism (CD) spectroscopy is a useful tool for the detection of chiral induction and helical

organization of chromophores in the aggregated state. In order to confirm this, we conducted circular dichroism measurements in the solution as well as in the solid state.

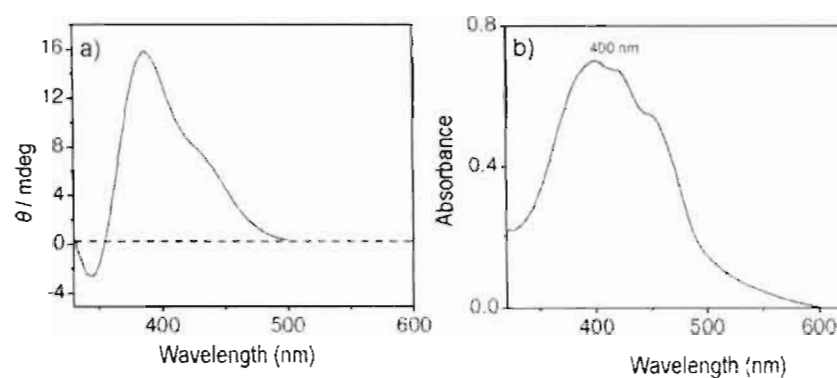


**Figure 3.11.** a) Circular dichroism spectra of CBP in the solid state (—) and in acetonitrile (---) ( $6 \times 10^{-6}$  M) and b) the corresponding absorption spectrum in the solid state.

In acetonitrile solution CBP ( $6 \times 10^{-6}$  M) is CD silent (Figure 3.11a). However, in the solid state significant CD response was obtained which may be due to the helical twist in the molecular aggregates. Furthermore, the CD spectrum is weak and nonbisignate, indicating a weak exciton coupling, probably due to the disorganized aggregation process, which prevents fluorescence quenching of CBP in the solid state.

### 3.3.5. Cation Binding Properties of CBP

Detailed metal ion titration study of CBP was conducted using alkali, alkaline and transition metal cations in acetonitrile. Titration of alkali and alkaline

metal cation perchlorates did not show much change to the optical properties of **CBP**. However, addition of transition metal ions such as  $\text{Ni}^{2+}$ ,  $\text{Co}^{2+}$ ,  $\text{Hg}^{2+}$ ,  $\text{Mn}^{2+}$  and  $\text{Zn}^{2+}$  imparts significant decrease in the absorption maxima at 408 nm with the concomitant formation of a new red shifted band at 454 nm. Most importantly, the emission of **CBP** at 537 nm was significantly quenched by  $\text{Cu}^{2+}$ ,  $\text{Hg}^{2+}$ ,  $\text{Co}^{2+}$  and  $\text{Mn}^{2+}$ , whereas the titration of  $\text{Zn}^{2+}$  resulted in a red shifted orange-red emission at 637 nm (Figure 3.12).

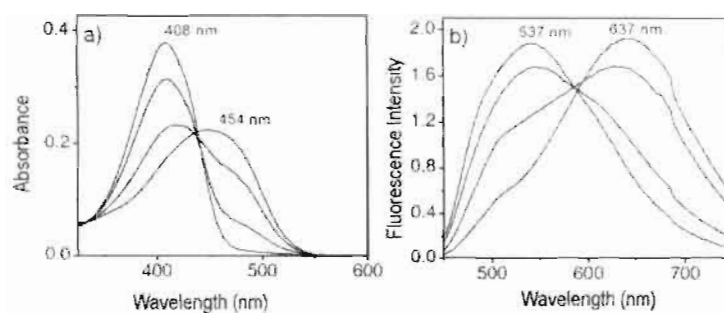


**Figure 3.12.** Changes in the a) absorption and b) emission spectra of **CBP** (6  $\mu\text{M}$ ) upon addition of  $\text{Zn}^{2+}$  (0-6  $\mu\text{M}$ ) in acetonitrile.

The observed red shift in the emission of **CBP** at 537 nm in solution (acetonitrile) when complexed with  $\text{Zn}^{2+}$  can be easily followed visually (Figure 3.13). The deep green fluorescence changes to orange-red when **CBP** complexed with  $\text{Zn}^{2+}$  ions. Binding of **CBP** with other transition metal ions such as  $\text{Cu}^{2+}$ ,  $\text{Ni}^{2+}$ ,  $\text{Co}^{2+}$  and  $\text{Mn}^{2+}$  resulted in significant quenching of emission at 537 nm. Binding of the cations leads to a red shift in absorption and emission maxima in

response to planarization of the bipyridyl unit with extended conjugation length, in conjunction with perturbation of the electronic system. Although many transition metals induce such a response, a selective fluorescence response to Zn<sup>2+</sup> can be achieved because, Zn<sup>2+</sup> has a closed-shell d<sup>10</sup> configuration and is diamagnetic; thus fluorophore appended ligands tend to remain emissive. In contrast, other metal ions likely to be encountered in the environment, such as Fe<sup>3+</sup> and Cu<sup>2+</sup>, are paramagnetic and are typically efficient emission quenchers. Heavier d<sup>10</sup> ions such as Cd<sup>2+</sup> and Hg<sup>2+</sup> also tend to yield less emissive complexes due to the fluorescence quenching via the classic heavy atom effect.

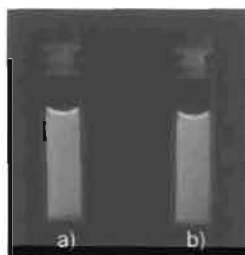


**Figure 3.13.** Visual fluorescence change of **CBP** ( $6 \times 10^{-6}$  M) in acetonitrile a) before and b) after binding with one equivalent of Zn<sup>2+</sup> ions.

The solid state emission of **CBP** after dispersing in a poly(methylmethacrylate) (PMMA) film before and exposure to zinc ions are shown in Figure 3.14a and Figure 3.14b, respectively. As expected, **CBP** exhibited an emission maximum at 535 nm with a high quantum yield which is ca. 25 times higher than that of **BP1** in PMMA matrix ( $\Phi_f = 0.018$ ). When the **CBP** dispersed PMMA film was immersed in a solution of Zn(ClO<sub>4</sub>)<sub>2</sub> ( $3 \times 10^{-4}$  M) in acetonitrile-

water (50% v/v), the absorption peak at 400 nm was red shifted to 484 nm. Similarly,  $\text{Cu}^{2+}$ ,  $\text{Hg}^{2+}$ ,  $\text{Ag}^+$ , and  $\text{Fe}^{3+}$  showed significant red shift to the absorption spectra revealing that these changes are not specific to  $\text{Zn}^{2+}$  ions. However, the fluorescence response was specific for  $\text{Zn}^{2+}$  ions. The fluorescence of **CBP** was significantly quenched with cations such as  $\text{Cu}^{2+}$ ,  $\text{Hg}^{2+}$ ,  $\text{Ag}^+$ , and  $\text{Fe}^{3+}$  except for  $\text{Zn}^{2+}$ . In the case of  $\text{Zn}^{2+}$ , the emission maximum was shifted to 640 nm with significant visual color change from green to red, thus allowing the specific visual detection (Figure 3.14b).

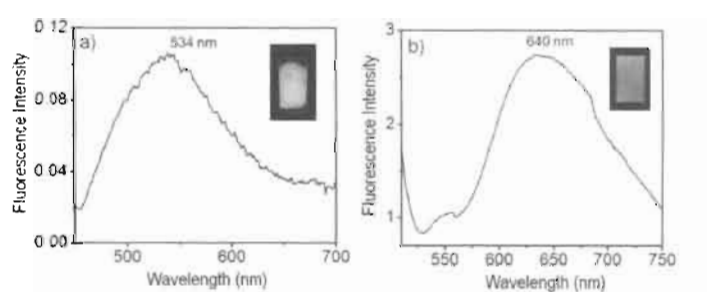


**Figure 3.14.** Solid state emission spectra of **CBP** in PMMA matrix, a) in the absence and b) in the presence of  $\text{Zn}^{2+}$  ions. Insets show emission colors of **CBP** and **CBP-Zn<sup>2+</sup>** complex in PMMA matrix when illuminated using 365 nm UV light.

The selectivity of the probe towards  $\text{Zn}^{2+}$  is tested by preparing a **CBP** coated plate which exhibited a bright greenish yellow fluorescence (Figure 3.15). Aqueous solutions of different metal salts ( $5 \times 10^{-3}$  M) were spotted on the plate, individually and as mixtures. Analysis of this plate reveals that the fluorescence of **CBP** changes from greenish-yellow to red in selective response to  $\text{Zn}^{2+}$  ions

(spots a-d). Promisingly, in a mixture of alkali, alkaline earth and transition metal cations that are mixed with Zn<sup>2+</sup> showed the red emission of the Zn<sup>2+</sup>-CBP complex, revealing the high selectivity of the probe. On the other hand, Ag<sup>+</sup>, Cu<sup>2+</sup>, Fe<sup>2+</sup>, and Hg<sup>2+</sup> salts which are spotted individually resulted in dark spots (spots e-h) due to fluorescence quenching whereas Na<sup>+</sup>, K<sup>+</sup>, Ca<sup>2+</sup> and Mg<sup>2+</sup> salts did not change the fluorescence of CBP much. A quantitative analysis of the specificity of Zn<sup>2+</sup> sensing in the solid state was carried out by measuring the relative fluorescence intensity of the CBP in the absence and presence of cations. Plots of the relative fluorescence intensities against the corresponding cations indicate that Zn<sup>2+</sup>, in the absence and presence of other cations, exhibits maximum relative fluorescence intensity (Figure 3.15b). Thus, a selective screening of Zn<sup>2+</sup> is possible by monitoring the emission color under illumination.

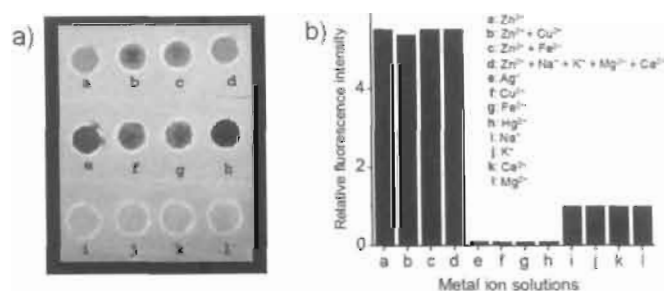


**Figure 3.15.** a) Screening of various metal ion solutions in water under neutral pH on a CBP coated plate under 365 nm UV-illumination. b) Plot of fluorescence intensity of CBP. a) Zn<sup>2+</sup>, b) Zn<sup>2+</sup> + Cu<sup>2+</sup> (1:1), c) Zn<sup>2+</sup> + Fe<sup>2+</sup> (1:1), d) Zn<sup>2+</sup> + Na<sup>+</sup> + K<sup>+</sup> + Mg<sup>2+</sup> + Ca<sup>2+</sup>(1:1:1:1:1), e) Ag<sup>+</sup>. f) Cu<sup>2+</sup>,

g)  $\text{Fe}^{2+}$ , h)  $\text{Hg}^{2+}$ , i)  $\text{Na}^+$ , j)  $\text{K}^+$ , k)  $\text{Ca}^{2+}$  and l)  $\text{Mg}^{2+}$  [metal ion concentration ( $5 \times 10^{-4} \text{ M}$ )]. The relative fluorescence intensity of CBP in presence of  $\text{Na}^+$  was taken as unity for normalization.

### 3.3.6. Design of Reusable Dipstick Probe for Zinc Ions using CBP

The above results encouraged us to develop a dipstick probe for the detection of  $\text{Zn}^{2+}$  in water, completely avoiding organic solvents.<sup>50</sup> For this purpose, CBP was adsorbed on alumina, a slurry of which was coated on a thermoplastic stick as support (Figure 3.16). The prepared stick as such was used for the detection purpose.

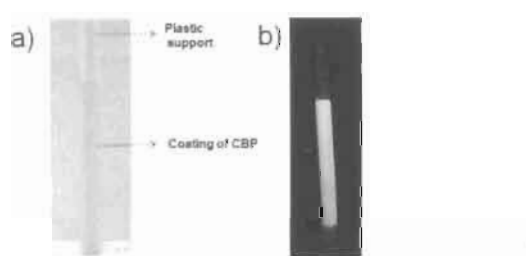


**Figure 3.16.** Photographs of dipstick coated with CBP in alumina matrix a) under ambient light, b) under 365 nm UV illumination.

The performance of the stick was tested by dipping it into a  $\text{Zn}(\text{ClO}_4)_2$  solution ( $5 \times 10^{-2} \text{ M}$ , 15 mL) in water under neutral pH. The color of the stick wherever in contact with  $\text{Zn}^{2+}$  was changed from greenish-yellow to orange which was accompanied by a fluorescence change from greenish yellow to deep red (Figure 3.17), upon illumination with 365 nm UV light. The detection limit of

**CBP** to  $Zn^{2+}$  in solution is in the order of  $10^{-7}$  M whereas in the solid state the visible detection limit is in the range of  $10^{-4}$  M.

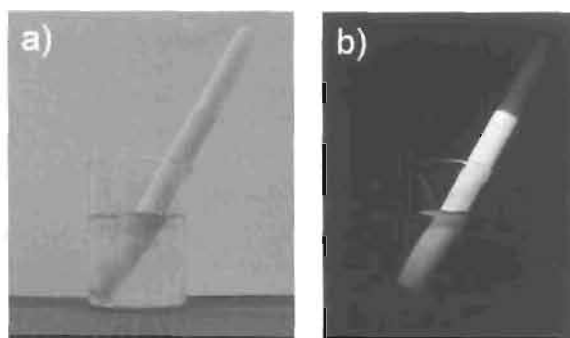


**Figure 3.17.** Photographs of dipstick coated with **CBP** in alumina matrix after immersing in aqueous medium (pH 7.2) containing  $Zn^{2+}$  ions ( $5 \times 10^{-4}$  M) a) in ambient light, b) under 365 nm UV illumination.

In the case of aqueous solutions containing cations such as  $Cu^{2+}$  and  $Fe^{3+}$  etc., the green emission of the stick is completely quenched. Comparison of the performance of the stick with  $Zn^{2+}$  and  $Cu^{2+}$  is shown in Figure 3.18. Alkali and alkaline earth metal cations such as  $Na^+$ ,  $K^+$ ,  $Ca^{2+}$  and  $Mg^{2+}$  (Figure 3.19) did not affect the green fluorescence of **CBP**. When the stick was dipped in a solution containing  $Fe^{3+}$ ,  $Cd^{2+}$  and  $Hg^{2+}$ , a visual color change has occurred in the surface of the stick, which indicates the binding of metal ions. However, in these cases, the fluorescence corresponding to the **CBP** derivative is completely quenched. Thus, only  $Zn^{2+}$  resulted in a fluorescence signal thereby making it possible to selectively sense  $Zn^{2+}$ .

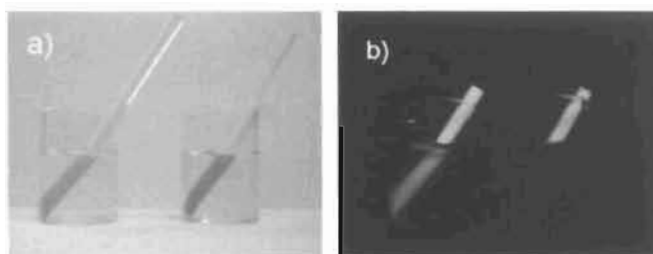


**Figure 3.18.** Photographs of dipstick coated with CBP after immersing in aqueous medium (pH 7.2) containing  $Zn^{2+}$  ( $5 \times 10^{-4}$  M) and  $Cu^{2+}$  ( $5 \times 10^{-4}$  M), a) under ambient light, and b) under 365 nm UV illumination for comparison.

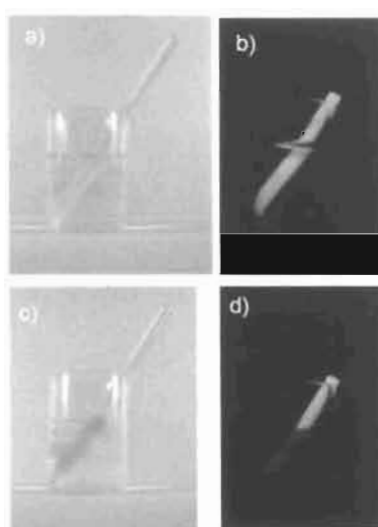


**Figure 3.19.** Photographs of the dipsticks coated with CBP after immersing in aqueous medium (pH 7.2) containing mixture of. a, b) alkali and alkaline earth metal cations such as  $Na^+$ ,  $K^+$ ,  $Ca^{2+}$  and  $Mg^{2+}$  and c)  $Fe^{2+}$  ( $5 \times 10^{-4}$  M). a, c) Under ambient light, and b, d) under 365 nm UV illumination.

The important criteria for the successful use of a practical sensor are its reusability and ability to detect a specific cation in the vicinity of other competing ions. In the present case, the reusability of the dip stick for the detection of  $Zn^{2+}$  was tested after washing the used stick with EDTA solution. Since EDTA is a good  $Zn^{2+}$  chelator, decomplexation of the bound cation occurs upon washing with EDTA solution. After washing and drying, the initial greenish yellow fluorescence of the stick was regained and was hence ready for another trial (Figure 3.20).

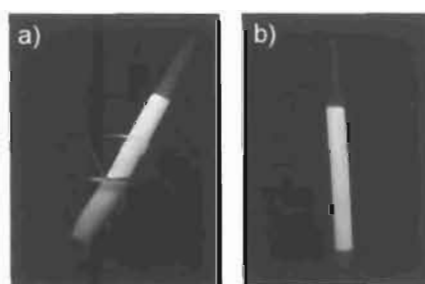


**Figure 3.20.** a) Photograph of dipstick coated with CBP after immersing in aqueous medium (pH 7.2) containing  $Zn^{2+}$  ( $5 \times 10^{-4}$  M) illuminated with 365 nm UV-light. b) Photograph of the dipstick used in (a) after washing with EDTA solution followed by illumination with UV-light.

The regenerated stick upon immersion in an aqueous solution of  $Zn^{2+}$  exhibited the bright red emission when illuminated. These processes were repeated 10 times without the loss of the emission intensity to any considerable extent, indicating the reusability of the probe even more number of times.

### 3.3.7. Cation Binding Properties of GBP

The bispyrrole derivative **GBP** with oxyethylene side chain showed better solubility in aqueous environments. Detailed metal ion binding studies were conducted and found that **GBP** shows selective fluorescence changes only with zinc ions. Figure 3.21 shows the change in absorption and emission spectra of **GBP** in 8:2 water-acetonitrile mixture (pH 7.2, HEPES, 0.01 M) upon addition of  $\text{Zn}(\text{ClO}_4)_2$  solution. Addition of zinc perchlorate induced a red shift in the absorption maximum at 403 nm to 450 nm through an isosbestic point at 430 nm. The Job plot and the Benesi-Hildebrand plot for the binding of  $\text{Zn}^{2+}$  to **GBP** shows 1:1 stoichiometry.

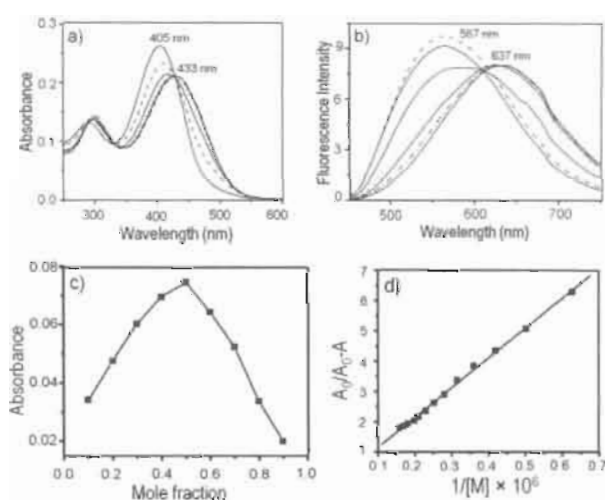


**Figure 3.21.** Changes in the a) absorption and b) emission spectra of **GBP** ( $6 \mu\text{M}$ ) with the addition of  $\text{Zn}^{2+}$  ( $0.6 \mu\text{M}$ ) in 8:2 water/acetonitrile (HEPES, pH 7.2). c) Job plot and d) Benesi-Hildebrand plot showing the binding of **GBP** to  $\text{Zn}^{2+}$  (in 8:2 water/acetonitrile).

The selectivity of **GBP** towards zinc ions were investigated by conducting the detailed metal ion titration experiments in presence of other bio-relevant metal cations. Alkali and alkaline earth metal cations exhibit no change in the absorption and emission properties of **GBP** and found that in a mixture of these cations the probe shows selectivity towards Zn<sup>2+</sup> ions (Figure 3.22a). For biological applications, it is necessary to establish that the metal ion binding and the corresponding changes in the photophysical properties should occur under aqueous biological pH. For this purpose, detailed study of the effect of pH on emission properties of **GBP** was carried out. The fluorescence changes of **GBP** and **GBP-Zn<sup>2+</sup>** complex are rather insensitive to changes in pH of the solution ranging from 6.4-7.4 except for a slight change in the intensity of the emission. In acidic pH range (<6.8), the fluorescence intensity of **GBP** is found to be very low due to the protonation at the bipyridine binding site. A plot of the fluorescence intensity variation in the pH range of 6.6-7.4 indicates that the emission is stable between pH 6.8-7.2 (Figure 3.22b).

### 3.3.8. Cell imaging study with GBP

We have examined the application of **GBP** for imaging Zn<sup>2+</sup> ions in cellular environments by using cultured **MCF-7** (human breast cancer) cell lines. Due to the presence of glycol side chain, the permeability of **GBP** through cell membrane was expected to be high. The cell lines were first incubated with 6  $\mu$ M **GBP** for about 30 min, which is sufficient for the cellular accumulation. After washing, the

stained cells were examined using a Leica fluorescence microscope at an excitation wavelength of 440 nm. Even though the intensity of emission from **GBP** decreases to a considerable extent, a bright green fluorescence was observed from the intracellular regions of **MCF-7** cell lines, which indicates the penetration of **GBP** inside the cell lines (Figure 3.23 a-b). The overlay image clearly shows the intracellular penetration of **GBP** in **MCF-7** cell lines (Figure 3.23c).

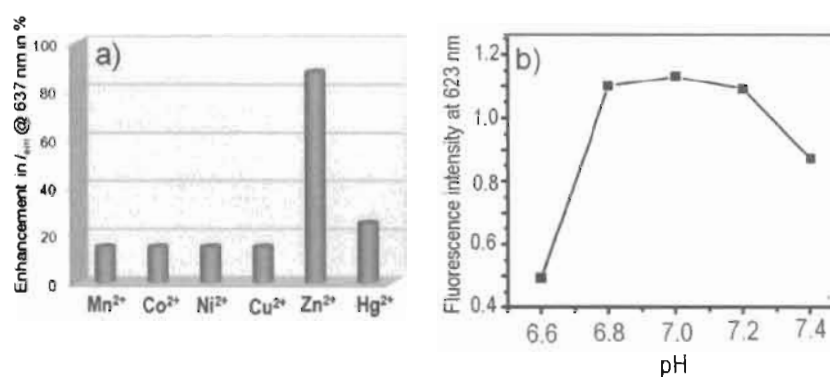


**Figure 3.22.** a) Plot of fluorescence intensity of **GBP** monitored at 637 nm with different metal ions in water/acetonitrile 8:2 mixture. b) Emission intensity variation of **GBP** after addition of  $Zn^{2+}$  monitored at 637 nm.

The intracellular  $Zn^{2+}$  imaging was conducted by loading the MCF cell lines with  $4 \mu M$   $Zn^{2+}$  for about 15 min. The  $Zn^{2+}$  loaded cells were incubated with **GBP** ( $6 \mu M$ ) for about 30 min. The cells were then examined using fluorescence microscopy with an excitation wavelength of 440 nm. The green emission was changed to deep red fluorescence corresponding to **GBP**- $Zn^{2+}$  complex (Figure

3.23 d-e). The overlay image clearly indicates the intracellular accumulation of **GBP** which in turn indicates complexation of zinc ions with the cell permeable derivative (Figure 3.23f). Thus, **GBP** has been proved as an excellent probe for the selective detection of zinc ions in cellular environments.

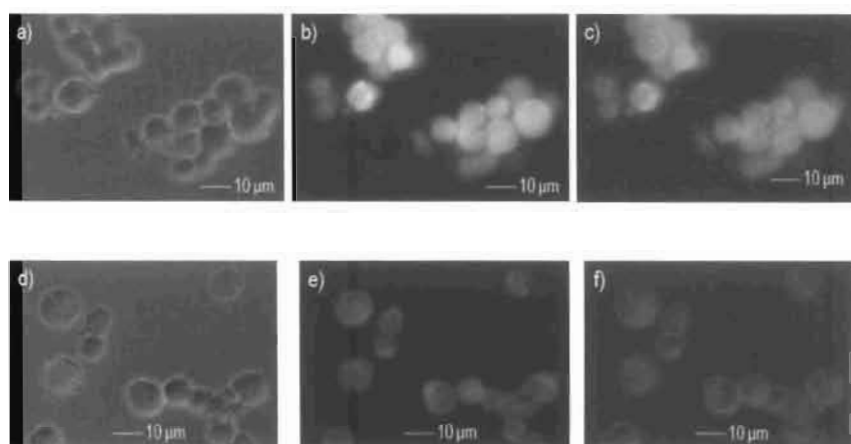


**Figure 3.23.** Epifluorescence images of **MCF-7** cell lines. a) Phase contrast image of cell lines incubated with **GBP**. b) Dark field image showing the fluorescence of **GBP**. c) Overlay image of a and b. d) Phase contrast image, e) dark field image and f) overlay image of d and e of Zn<sup>2+</sup> containing cells after incubation with **GBP**.

### 3.4. Conclusions

The 2, 2'-bipyridine bridged fluorophores as described are found to be useful for the imaging and detection of Zn<sup>2+</sup> ions in cellular as well as in aqueous conditions. The glycol chain attached derivative **GBP** is found to be suitable for the intracellular imaging of zinc ions. The cellular uptake of **GBP** and imaging Zn<sup>2+</sup> ions using **GBP** were demonstrated with **MCF-7** cell lines. Apart from this,

we found that the chiral bipyridyl ligand (CBP) exhibited 25 times more fluorescence in PMMA matrix and in the powder form when compared to an analogous achiral derivative. This phenomenon has been exploited to the fabrication of a reusable solid state fluorescent dipstick which selectively detects  $Zn^{2+}$  in presence of other competing cations in water. The present strategy which uses the property of enhanced solid state emission of a chiral organic fluorophore for the visual detection of a biologically relevant cation in water is a novel approach when compared to other known methods. Moreover, this method allows the imaging of  $Zn^{2+}$  in analytical samples which expand the future scope of this strategy.

### 3.5. Experimental Section

#### 3.5.1. Synthesis and Characterization

All solvents were purified and dried by standard methods prior to use. Melting points were determined with a Mel-Temp-II melting point apparatus. NMR spectra were recorded on 300 MHz Bruker Avance DPX spectrometer. FT-IR spectra were recorded on a Nicolet Impact 400D infrared spectrophotometer. High-resolution mass spectra were obtained on a JEOL JM AX 505 HA mass spectrometer. Electronic absorption spectra were recorded on a Shimadzu UV-3101 PC NIR scanning spectrophotometer and the emission spectra were measured on a SPEX-Fluorolog F112X spectrofluorimeter. CD spectra were

recorded on JASCO-J-810 spectropolarimeter equipped with a JASCO PTC-423S Peltier type temperature control system.

### 3.5.2. Preparation of 5, 5'-Bis(bromomethyl)-2, 2'-bipyridine (7)

To a solution of 5, 5'-dimethyl-2, 2'-bipyridine (6) (1.84 g, 10 mmol) in 50 mL of dry carbontetrachloride was added *N*-bromosuccinimide (3.5 g, 20.5 mmol) and AIBN. The reaction mixture was refluxed for 18-20 h., cooled, filtered and the solvents were removed under reduced pressure to give the crude product which was further purified by recrystallization from CCl<sub>4</sub>. Yield 80-90%; mp. 188 °C; <sup>1</sup>H NMR (CDCl<sub>3</sub>, 300 MHz) δ (ppm): 8.61 (m, 2H, aromatic), 8.34 (m, 2H, aromatic), 7.79 (m, 2H, aromatic), 4.53 (s, 4H, CH<sub>2</sub>Br); <sup>13</sup>C NMR (CDCl<sub>3</sub>, 75 MHz) δ (ppm): 155.19, 149.27, 137.70, 133.28, 121.25, 29.43.

### 3.5.3. Preparation of 5, 5'-Bis(diethyl phosphonomethyl)-2, 2'-bipyridine (8)

The bisphosphonate (8) was prepared by the reaction of the corresponding bisbromomethyl derivative (7) (680 mg, 2 mmol) with 3 mL of triethyl phosphite at 80-85 °C for 10-12 h followed by the removal of the unreacted triethyl phosphite under vacuum. Yield 90- 95%; <sup>1</sup>H NMR (CDCl<sub>3</sub>, 300 MHz) δ (ppm): 8.30 (m, 2H, aromatic), 8.01 (m, 2H, aromatic), 7.34 (m, 2H, aromatic), 4.14 (m, 8H, OCH<sub>2</sub>), 3.21 (s, 4H, CH<sub>2</sub>P), 1.12 (m, 12H, CH<sub>3</sub>).

#### 3.5.4. Preparation of BP1, CBP and GBP

A suspension of sodium hydride (290 mg, 12 mmol) in dry THF (50 mL) was added slowly to a solution of the tetraethyl 2, 2'-bipyridine-5, 5'-diylbis(methylene)diphosphonate, **8** (0.9 g, 2 mmol) and the respective alkylated pyrrole-2-carbaldehyde **10a-c** (4 mmol) in THF. After refluxing for 12 h, the fluorescent reaction mixture obtained was cooled followed by the removal of THF under reduced pressure to give a pasty residue. The residue was suspended in water and extracted with dichloromethane. The organic layer was washed with brine, dried over Na<sub>2</sub>SO<sub>4</sub> and concentrated to give the crude product, which was further purified by column chromatography over basic alumina using ethyl acetate-petroleum ether as eluent. Yields, melting points, and spectral details of each product are given below.

**BP1**: Yield 48%; mp. 92-93 °C; FT-IR (KBr)  $\nu_{\max}$  2912, 2846, 1699, 1626, 1460, 1288, 1082, 1016, 850, 704 cm<sup>-1</sup>; <sup>1</sup>H NMR (CDCl<sub>3</sub>, 300 MHz)  $\delta$  (ppm): 8.70 (m, 2H, aromatic), 8.30 (d, 2H, aromatic), 7.85 (m, 2H, aromatic), 7.07 (d, 2H, vinylic,  $J = 16.08$  Hz), 6.87 (d, 2H, vinylic,  $J = 16.07$  Hz), 6.71 (s, 2H, aromatic), 6.57 (m, 2H, aromatic), 6.18 (m, 2H, aromatic), 3.98 (t, 4H, NCH<sub>2</sub>), 1.95 (m, 4H, CH<sub>2</sub>), 1.77 (m, 8H, CH<sub>2</sub>), 1.24 (m, 28H, CH<sub>2</sub>), 0.86 (t, 6H, CH<sub>3</sub>); <sup>13</sup>C NMR (CDCl<sub>3</sub>, 75 MHz)  $\delta$  (ppm): 153.97, 147.45, 133.55, 132.68, 130.92, 123.30, 121.46, 120.70, 119.06, 108.56, 107.48, 47.11, 31.89, 31.63, 29.59, 29.54, 29.49, 29.31, 29.19.

26.80, 22.65, 14.07; MALDI-TOF: [M+H]<sup>+</sup> Calcd for C<sub>46</sub>H<sub>70</sub>N<sub>4</sub>, 678.56; found 679.13.

**CBP**: Yield 41%; mp. 82 °C; IR (KBr)  $\nu_{\max}$  2925, 2853, 1699, 1626, 1467, 1209, 1045, 950, 850, 727 cm<sup>-1</sup>; <sup>1</sup>H NMR (CDCl<sub>3</sub>, 300 MHz)  $\delta$  (ppm): 8.70 (s, 2H, aromatic), 8.34 (d, 2H, aromatic), 7.84 (m, 2H, aromatic), 7.05 (d, 2H, vinylic, *J* = 16.02 Hz), 6.85 (d, 2H, vinylic, *J* = 16.08 Hz), 6.71 (s, 2H, aromatic), 6.57 (d, 2H, aromatic), 6.17 (t, 2H, aromatic), 3.97 (m, 4H, NCH<sub>2</sub>), 1.71 (m, 2H, CH), 1.12 (m, 16H, CH<sub>2</sub>), 0.83 (m, 12H, CH<sub>3</sub>); <sup>13</sup>C NMR (CDCl<sub>3</sub>, 75 MHz)  $\delta$  (ppm): 153.87, 147.36, 133.53, 132.58, 130.96, 124.08, 121.20, 120.70, 119.16, 108.37, 107.34, 50.88, 41.27, 30.54, 29.65, 28.56, 23.86, 22.94, 13.98, 10.63; HRMS-FAB: [M+H]<sup>+</sup>: Calculated for C<sub>42</sub>H<sub>58</sub>N<sub>4</sub>: 619.47. Obtained: 619.76.

**GBP**: Yield 45%; (Pasty solid); <sup>1</sup>H NMR (CDCl<sub>3</sub>, 300 MHz)  $\delta$  (ppm): 8.61 (s, 2H, aromatic), 8.29 (d, 2H, aromatic), 7.84 (d, 2H, aromatic), 7.08 (d, 2H, vinylic, *J* = 16.05 Hz), 6.80 (d, 2H, vinylic, *J* = 16.05 Hz), 6.70 (s, 2H, aromatic), 6.51 (m, 2H, aromatic), 6.12 (m, 2H, aromatic), 4.12 (t, 4H, NCH<sub>2</sub>), 3.69 (t, 4H, OCH<sub>2</sub>), 3.49 (m, 12H, OCH<sub>2</sub>), 3.43 (m, 4H, OCH<sub>2</sub>), 3.27 (s, 6H, OCH<sub>3</sub>); <sup>13</sup>C NMR (CDCl<sub>3</sub>, 75.4 MHz)  $\delta$  (ppm): 153.93, 147.69, 133.74, 132.84, 131.42, 123.98, 121.68, 120.94, 119.47, 109.13, 107.70, 72.05, 71.29, 71.00, 70.76, 59.16, 47.06; HRMS-FAB: [M]<sup>+</sup> Calcd for C<sub>30</sub>H<sub>46</sub>N<sub>4</sub>O<sub>6</sub>: 630.77; Found 630.76.

### 3.5.5. Details of the Preparation of Dipstick for Zn<sup>2+</sup> Detection

Thermoplastic or glass rods having 4 mm radius were cut into small units having 10 cm length. 10 mg of CBP was dissolved in 15 mL chloroform. To this solution was added 2 gm of finely powdered alumina. The mixture was kept 10 minutes for the solvent to evaporate off. The assay containing finely powdered alumina was yellow in color with a greenish yellow fluorescence under 365 nm UV illumination. The alumina was coated over the stick up to a length of 5 cm from the bottom of the stick. Agitation of the dipstick in the test sample is preferred to enhance contact between the test area and the analyte to be detected. Agitation was performed manually or mechanically by motion of the dipstick or test sample or both. The dipstick was made reusable after Zn<sup>2+</sup> detection by rinsing with aqueous EDTA solution. After EDTA treatment, the stick was washed with pure water followed by drying.

### 3.5.6. Details of Cell Culturing and Imaging:

#### 3.5.6.1. Preparation of the Culture Medium

The culture medium was prepared by dissolving 8.4 g of RPMI-1640 (Sigma, USA) in one litre of distilled water. Sodium bicarbonate (2 g/L) was added to the medium and pH of the medium was adjusted to 7.3. This medium was then sterilized by passing through sterile filter assembly fitted with 0.22 µm filter (Millipore, USA) using vacuum pump. Later, the medium was stored in pre-sterilized Borosil polypropylene bottles, at 4 °C, for further use.

### 3.5.6.2. Preparation of Complete Medium

To the prepared culture medium an antibiotic mixture (20 µL/mL of 100x concentrate, Sigma, USA) was added. Fetal calf serum (FCS) (Sigma, USA) was also added to the medium to give a final concentration of 10% (to 900 mL medium, 100 mL of FCS was added).

### 3.5.6.3. Cell Revival

Breast cancer cell lines (MCF-7), were stored in cryovials at -180 °C in liquid nitrogen, in a medium containing 70% FCS, 10 % Dimethyl sulfoxide (DMSO) and 20% RPMI-1640 media. For revival, the vials were thawed by placing them in a water-bath maintained at 37 °C. Cells were then transferred into a radiation sterilized culturing flask, T-25cm<sup>2</sup> (Corning, USA) inside the laminar flow. Subsequently, the flask was placed in CO<sub>2</sub> incubator for 2 h. The viable cells, stick to the culture flask while the dead cells remain in the medium. Later the medium was replaced with fresh medium containing 10% FCS and incubated till a monolayer was formed.

### 3.5.6.4. Subculturing of MCF-7 Cells

A 25 cm<sup>2</sup> cell culture flask, which had a uniform monolayer of MCF-7 cells, was taken and its medium was then discarded. Since the MCF-7 cells are adherent in nature, they were trypsinised by using 5 mL of trypsin (0.25%)-EDTA (0.53 mM) buffer containing 0.9% sodium chloride for 5 min. The cells were then transferred to a centrifuge tube and centrifuged at 2000 rpm for 10 min., followed by the

removal of the supernatant. For sub culturing, fresh RPMI-1640 media containing 10 % FCS was added under aseptic conditions. Cells were flushed with the help of pipette tip (1 mL) till all the cells come into the medium. The cells were then diluted in a sterile complete medium at 1:3 times and transferred into fresh culture flasks. Then the flasks were placed inside CO<sub>2</sub> incubator.

#### 3.5.6.5. Cell Imaging

For imaging, the cells were taken after trypsinisation and addition of fresh media. Approximately,  $1 \times 10^6$  cells/mL was incubated with **GBP** (6  $\mu$ M) for 30 min. For the removal of background fluorescence in the medium, the cells were centrifuged at 2000 rpm for 10 minutes and were resuspended in fresh medium. These cells were then imaged using fluorescence microscope at an excitation source of 440 nm.

### 3.6. References

1. H. Hu, M. McCally (ed), *Life Support: Human Health and Heavy Metal Exposure*, Chapter 4, MIT Press, Boston, **2002**.
2. J. P. Desvergne, A. W. Czarnik, Eds. *Chemosensors for Ion and Molecule Recognition*; Kluwer Academic Publishers: Dordrecht, The Netherlands, **1997**.
3. J. R. Lakowicz, *Principles of Fluorescence Spectroscopy*, 2<sup>nd</sup> ed. Kluwer Academic/Plenum: New York, **1999**.
4. E. Kimura and T. Koike, *Chem. Soc. Rev.* **1998**, 27, 179.

5. N. C. Lim, H. C. Freake and C. Brückner, *Chem.-Eur. J.* **2005**, *11*, 38.
6. Z. Dai and J. W. Canary, *New J. Chem.* **2007**, *31*, 1708.
7. S. A. de Silva, A. Zavaleta, D. E. Baron, O. Allam, E. V. Isidor, N. Kashimura, J. M. Percarpio, *Tetrahedron Lett.* **1997**, *38*, 2237.
8. P. Carol, S. Sreejith, A. Ajayaghosh, *Chem. Asian J.* **2007**, *2*, 338.
9. E. L. Que, D. W. Domaille, C. J. Chang, *Chem. Rev.* **2008**, *108*, 1517.
10. D. W. Domaille, E. L. Que, C. J. Chang, *Nat. Chem. Biol.* **2008**, *4*, 168.
11. K. Kikuchi, K. Komatsu, T. Nagano, Zinc sensing for cellular application. *Curr. Opin. Chem. Biol.* **2004**, *8*, 182.
12. G. K. Walkup, S. C. Burdette, S. J. Lippard, R. Y. Tsien, *J. Am. Chem. Soc.* **2000**, *122*, 5644.
13. S. C. Burdette, G. K. Walkup, B. Spingler, R. Y. Tsien, S. J. Lippard, *J. Am. Chem. Soc.* **2001**, *123*, 7831.
14. S. C. Burdette, C. J. Frederickson, W. M. Bu, S. J. Lippard, *J. Am. Chem. Soc.* **2003**, *125*, 1778.
15. C. C. Woodrooffe, R. Masalha, K. R. Barnes, C. J. Frederickson, S. J. Lippard, *Chem. Biol.* **2004**, *11*, 1659.
16. C. C. Woodrooffe, S. J. Lippard, *J. Am. Chem. Soc.* **2003**, *125*, 11458.
17. X. -a. Zhang, D. Hayes, S. J. Smith, S. Friedle, S. J. Lippard, *J. Am. Chem. Soc.* **2008**, *130*, 15788.

18. J. R. Lakowicz, *Principles of Fluorescence Spectroscopy*, 2nd ed., Kluwer Academic/Plenum, New York, **1999**.
19. C. Kaes, A. Katz and M. W. Hosseini, *Chem. Rev.* **2000**, *100*, 3553.
20. A. E. Dennis, R. C. Smith, *Chem. Commun.* **2007**, 4641.
21. L. Zhang, R. J. Clark, L. Zhu, *Chem. Eur. J.* **2008**, *14*, 2894.
22. Y. Takahashi, H. Kasai, H. Nakanishi, T. M. Suzuki, *Angew. Chem. Int. Ed.* **2006**, *45*, 913.
23. J. C. de Mello, H. F. Wittmann, R. H. Friend, *Adv. Mater.* **1997**, *9*, 230.
24. J. Cornil, D. A. dos Santos, X. Crispin, R. Sibey, J. L. Brédas, *J. Am. Chem. Soc.* **1998**, *120*, 1289.
25. J. Cornil, D. Beljonne, J. P. Calbert, J. L. Brédas, *Adv. Mater.* **2001**, *13*, 1053.
26. S. Siddiqui, F. C. Spano, *Chem. Phys. Lett.* **1999**, *308*, 99.
27. A. Ajayaghosh, P. Carol, S. Sreejith, *J. Am. Chem. Soc.* **2007**, *127*, 14962.
28. L.-O. Pålsson and A. P. Monkman, *Adv. Mater.* **2002**, *14*, 757.
29. J. C. de Mello, H. F. Wittmann and R. H. Friend, *Adv. Mater.* **1997**, *9*, 230.
30. S. Sreejith, K. P. Divya, A. Ajayaghosh, *Chem. Commun.* **2008**, 2903.

---

### Excited State Charge Transfer Modulation and Molecular Logic Operations in a Bipyridine Integrated Fluorophore

---

#### 4.1. Abstract

*Construction of molecular systems that respond to chemical inputs are important as analyte sensors and molecular logic gates. In this chapter, details of the synthesis and photophysical properties of a new donor- $\pi$ -acceptor- $\pi$ -donor type fluorophore **10** which is capable of performing multiple Boolean operations is described. The molecule **10**, by virtue of the excited state charge transfer interaction allows reversible modulation of emission from one state to the other in response to multiple chemical inputs resulting in optical outputs at three different wavelengths. The intramolecular charge transfer (ICT) emission of **10** at 574 nm is modulated to give two different emission outputs (464 nm and 488 nm) using different chemical inputs ( $Zn^{2+}$ ,  $H^+$ , and EDTA). Thus, different logic operations such as AND, 2-input-INH, 3-input-INH, IMP and a combination of these logic operations could be achieved. The demonstration of generation of various emission outputs from **10** with respect to the respective chemical inputs are demonstrated using a paper microfluidic technique.*

## 4.2. Introduction

The tremendous pace in the development of information technology is rapidly approaching a limit.<sup>1,2</sup> Alternative materials and operating principles for the elaboration and communication of data in electronic circuits and optical networks must be identified.<sup>3</sup> Molecular computing is predicted as the ultimate solution to overcome the present limitation of computing devices.<sup>4</sup> Their attractive features are the miniaturized dimensions and the high degree of control on molecular design through chemical synthesis. In particular, molecules can be designed to switch from one state to another, when addressed with chemical, electrical, or optical stimulations, to produce a detectable signal output. Binary data can be encoded on the input stimulations and output signals using logic conventions and assumptions similar to those of digital electronics. Thus, binary inputs can be transduced into binary outputs relying on molecular switches. Following these design principles, the three basic logic operations (AND,<sup>5-8</sup> OR,<sup>9,10</sup> YES<sup>11</sup> and NOT<sup>12</sup>) and more complex logic functions (NOR,<sup>13,14</sup> INH,<sup>15,16</sup> XOR<sup>17</sup> and XNOR<sup>18</sup>) have already been demonstrated at the molecular level.

Chemical switches with optical readout are usually based on the photophysical phenomena such as photoinduced electron transfer (PET), photoinduced charge transfer (PCT), electronic energy transfer (EET), excimer/excimer formation and reorganization of electronic structure of transition-metal based chromophores/fluorophores.<sup>19,20</sup> PET-based luminescent

switches can be triggered by various chemical and physical stimuli such as protons, metal cations, anions, neutral organic molecules, and even nanoparticles. Depending on the desired spectral properties and lifetime of the fluorescent switch, the molecular assembly may include various organic (eg. anthracene, pyrene, naphthalimides, pyromellitimide, coumarins, fluoresceins, pyrazolobenzothiazoles, and diphenylpyrazoles) or inorganic fluorophores (eg. polypyridine Ru (II) complexes and lanthanide complexes).<sup>21</sup> Selectivity and sensitivity of these systems are controlled by careful design of the receptor part. The large diversity of possible organic ligands enables the design of fluorophores that respond to a variety of inputs suitable for sensing and logic operations.<sup>22</sup>

Another category of chemically driven optical switches encompasses the phenomenon of photoinduced charge transfer (PCT) systems.<sup>20, 22</sup> In contrast to PET based switches, the receptor and fluorophore (chromophore) moieties are connected in a way that provides extensive orbital delocalization between these two parts. One end of such a molecule needs to be electron rich, while the other side electron poor. Upon interaction with a suitable input, the electron distribution may significantly change, thus varying the optical properties of the switch. In such push-pull systems, photoexcitation leads to redistribution of electron density and generation of dipole moment. If the receptor binds a charged trigger species, the additional charge interacts with the photogenerated dipole, thus modifying the fluorescence spectrum. For example, interaction of a charged species to the donor

moiety (D) will result in the hypsochromic shift of the spectral properties (absorption/emission bands) while interaction with acceptor moiety (A) results in a bathochromic shift of absorption and emission bands (Figure 4.1).

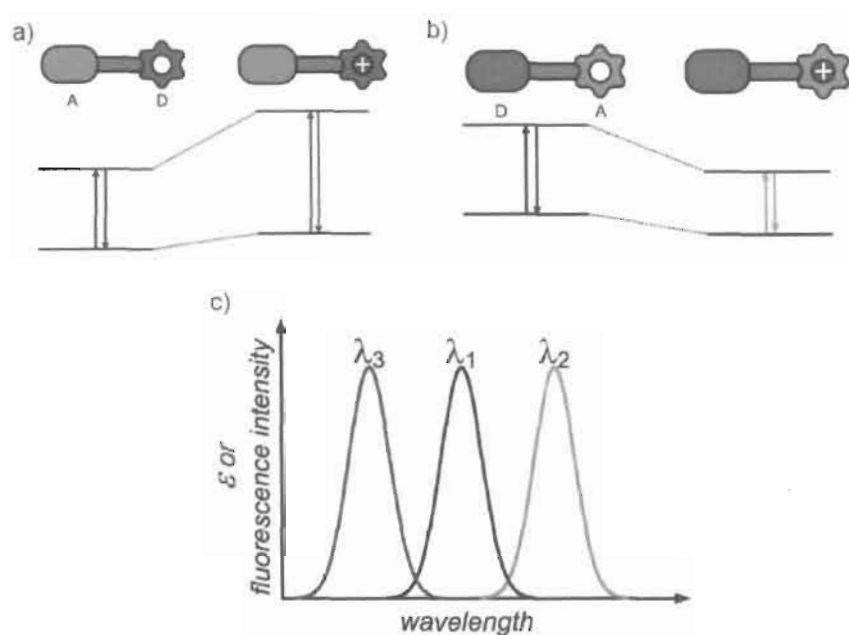


**Figure 4.1.** Principle of the PCT driven luminescent molecular switch based on the donor-spacer-acceptor architecture. Binding of a cationic trigger to the donor (green) moiety results in the hypsochromic shift of the absorption (emission) band (a), and binding of the same trigger to the acceptor moiety (red) results in a bathochromic shift of the corresponding transition (b). The multireceptor system may exhibit both bathochromic and hypsochromic shifts upon binding with different trigger ions (c), which results in a multistate molecular switch.

Tor et al. have reported the switching of CT emission in a phenanthroline appended phenylethyne based D-A-D system, **1**.<sup>23</sup> Increasing the donor strength in the molecular backbone results in a red-shift in the emission of the fluorophore **1a-c** from blue to orange (Figure 4.2). All derivatives exhibit solvatochromic shift from nonpolar to polar solvents. Addition of exogenous ions such as  $Zn^{2+}$  and  $H^+$  to **1b** results in the generation of new emitting species by the modulation of the CT process (Figure 4.3).

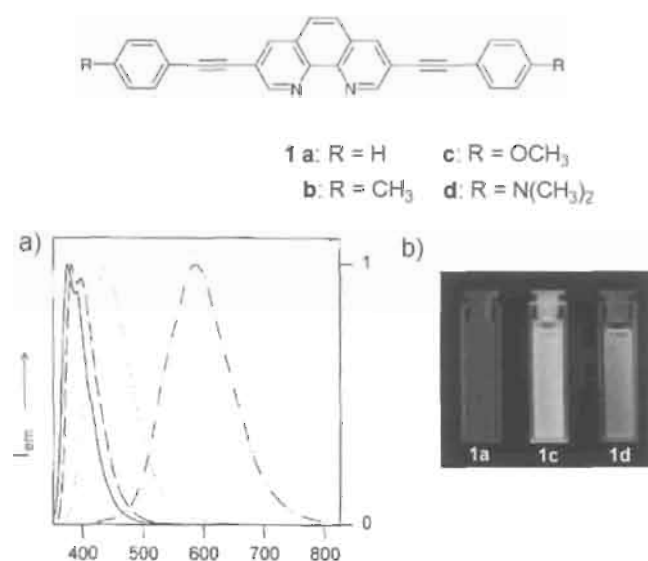


**Figure 4.2.** Conjugated 1,10 phenanthroline derivatives **1a-d**. a) Normalized emission spectra of **1a** (—), **1b** (---), **1c** (····), and **1d** (— ·) in acetonitrile. b) Photograph showing visual emission color change of **1a**, **1c** and **1d**.

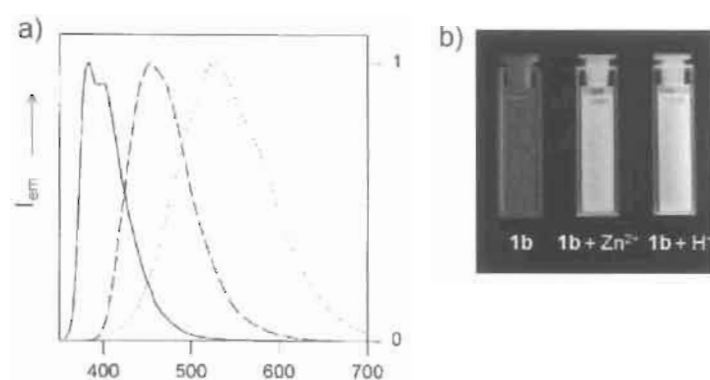
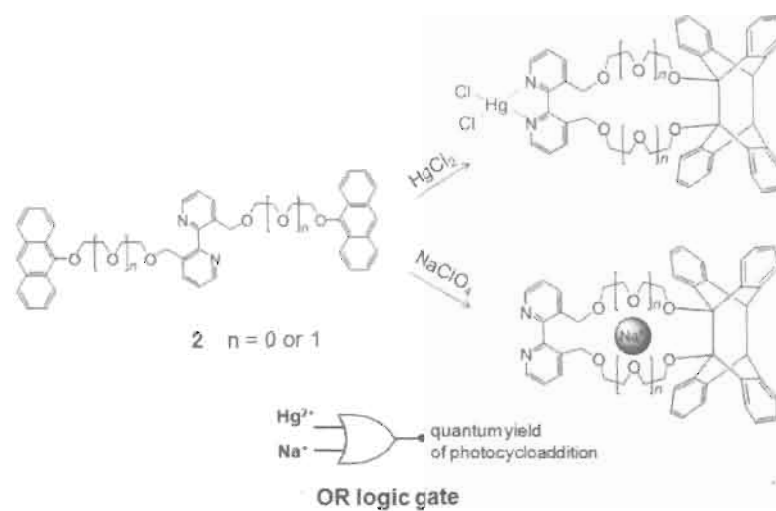


**Figure 4.3.** Normalized emission spectra of **1b** (—), **1b**-excess  $Zn^{2+}$  (---), and **1b**-excess methanesulfonic acid (···) in acetonitrile. b) Photograph showing corresponding visual emission color change with the addition of external inputs.

The main advantage of the PCT switches over the PET switches is the possibility of control on charge transfer interactions and fluorescence modulation which allow the usage of several wavelengths to analyze the state of the switch. From a Boolean logic view point, it enables parallel generation of several binary variables. In other words, it creates numerous independent information channels. In this context, the switches with pronounced concomitant absorption and fluorescence changes are of special interest. Numerous complex logic systems, including a molecular arithmetic device, have been reported in the literature (*vide infra*).

Bipyridyl moiety is known to be a good chelator for transition metal cations.<sup>24</sup> Desvergne et al., have reported a 2, 2'-bipyridine appended

photochromic system **2**, which can perform OR logic operation with respect to  $\text{Hg}^{2+}$  and  $\text{Na}^+$  ions as inputs and fluorescence as the readable output (Scheme 4.1).<sup>25</sup>



**Scheme 4.1.** Schematic representation of the conformational changes in **2** as a result of metal ion interaction and the corresponding representation of OR logic gate.

de Silva and co-workers have reported a molecular logic gate based on an anthracene appended bipyridine derivative **3**.<sup>26</sup> The cation bound receptor is sufficiently electron deficient and planar so as to allow rapid PET process from the anthracene fluorophore. Therefore, significant quenching of the anthracene emission is observed. A NOR operation was followed with respect to changes in fluorescence from **3** based on the chemical input such as  $\text{Zn}^{2+}$  and  $\text{H}^+$  (Figure 4.4).

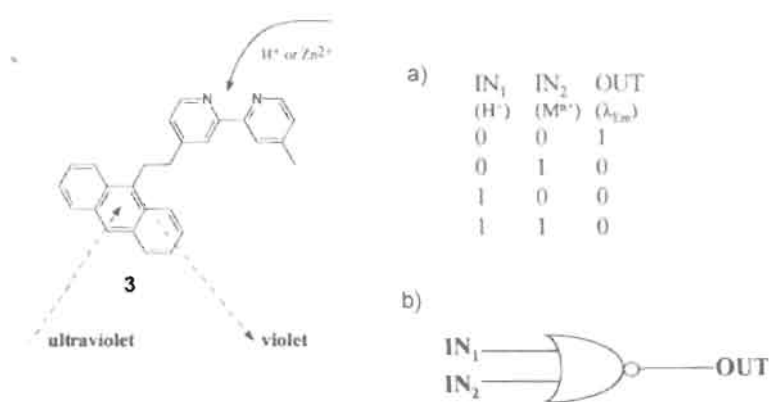


**Figure 4.4.** 2, 2'-bipyridyl based "fluorophore-spacer-receptor" system **3**. a) Truth table corresponding to the fluorescence changes with chemical inputs. b) Representation of the NOR logic gate.

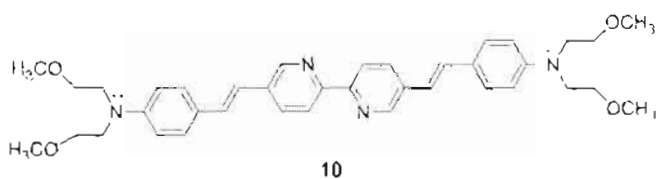
In the present work, synthesis, photophysical properties and molecular logic operations of a D- $\pi$ -A- $\pi$ -D based fluorophore **10**, having 2, 2'-bipyridine and *N, N'* dimethoxy aniline core as the receptor sites are described.

### 4.3. Results and Discussion

#### 4.3.1. The Design Strategy

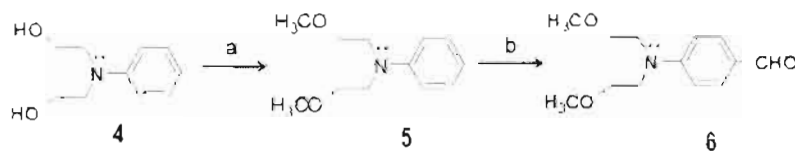
We have designed the bismethoxyethyl aniline derivative **10** based on a donor-acceptor-donor (D-A-D) strategy. The, *N, N*-methoxyethyl substituted aniline moieties are connected to a bipyridine core using two vinylic linkages. Aniline moieties act as strong heteroaromatic donor groups whereas bipyridine moiety acts as the acceptor. In this design, the donor as well as the acceptor moieties acts as receptor sites for various inputs such as H<sup>+</sup> and metal ions, which

allow significant control on the modulation of the excited state properties. Thus, different fluorescence outputs may be generated against different chemical inputs. The optical outputs thus generated from **10** can be defined in terms of different logic operations. With the above design strategy and properties in mind we have designed and synthesized the bipyridine attached fluorophore **10**



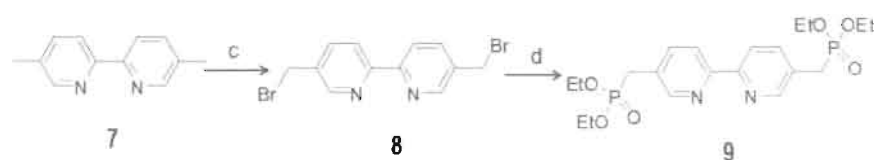
#### 4.3.2. Synthesis of **10**

The required starting materials 4-bis(2-methoxyethyl)amino)benzaldehyde (**6**) and the bisphosphonate ester (**9**) have been prepared according to standard procedures. Reaction of *N*-phenyldiethanolamine (**4**) with methyl iodide in presence of NaH in THF gave *N,N*-bis(2-methoxyethyl)aniline (**5**) in 62% yield which upon Vilsmeier formylation with DMF and POCl<sub>3</sub> afforded the aldehyde **6**, in 78% yield (Scheme 4.1).



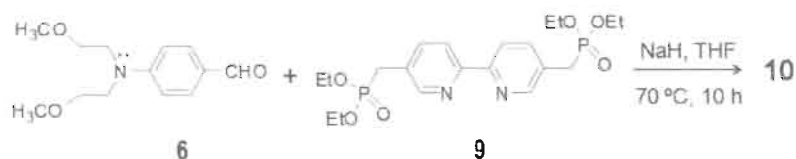
**Scheme 4.1.** Reagents and conditions. a) CH<sub>3</sub>I, NaH, THF (room temperature), 8 h (62%); b) DMF, POCl<sub>3</sub>, 5-10 °C, 45 min (78%).

Compound **9** was prepared starting from 5,5'-dimethyl-2,2'-bipyridine (Scheme 4.2). Bromination of **7** was carried out with *N*-bromosuccinimide. The bisbromomethyl derivative (**8**) was converted to the corresponding bisphosphonate ester by Michaelis-Arbuzov reaction in 90-92% yield.



**Scheme 4.2.** Reagents and conditions: a) NBS, CCl<sub>4</sub> 18 h; b) P(OEt)<sub>3</sub>, 100 °C, 12 h (90-92%).

The bismethoxyethyl aniline substituted bipyridine derivative (**10**) was prepared by the Wittig-Horner-Emmons olefination reaction of the bisphosphonate ester **9** and the 4-(bis(2-methoxyethyl)amino) benzaldehyde (**6**) using NaH in 62% yield (Scheme 4.3).



**Scheme 4.3.** Synthesis of **10**.

The compound **10** was characterized by <sup>1</sup>H NMR, <sup>13</sup>C NMR, IR and HRMS-FAB. FT-IR spectrum of **10** showed characteristic C-O stretching peak at 1116-1118 cm<sup>-1</sup> and the C-N stretching peak at 1517-1602 cm<sup>-1</sup>. <sup>1</sup>H NMR spectrum of the **10** showed strong *trans* coupling ( $J = 16-17$  Hz) for the vinylic linkages. The

N-CH<sub>2</sub> and -OCH<sub>2</sub> protons appeared as a multiplet at  $\delta$  3.5 ppm. The -OCH<sub>3</sub> protons of phenyl ring were observed at  $\delta$  3.3 ppm as a singlet.

#### 4.3.3. Optical Properties of **10**

The molecule **10** in chloroform ( $c = 6 \times 10^{-6}$  M) exhibited an absorption spectrum in the range of 350-475 nm with a maximum at 424 nm ( $\epsilon = 3.2 \times 10^4$  M<sup>-1</sup> cm<sup>-1</sup>) due to the  $\pi$ - $\pi^*$  transition. The spectrum did not show any considerable change in solvents such as toluene and acetonitrile except a small blue shift of about 4 nm (Figure 4.5a). However, as the polarity of the solvent is increased from hexane to acetonitrile, a 90 nm redshift is observed in the emission maximum which is at 484 nm in hexane and 574 nm in acetonitrile when excited at 440 nm. The quantum yields ( $\phi_f$ ) of the emission in hexane, chloroform and acetonitrile are 0.24, 0.34 and 0.31, respectively (quinine sulphate as standard). The observed solvent dependency of emission is attributed to the possibility of intramolecular charge transfer (ICT) associated with the D- $\pi$ -A- $\pi$ -D backbone of **10**. The solvent dependency of emission could be followed visually through a color change from blue to yellow when the solvent is changed from toluene to acetonitrile (Figure 4.6).

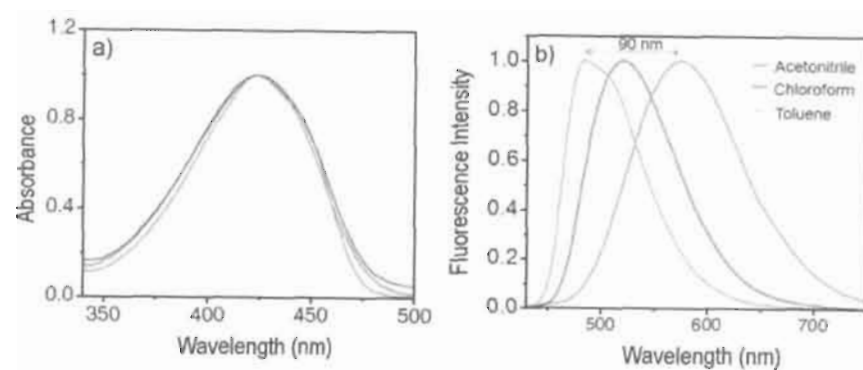


**Figure 4.5.** Normalized a) absorption and b) emission spectra of **10** in toluene, chloroform and acetonitrile ( $c = 6 \times 10^{-6}$  M,  $\lambda_{\text{ex}} = 420$  nm).

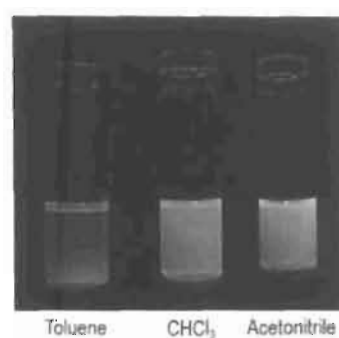


**Figure 4.6.** Photograph showing the visual color change in the fluorescence of **10** in toluene, chloroform and acetonitrile.

For more sights on the ICT process, time resolved fluorescence decay profiles were recorded in different solvents of varying polarity (Figure 4.7). Since polar solvents stabilize the CT state, excited state lifetime of **10** in acetonitrile was found to be high ( $\tau = 2.02$  ns) when compared to that in less polar solvents such as

chloroform ( $\tau = 1.19$  ns) and hexane ( $\tau = 0.96$  ns) (Table 1) with characteristic monoexponential decay profiles.

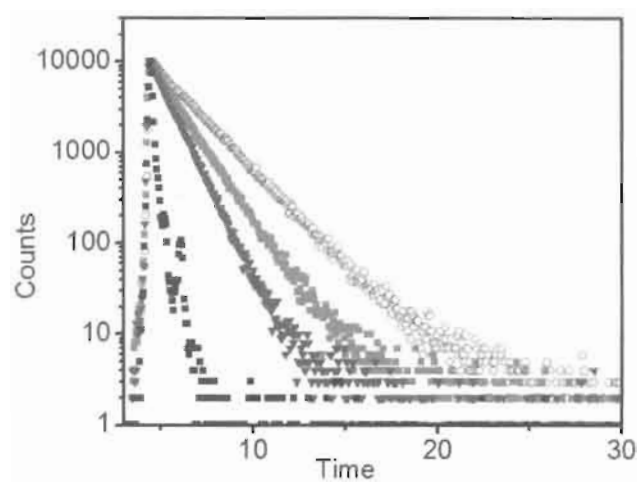


**Figure 4.7.** Comparison of the fluorescence decay profiles of **10** ( $6 \times 10^{-6}$  M) in acetonitrile ( $\circ$ ), chloroform ( $\blacksquare$ ), hexane ( $\blacktriangledown$ ) (polarity index 0.1, 4.1 and 5.8).

**Table 1.** Table showing the photophysical parameters of **10** in different solvents ( $6 \times 10^{-6}$  M).

Solvents	$\lambda_{em}$ (nm)	$\Phi_f$	$\tau$ (ns)
Hexane	464, 480	0.28	0.96
Chloroform	520	0.34	1.19
Acetonitrile	574	0.31	2.02

#### 4.3.4. Absorption and Emission Studies of **10** in Presence of Different Chemical Inputs

Photophysical properties of **10** are found to be highly sensitive to the presence of various chemical inputs. Since the molecule **10** contains three receptor sites which includes the central bipyridyl moiety, and the two tertiary nitrogen atoms in the donor part, the absorption and emission could be modulated by the addition of different inputs such as  $\text{Zn}^{2+}$  and  $\text{H}^+$ . For example, upon addition of trifluoroacetic acid (TFA) at pH 5.2, the absorption maximum is shifted to 510 nm (Figure 4.8), corresponding to a nonemissive CT state which is due to the protonation of the bipyridyl moieties. Further addition of TFA at pH 2.3 exhibited a shift of the CT band to 494 nm with a decreased intensity. Simultaneously, an additional band at 371 nm is formed. While the absorption band at 494 is nonemissive, the band at 371 nm is emissive. Interestingly, the emission at 574 nm (output 1) of **10** is blue shifted to 488 nm ( $\lambda_{ex}$  @ 400 nm,  $\Phi_f = 0.36$ ) (output 2) upon addition of TFA at pH 2.3 (input 1). Inset of Figure 4.8 b shows the visual color change for fluorescence output from yellow to pale blue. The optical output at 488 nm could be reversed to the initial fluorescence of **10** with the addition of tetra sodium salt of ethylene diamine tetra acetic acid (EDTA). These observations indicate the possibility of a stepwise protonation of the bipyridine and the aromatic amine moieties in presence of TFA at different pH, thereby changing the extent of the donor-acceptor interactions.

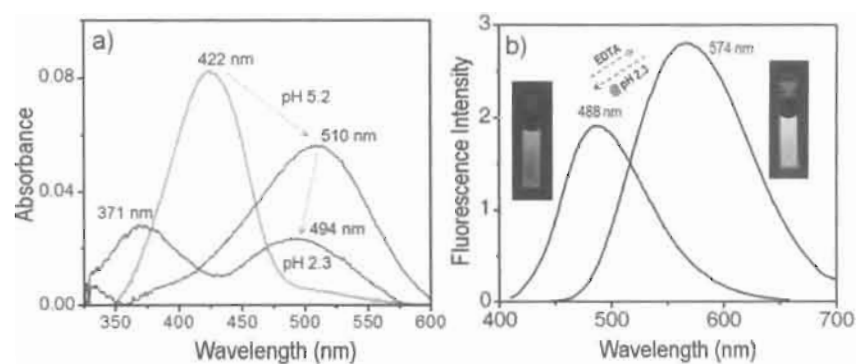


**Figure 4.8.** a) Changes in the absorption spectra of **10** ( $6 \times 10^{-6}$  M) (—) with the addition of TFA at pH 5.2 (---) and 2.3 (---). b) Shift in the emission output of **10** in acetonitrile upon addition of TFA at pH 2.3. Inset photographs show the visual change in the emission of **10** from yellow to blue in acetonitrile with the addition of TFA at pH 2.3 and the reversible change from blue to yellow with the addition of EDTA.

$^1\text{H}$  NMR titration of **10** in acetonitrile using TFA solution at different pH indicates the step-wise protonation of the bipyridyl units followed by the amine groups, that exhibited a gradual shift of the resonance peaks (Figure 4.9 and 4.10). When the pH of the solution is increased to 5.2, the bipyridine proton ( $\text{H}_a$ ) at 3-position ( $\delta = 7.9$  ppm) is deshielded gradually to  $\delta$  8.2 ppm. With the addition of excess TFA all aromatic protons were completely deshielded. The aliphatic  $-\text{NCH}_2$  and  $-\text{OCH}_2$  protons which appeared as a multiplet at  $\delta$  3.5 ppm were shifted as two triplets at  $\delta$  3.4 and 3.7 ppm upon addition of excess TFA, indicating the protonation of the two amine moieties.

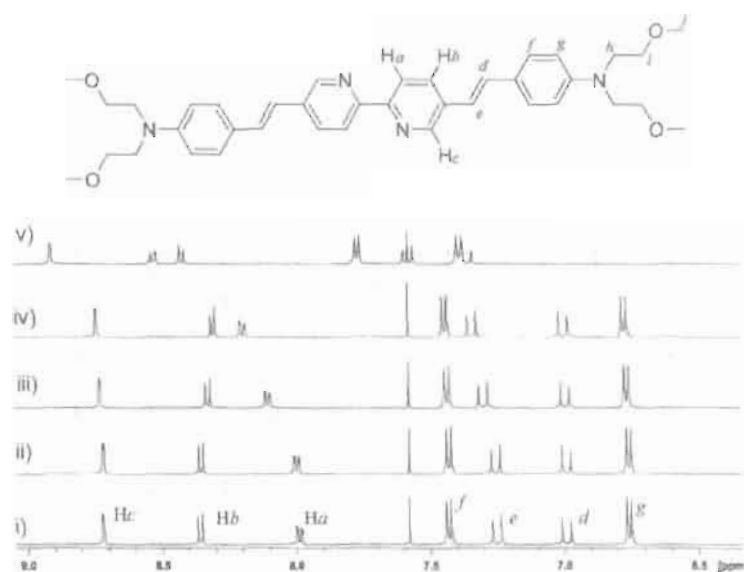


**Figure 4.9.** Partial <sup>1</sup>H NMR spectra of **10** (aromatic region) with the addition of TFA showing the initial protonation of the bipyridine moiety. i) **10** alone, ii) **10**+ TFA at pH 6.0, iii) **10**+ TFA at pH 5.5, iv) **10**+ TFA at pH 5.2 and v) **10** + excess TFA.

Addition of excess TFA, at pH 2.3 may protonate the donor as well as the acceptor sites which results in the complete arrest of the electronic communication between the donor and the acceptor thereby reducing the chance for ICT as shown in Scheme 4.4.

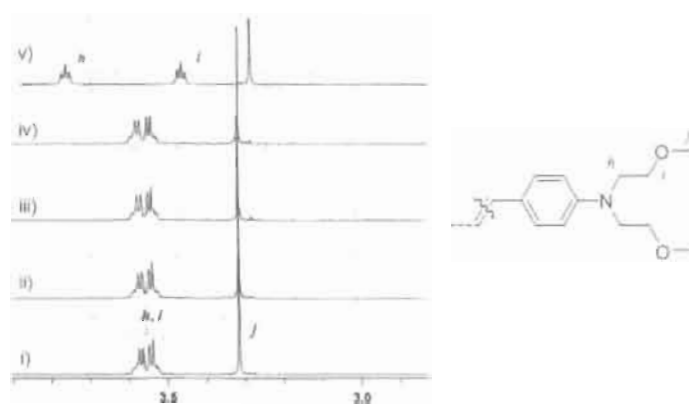
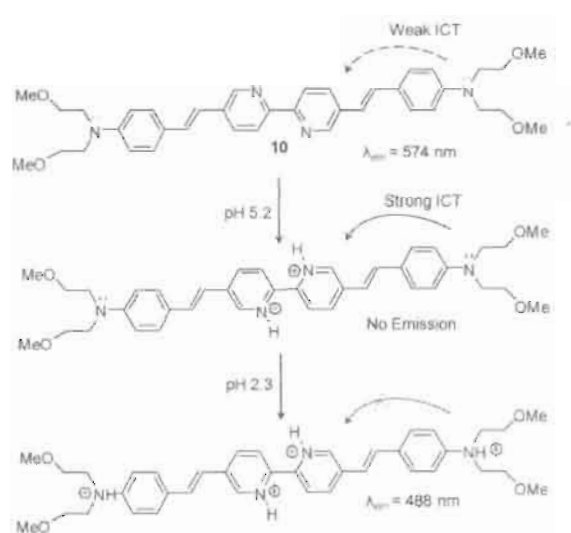


**Figure 4.10.** Partial  $^1\text{H}$  NMR spectra of **10** (aliphatic region) showing changes with the addition of TFA. i) **10** alone ii) **10**+ TFA at pH 6.0, iii) **10**+ TFA at pH 5.5, iv) **10**+ TFA at pH 5.2 and v) **10** + excess TFA.



**Scheme 4.4.** Possible mechanism of ICT modulated emission **10** with the addition of TFA at pH 5.2 and 2.3.

When one equivalent of  $\text{Zn}(\text{ClO}_4)_2$  is added to a solution of **10**, the emission output at 574 nm is completely quenched. Sequential addition of TFA at pH 2 resulted in the regeneration of a new emission (output 3) at 464 nm ( $\lambda_{\text{exc}}$  @ 390 nm,  $\Phi_f = 0.44$ ) (Figure 4.11). With the addition of excess EDTA solution, the emission output at 574 nm corresponding to **10** is regenerated without considerable loss of the emission intensity. The absorption maximum of **10** at 422 nm is red shifted to 486 nm upon addition of  $\text{Zn}(\text{ClO}_4)_2$  which subsequently is blue shifted to 377 nm with considerable decrease in intensity upon protonation with TFA and then to the original absorption at 422 nm with addition of EDTA (Figure 4.11a).

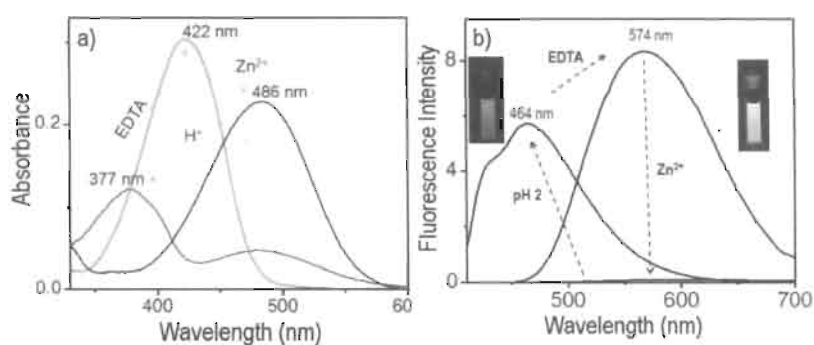


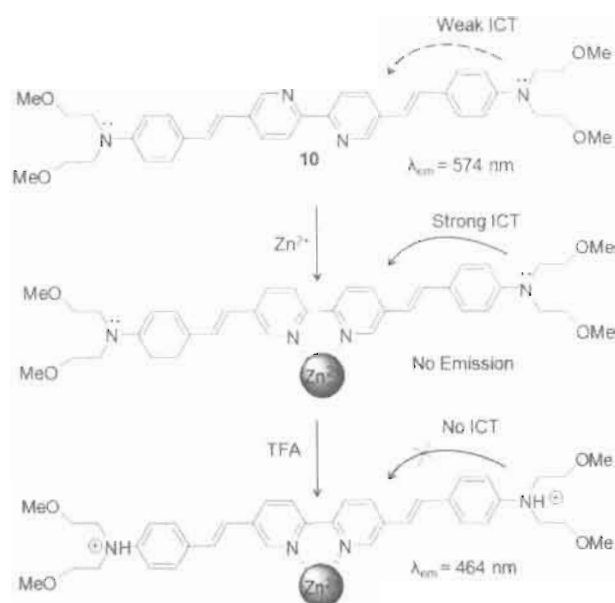
**Figure 4.11.** a) Changes in the absorption spectrum of **10** ( $6 \times 10^{-6}$  M) (—) with the addition of one equivalent of  $\text{Zn}^{2+}$  ions (---) and followed by the addition of TFA (· · ·). b) Shift in the emission output of **10** at 574 nm ( $\Phi_f = 0.31$ ) in acetonitrile to 464 nm ( $\Phi_f = 0.44$ ) upon addition of  $\text{Zn}^{2+}$  and TFA. Inset photographs show the corresponding reversible change in the emission color of **10** with the addition of  $\text{Zn}^{2+}$  and TFA (left) and the addition of EDTA (right).

Change in the emission output of **10** with the sequential addition of  $\text{Zn}(\text{ClO}_4)$ , TFA and EDTA are shown in Figure 4.11b. When  $\text{Zn}^{2+}$  is complexed with the bipyridine receptor site, the excited state ICT process is strengthened which resulted in a complete quenching of the emission of **10** at 574 nm (Figure 4.11b). When TFA solution with pH 2 is added to **10**- $\text{Zn}^{2+}$  complex, protonation occurs at both amine donor sites thereby blocking the ICT channel which in turn resulted in the generation of a new emission output at 464 nm. The mechanism involved in the fluorescence output changes upon addition of different inputs are shown in Scheme 4.5. The main advantage of such ICT based fluorescence change is the possibility of using multiple wavelengths to address the state of the switch, which ultimately enables parallel generation of several binary variables and logic operations.

#### 4.3.5. Logic Operations of **10**

The in situ generation of three different fluorescence outputs from the fluorophore **10**, allow four different multiple input logic functions which define INHIBIT (*INH*, 2 inputs-1 output), INHIBIT (*INH*, 3 inputs-1 output), IMPLICATION (*IMP*, 2 inputs-1 output), and AND (2 inputs-1 output) logic operations. For example, the changes in the fluorescence of **10** with  $\text{H}^+$ , EDTA and  $\text{Zn}^{2+}$  can be represented by two different logic operations corresponding to an INHIBIT and an IMPLICATION logic gates. An INHIBIT (*INH*) operation is described by the truth table as shown in Figure 4.12e, which is a concatenation of

AND and NOT logic functions and therefore expresses a noncommutative behavior.



**Scheme 4.3.** Mechanism of multiple fluorescence expressions through excited state intramolecular charge transfer in **10** with respect to inputs such as  $\text{Zn}^{2+}$  and  $\text{H}^+$ .

A combination of sequential inputs of pII 2.3 and EDTA results in reversible optical output at 488 nm equivalent to an *INH* logic system (Figure 4.12a). The emission intensity variation and the corresponding truth table are shown in Figure 4.12c and 4.12e, respectively. At the same time, a complementary logic operation is possible when the emission output at 574 nm is addressed in combination with  $\text{Zn}^{2+}$  and EDTA as inputs (Figure 4.12b). This is equivalent to an IMPLICATION

(*IMP*) logic interpretation<sup>27</sup> as shown in the truth table in Figure 4.12f. The corresponding fluorescence output variations against the inputs are shown in Figure 4.12d. Thus, we could achieve simultaneous and separate operation of both *INH* and *IMP* gates using **10**. This is possible due to the three emission states generated by ICT modulation in **10** at 488, 574 nm (on states) and a quenched state (off state).

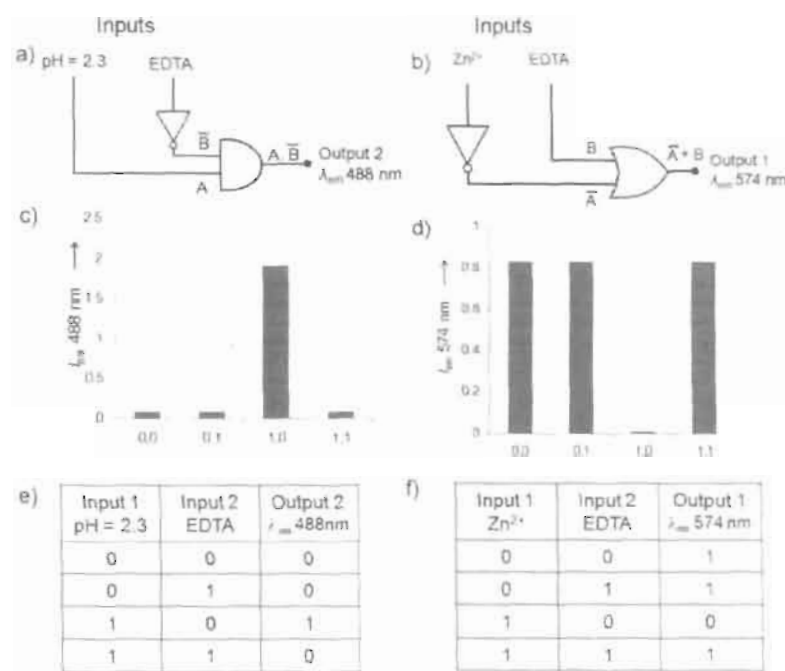


**Figure 4.12.** Logic circuits, emission intensity variation plots at two independent wavelengths (488 nm & 574 nm) and the corresponding truth tables representing INHIBIT (combination of NOT and AND gates) (a, c and e) and IMPLICATION (combination of NOT and OR gates) (b, d and f) with respect to a set of inputs.

A third option with **10** is an AND logic operation which needs two inputs at a time to get an output. In all other operations, the output will be zero. In the present case, a two input AND logic operation can be defined by considering  $Zn^{2+}$  and pH 2 as chemical inputs and emission maximum at 464 nm as optical output (output 3) (Figure 4.13a & 4.13b). In addition, a molecular logic gate with 3-input-*INH* logic operation can also be demonstrated by monitoring emission at 464 nm (output 3) using  $Zn^{2+}$ , pH 2 and EDTA (in excess) as chemical inputs (Figure 4.13c and 4.13d). A 3-input-*INH* is a combination of NOT gate and a 3-input AND logic gate. Thus, the molecule **10** allows the design of four different binary logic operations by choosing the appropriate chemical inputs and optical outputs.

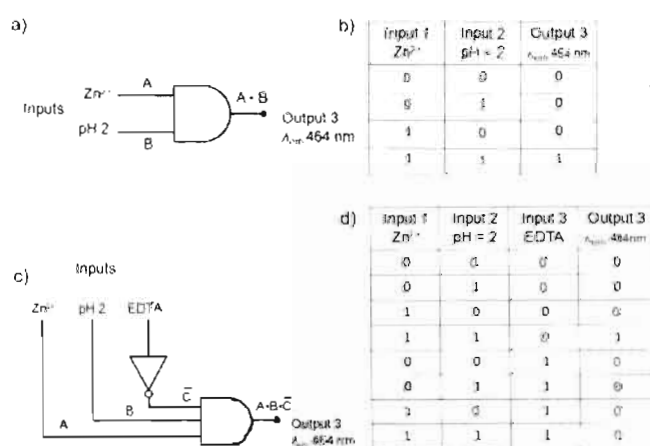


**Figure 4.13.** Logic circuit representation and the corresponding truth table for AND (a & b) and 3-input-*INH* logic gates (c & d) with respect to a set of sequential inputs of output at 464 nm.

An added advantage of the molecule **10** is the possibility to construct integrated logic circuits. Thus, a combined logic scheme could be designed based on three chemical inputs of  $\text{Zn}^{2+}$ , pH 2 and EDTA with two state distinct emission outputs at 574 nm and 464 nm. Such an integrated logic circuit comprises of a combination of several basic logic operations. For example, a combination of three NOT gates, along with a 2-input AND, a 3 input AND and an OR gates has been demonstrated with the molecule **10** by monitoring two different outputs at 574 and 464 nm (Figure 4.14). Thus, integration of different logic gates could be achieved by combining different Boolean operations in a single circuit with a specific function as indicated in the corresponding truth table (Figure 4.14b).

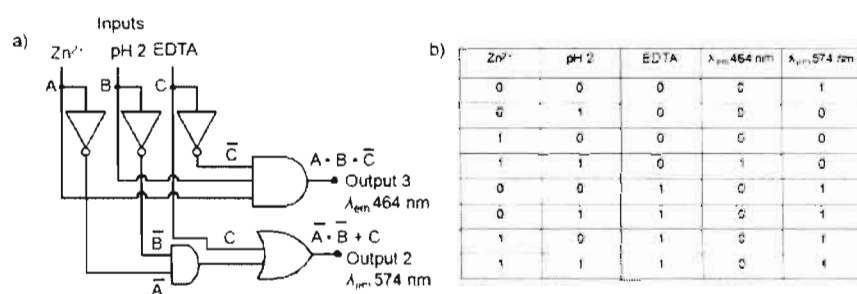


**Figure 4.14.** a) A three-input, two-output combinatorial logic circuit representation with fluorescence outputs at  $\lambda_{em}$  464 nm and  $\lambda_{em}$  574 nm triggered by chemical inputs of  $\text{Zn}^{2+}$ ,  $\text{H}^+$  and EDTA . b) The corresponding truth table.

#### 4.3.6. Paper Microfluidic Demonstration of Fluorescence Modulation with Various Inputs

Construction of integrated circuits with molecular logic gates is a challenging task. We have attempted a demonstration of multiple logic definitions of the molecular logic gate **10** using micro channels in a filter paper substrate. Whitesides et al., have recently described the development of microchannels in filter paper using poly(dimethyl siloxane) (PDMS).<sup>28-30</sup> We have adopted a similar strategy for the preparation of micro channels and logic operation display chambers. A hexane solution of the hydrophobic polymer PDMS is coated over small pieces of Whatman 40 filter paper as shown in Figure 4.15. PDMS penetrates to the depth of the paper and forms a hydrophobic wall through which aqueous solutions cannot cross. The design of micro channel circuitry comprises of four display reservoirs (DR) and a main reservoir (MR). Four sides of the filter paper are coated with PDMS except for the “on” input channel (green color) which is allowed to be in contact with aqueous solutions of different inputs. The capillary action pulls the chemical inputs to reach the display chamber. The main reservoir as well as the display reservoirs was preoccupied by **10**.

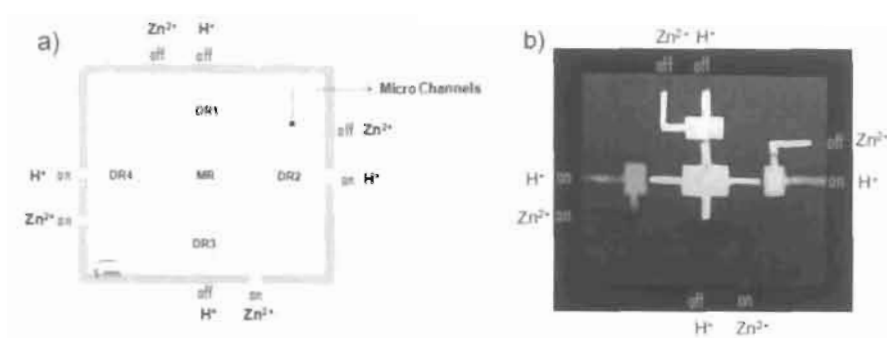


**Figure 4.15.** Demonstration of a hydrophilic microchannel display circuitry in a filter paper by using PDMS to represent various logic operations. a) Design strategy for the microcircuitry. b) Photograph showing various emission outputs from four display chambers with respect to the chemical inputs at the opened microchannels.

In order to visualize different optical outputs from **10** with respect to various chemical inputs, the entire micro channel circuitry was illuminated with a 365 nm UV light. The main reservoir as well as the display reservoirs show yellow emission (574 nm) (output 1) corresponding to **10** (Figure 4.15) (see MR, DR 1). Through the “on” channel of DR2, a solution of TFA at pH 2.3 is allowed to enter the micro channel, thus resulting in the emission output at 488 nm (output 2, pale blue emission) (Figure 4.15). The “on” state of DR3 allows only  $Zn^{2+}$  to enter into the channel and results in the complete quenching of the emission of **10** at 574 nm. The micro channel in DR4 is in the “on” state for both chemical inputs of  $Zn^{2+}$  and  $H^+$ . Allowing sequential entrance of  $Zn^{2+}$  solution and TFA at pH 2 resulted in the emission output at 464 nm (output 3). The three intrinsically generated fluorescence responses at DR2, DR3 and DR4 are reversible when all the four

channels are allowed to be in contact with the third chemical input EDTA. Thus, DR2 represents *INH* operation using 488 nm emission output with pH and EDTA as inputs, while DR3 represents *IMP* operation using 574 nm emission output and  $Zn^{2+}$  and EDTA as inputs. Finally, DR4 represents AND and 3-input-*INH* operations using emission output at 464 nm and  $Zn^{2+}$ ,  $H^+$  and EDTA as inputs (Figure 4.15).

#### 4.4. Conclusions

The bipyridine based fluorophore **10** described here shows significant solvatochromic emission shift in different solvents due to an excited state CT modulation. The donor-acceptor strength in **10** could be altered by different chemical inputs resulting in different optical outputs. This property of **10** could be addressed in the form of binary logic operations which include 2-input-INHIBIT, IMPLICATION, AND and 3-input-INHIBIT. In addition, combinations of these basic logic operations are demonstrated in a single integrated circuit. Finally, a microchannel display of the four stage intrinsic fluorescence outputs and the corresponding logic operations are demonstrated using a paper microfluidic technique which may find application in logic controlled design of “lab on a chip” for micro analytical purposes.

## 4.5. Experimental Section

### 4.5.1. Synthesis and Characterization

Solvents and reagents were purified and dried by usual methods. All starting materials were obtained from commercial suppliers and used as received. Melting points were determined with Mel-Temp-II melting point apparatus.  $^1\text{H}$  and  $^{13}\text{C}$  NMR were measured on a 500 MHz Bruker Avance II Spectrometer. High Resolution Mass Spectra were recorded with a JEOL JMS600. Electronic absorption spectra were recorded on a Shimadzu UV-3101 PC NIR scanning spectrophotometer and the emission spectra were measured on a SPEX-Fluorolog F112X spectrofluorimeter. Fluorescence quantum yields were determined in spectroscopic grade  $\text{CH}_3\text{CN}$  using optically matching solutions of Quinine Sulfate ( $\Phi_f = 0.546$  in  $0.1\text{N H}_2\text{SO}_4$ ) as standard at an excitation wavelength of 360 nm. The quantum yield was calculated using equation 1.

$$\Phi_f = \Phi_f (A_r F_s / A_s F_r) (\eta_s^2 / \eta_r^2) \dots\dots\dots (1)$$

where,  $A_s$  and  $A_r$  are the absorbance of the sample and reference solutions, respectively at the same excitation wavelength,  $F_s$  and  $F_r$  are the corresponding relative integrated fluorescence intensities and  $\eta$  is the refractive index of the solvent.

Fluorescence lifetimes were measured using IBII (FluoroCube) time-correlated picosecond single photon counting (TCSPC) system. Solutions were excited with a pulsed diode laser (<100 ps pulse duration) at a wavelength of 375

nm (NanoLED-11) with a repetition rate of 1 MHz. The detection system consists of a microchannel plate photomultiplier (5000U-09B, Hamamatsu) with a 38.6 ps response time coupled to a monochromator (5000M) and TCSPC electronics (Data Station Hub including Hub-NL, NanoLED controller and preinstalled Fluorescence Measurement and Analysis Studio (FMAS) software). The fluorescence lifetime values were determined by deconvoluting the instrument response function with bi-exponential decay using DAS6 decay analysis software. The quality of the fit was judged by the fitting parameters such as  $\chi^2$  (< 1.2) as well as the visual inspection of the residuals.

#### 4.5.2. Preparation of *N,N*-bis(2-methoxyethyl)aniline (5)

To a two-necked round bottom flask placed with **4** (0.9 g, 5 mmol) in dry THF, a suspension of NaH (30 mmol) in THF was added. After stirring for 10 min, CH<sub>3</sub>I (10 mmol) was added dropwise into the reaction mixture. After stirring for 12 h, THF was removed under reduced pressure to give a pasty residue. The residue was suspended in water and extracted with dichloromethane. The organic layer was washed with brine, dried over Na<sub>2</sub>SO<sub>4</sub> and concentrated to give a crude product, which was further purified by column chromatography over alumina using ethylacetate (2%)-petroleum ether as the eluent.

Yield 83%; <sup>1</sup>H NMR (CDCl<sub>3</sub>, 500 MHz)  $\delta$  (ppm): 7.2 (2H, aromatic), 6.94 (2H, aromatic), 6.79 (1H, aromatic), 4.18 (t, 2H), 3.73 (t, 2H), 3.3 (s, -OCH<sub>3</sub>); <sup>13</sup>C NMR (CDCl<sub>3</sub>, 125 MHz)  $\delta$  (ppm): 149.6, 129.6, 121.9, 114.3, 70.3, 59.2.

#### 4.5.3. Preparation of 4-(bis(2-methoxyethyl)amino)benzaldehyde (6)

To a solution of dry DMF (35 mmol) and phosphorus oxychloride (9 mmol) at 10-20 °C, *N,N*-bis(2-methoxyethyl)aniline (5) (1.8 g, 9 mmol) in dry DMF was added slowly with stirring. The mixture was stirred at 35 °C for 45 min., and then poured into crushed ice. The clear solution formed at 20-30 °C was neutralized with aqueous NaOH. The mixture was boiled for 1 min, cooled to room temperature and extracted with diethyl ether. Removal of the solvent gave a viscous liquid, which was chromatographed on silica gel using petroleum ether-ethylacetate (9.5:0.5) to give the (6).

Yield 70%; <sup>1</sup>H NMR (CDCl<sub>3</sub>, 500 MHz) δ (ppm): 9.88 (s, 1H, -CHO), 7.14 (2H, aromatic), 6.95 (2H, aromatic), 4.18 (t, 2H), 3.73 (t, 2H), 3.3 (s, -OCH<sub>3</sub>); <sup>13</sup>C NMR (CDCl<sub>3</sub>, 125 MHz) δ (ppm): 191.0, 155.4, 130.8, 126.4, 112.3, 70.3, 59.2.

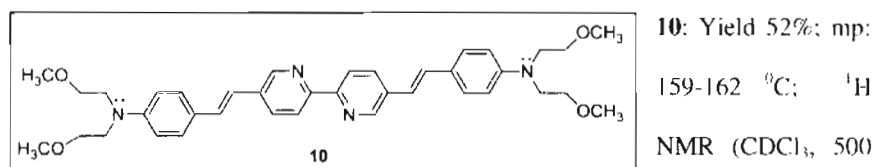
#### 4.5.4. Preparation of 5,5'-bis(bromomethyl)-2,2'-bipyridine (8) and bisphosphonate (9) derivatives

Details of the synthesis and characterization of 8 and 9 were discussed in Chapter 3.

#### 4.5.5. Procedure for the Synthesis of 10

A suspension of sodium hydride (0.3 g, 12 mmol) in dry THF was added slowly to a solution of the bisphosphonate (0.9 g, 2 mmol) and 4-(bis(2-methoxyethyl)amino) benzaldehyde (1g, 4 mmol) in THF. After refluxing for 12 h, the

fluorescent reaction mixture obtained was cooled followed by the removal of THF under reduced pressure to give a pasty residue. The residue was suspended in water and extracted with dichloromethane. The organic layer was washed with brine, dried over  $\text{Na}_2\text{SO}_4$  and concentrated to give the crude product, which was further purified by column chromatography over alumina using ethylacetate (10%)-petroleum ether as eluent. Yields, melting points, and spectral details of **10** are given below.



MHz)  $\delta$  (ppm): 8.7 (s, 1H, aromatic), 8.3 (s, 1H, aromatic), 7.9 (d, 1H, aromatic), 7.4 (d, 2H, aromatic), 7.2 (d, 1H, vinylic,  $J = 16.41$  Hz), 6.95 (d, 1H, vinylic,  $J = 16.38$  Hz), 6.7 (d, 2H, aromatic), 3.57 (m, 4H,  $-\text{NCH}_2$ ), 3.52 (m, 4H,  $-\text{OCH}_2$ ), 3.3 (s, 6H,  $-\text{OCH}_3$ );  $^{13}\text{C}$  NMR ( $\text{CDCl}_3$ , 125 MHz)  $\delta$  (ppm): 153.90, 147.94, 147.69, 133.65, 132.65, 130.78, 128.09, 124.96, 120.14, 112.58, 111.85, 109.61, 70.1, 59.02, 50.97; FT-IR (KBr)  $\nu_{\text{max}}$ : 835, 964, 1116, 1184, 1274, 1354, 1517, 1602, 1745, 2814  $\text{cm}^{-1}$ ; HRMS-FAB:  $[\text{M}]^+$ : Calculated for  $\text{C}_{42}\text{H}_{58}\text{N}_4$ : 623.8, Obtained: 624.0.

#### 4.6. References

1. P. Ball, *Nature* **2000**, *406*, 118.
2. *International Technology Roadmap for Semiconductors*, International SEMATECH, Austin, TX **2000**.
3. G. Bell, J. N. Gray in *Beyond Calculation: The Next Fifty Years of Computing* (Eds.: P. J. Denning, R. M. Metcalfe), Copernicus/Springer, New York, **1997**, p. 30.
4. A. P. de Silva, N. D. McClenaghan and C. P. McCoy, *Molecular-Level Electronics. Imaging and Information, Energy and Environment, in Electron Transfer in Chemistry*, ed. V. Balzani, Vol. 5, Wiley-VCH, Weinheim, **2001**
5. A. P. de Silva, H. Q. N. Gunaratne, C. P. McCoy, *Nature*, **1993**, *364*, 42.
6. A. P. de Silva, H. Q. N. Gunaratne, C. P. McCoy, *J. Am. Chem. Soc.*, **1997**, *119*, 7891.
7. A. P. de Silva, G. D. McClean, S. Pagliari, *Chem. Commun.*, **2003**, 2010.
8. S. Uchiyama, N. Kawai, A. P. de Silva, K. Iwai, *J. Am. Chem. Soc.*, **2004**, *126*, 3032.
9. P. Ghosh, P. K. Bharadwaj, S. Mandal, S. Ghosh, *J. Am. Chem. Soc.*, **1996**, *118*, 1553.
10. G. McSkinning, J. H. R. Tucker, H. Bouas-Laurent, J. -P. Desvergne, *Angew. Chem. Int. Ed.*, **2000**, *39*, 2167.

11. J. F. Callan, A. P. de Silva and N. D. McClenaghan, *Chem. Commun.*, **2004**, 2048.
12. A. P. de Silva, T. Gunnlaugsson and C. P. McCoy, *J. Chem. Educ.*, **1997**, *74*, 53.
13. A. P. de Silva, I. M. Dixon, H. Q. N. Gunaratne, T. Gunnlaugsson, P. R. S. Maxwell and T. E. Rice, *J. Am. Chem. Soc.*, **1999**, *121*, 1393.
14. B. Turfan and E. U. Akkaya, *Org. Lett.*, **2002**, *4*, 2857.
15. T. Gunnlaugsson, D. A. Mac Dónail, D. Parker, *Chem. Commun.*, **2000**, 93.
16. T. Gunnlaugsson, D. A. Mac Dónail, D. Parker, *J. Am. Chem. Soc.*, **2001**, *123*, 12866.
17. A. Credi, V. Balzani, S. J. Langford and J. F. Stoddart, *J. Am. Chem. Soc.*, **1997**, *119*, 2679.
18. S. H. Lee, J. Y. Kim, S. K. Kim, J. H. Lee and J. S. Kim, *Tetrahedron*, **2004**, *60*, 5171.
19. *Molecular Switches* (Ed: B. L. Feringa), Wiley-VCH, Weinheim, **2001**.
20. A. P. de Silva, H. Q. N. Gunaratne, T. Gunnlaugsson, A. J. M. Huxley, C. P. McCoy, J. T. Rademacher, T. E. Rice, *Chem. Rev.* **1997**, *97*, 1515.
21. J. R. Lakowicz, *Anal. Biochem.* **2001**, *298*, 1.
22. K. Szacilowski, *Chem. Rev.* **2008**, *108*, 3481.
23. H. S. Joshi, R. Jamshidi, Y. Tor, *Angew. Chem. Int. Ed.* **1999**, *38*, 2722.
24. C. Kaes, A. Katz and M. W. Hosseini, *Chem. Rev.* **2000**, *100*, 3553.
25. G. McSkimming, J. H. R. Tucker, H. Bouas-Laurent, J. -P. Desvergne, *Angew. Chem. Int. Ed.* **2000**, *39*, 2167.

26. A. P. de Silva, I. M. Dixon, H. Q. N. Gunaratne, T. Gunnlaugsson, P. R. S. Maxwell, T. E. Rice, *J. Am. Chem. Soc.* **1999**, *121*, 1393.
27. K. Rurack, C. Trieflinger, A. Koval'chuck, J. Daub, *Chem. Eur. J.* **2007**, *13*, 8998.
28. D. A. Bruzewicz, M. Reches, G. M. Whitesides, *Anal. Chem.* **2008**, *80*, 3387.
29. A. W. Martinez, S. T. Philips, E. Carrilho, S. W. Thomas III, hayat Sindi, G. M. Whitesides *Anal. Chem.* **2008**, *80*, 3699.
30. A. W. Martinez, S. T. Philips, G. M. Whitesides *Proc. Natl. Acad. Sci. USA*, **2008**, *105*, 19606.

## LIST OF PUBLICATIONS

1. A Ratiometric Fluorescence Probe for Selective Visual Sensing of Zn<sup>2+</sup>.  
A. Ajayaghosh, P. Carol, S. Sreejith  
*J. Am. Chem. Soc.* **2005**, *127*, 14962-14963.
2. Ratiometric and Near-Infrared Molecular Probes for the Detection and Imaging of Zinc Ions.  
P. Carol, S. Sreejith, A. Ajayaghosh  
*Chem. Asian J.* **2007**, *2*, 338-348. (Focus Review)
3. Squaraine Dyes: a mine of molecular materials.  
S. Sreejith, P. Carol, P. Chithra, A. Ajayaghosh  
*J. Mater. Chem.* **2008**, *18*, 264-274. (Feature Article)
4. Detection of zinc ions under aqueous conditions using chirality assisted solid-state fluorescence of a bipyridyl based fluorophore.  
S. Sreejith, K. P. Divya, A. Ajayaghosh  
*Chem. Commun.* **2008**, 2903-2905.
5. A Near-Infrared Squaraine Dye as a Latent Ratiometric Fluorophore for the Detection of Amino-thiol Content in Blood Plasma.  
S. Sreejith, K. P. Divya, A. Ajayaghosh  
*Angew. Chem. Int. Ed.* **2008**, *47*, 7883-7887.

## PATENTS FILED

1. Pyrrole end-capped bipyridine assay powder for selective detection of zinc ions and a process for the preparation thereof.  
A. Ajayaghosh, S. Sreejith  
Int. Appl. No. *PCT/IN2008/00374*

## POSTERS PRESENTED AT CONFERENCES

1. Design of Reusable Dipstick Sensor for the Detection of Zinc Ions under Aqueous Conditions  
S. Sreejith and A. Ajayaghosh  
3<sup>rd</sup> JNC Conference on Chemistry of Materials, September 27-29, 2007, Munnar, Kerala, India.
  
2. Chirality Induced Enhanced Solid-state Fluorescence of a Bipyridyl Based Chelator: Design of Molecular Probes for Zn<sup>2+</sup>  
S. Sreejith and A. Ajayaghosh  
Indo-Japan Cooperative Science Programme: "Recent Trends in Molecular Materials Research", January 20-22, 2008, Trivandrum, India.
  
3. Detection of Total Amino-thiol Content in Blood Plasma using a Novel Ratiometric Probe  
S. Sreejith and A. Ajayaghosh  
11<sup>th</sup> CRSI Symposium in Chemistry, February 06-08, 2009, National Chemical Laboratory, Pune, India.